universiteit
hasselt
KNOWLEDGE IN ACTION

2015 | Faculty of Sciences

DOCTORAL DISSERTATION

Functionalization of Boron-Doped Diamond Surfaces for (Bio)Molecular Electronics

Doctoral dissertation submitted to obtain the degree of
Doctor of Science: Chemistry, to be defended by

Weng Siang Yeap

Promoter: Prof. Dr Ken Haenen | UHasselt
Co-promoter: Prof. Dr Wouter Maes | UHasselt

D/2015/2451/10

universiteit hasselt | imec

IMO - IMOMEC
INSTITUUT VOOR MATERIAALONDERZOEK

Jury

Chair: Prof. Dr. K. Coninx
Hasselt University

Promoter: Prof. Dr. K. Haenen
Hasselt University & IMEC vzw

Co-promoter: Prof. Dr. W. Maes
Hasselt University & IMEC vzw

Members of the Jury: Prof. Dr. A. Krueger
Universität Würzburg, Institut Für Organische Chemie, Germany

Prof. Dr. L. Kavan
Academy of Sciences of the Czech Republic, J. Heyrovskỳ Institute of Physical Chemistry, Czech Republic

Prof. Dr. M. Fahlman
Linköping University, Department of Physics, Chemistry and Biology, Sweden

Prof. Dr. M. Nesládek
Hasselt University & IMEC vzw

Prof. Dr. P. Wagner
Katholieke Universiteit Leuven, Department of Physics and Astronomy, Belgium

Prof. Dr. W. Guedens
Hasselt University & IMEC vzw

Dr. L. Lutsen
Hasselt University & IMEC vzw

Acknowledgements

I would like to take this opportunity to express my gratitude to the following people who have shown me guidance and rendered me support during my PhD studies.

First of all, I would like to express my sincerest gratitude to my supervisor, Prof. Dr. Ken Haenen, and co-supervisor, Prof. Dr. Wouter Maes, for their kind guidance, support and encouragement throughout my research work. Without their unwavering support, I could not have completed this thesis work.

I would like to thank Prof. Dr. Ladislav Kavan, Prof. Dr. Mats Fahlman, Prof. Dr. Anke Krueger, Prof. Dr. Miloš Nesládek, Prof. Dr. Wanda Guedens, Prof. Dr. Patrick Wagner, and Dr. Lauren Lutsen for their acceptance to be in the jury committee of my PhD degree thesis. They took part in my thesis committee and provided valuable feedback and suggestions.

I am especially indebted to Dr. Liu Xianjie from Linköping University who has dedicated considerable amount of time in measuring all my diamond samples with endless tolerance and patience. Also special thanks to Dr. David Bevk who has provided me with many valuable suggestions in order to help me to complete my work in the MOLESOL project. I deeply acknowledge Dr. Alberto Pasquarelli from Ulm University who welcomed me for a short stay at his lab. A deep thank you also to Dr. Mohammed S. Murib for his help, support, and in-depth discussions.

A big thank you to the laboratory staff, Huguette Penxten, Christel Willems, Johnny Baccus, Hilde Pellaers, Bart Ruttens, Ing. Erik Thoonen and many more, for their technical support and guidance in the lab.

I am thankful to all the current and former members of the WBGM group and the office mates (Room 1.39) from IMOMEC for their help and friendship. Many thanks to Lea, Relinde, Ellen and Marina for their help with the official documents. My gratitude also goes out to Qiushi, Lianchen, Hong and Haixin for being such great friends and the lunch breaks we had together whilst listening to each other's problems. I am also grateful to my family and friends for their invaluable love and support. Without them, I wouldn't be where I am today. My sincere best wishes go out to other family members, friends and colleagues as they are equally important. Even if I did not mention all the names, I am so grateful to all and will always be forever thankful.

Last but not least, I would like to acknowledge Hasselt University for providing me with the financial support and the facilities to carry out the research work.

Table of Contents

Abstract

In this thesis work, we have contributed to the development and optimization of specific surface functionalization methods for the introduction of different organic (bio)molecules on mainly boron-doped diamond (BDD) surfaces. These methods are based on electrochemical and wet-chemical concepts. The functionalized diamond platform was also tested for its possible applications.

In the first part of Chapter 1, a general description on diamond classification and a brief explanation on how to grow boron-doped diamond is given. Then, the surface properties of diamond and the electrochemical properties of boron-doped diamond are discussed. The last part of this chapter focuses on the surface chemistry of diamond.

In Chapter 2, a general introduction to all the characterization techniques used throughout this thesis is given, such as X-ray Photoelectron Spectroscopy (XPS), Ultra-violet Photoelectron Spectroscopy (UPS), Near-Edge X-ray Absorption Fine Structure Spectroscopy (NEXAFS), Cyclic Voltammetry (CV), and Impedance Spectroscopy.

In Chapter 3, we show that N3 dye molecules [*cis*-*bis*(isothiocyanato)-*bis*(2,2'-bipyridyl-4,4'-dicarboxylato)-ruthenium(II)] can be covalently attached onto boron-doped nanocrystalline diamond (B:NCD) thin films through a combination of coupling chemistries, i.e. diazonium, Suzuki and EDC-NHS. Spectroscopic techniques such as XPS, UPS, and NEXAFS were used to verify the covalent bonding of the dye on the B:NCD surface. The spectroscopic results confirmed the presence of a dense N3 chromophore layer. The positions of the frontier orbitals of the dye relative to the band edge of the B:NCD thin film were inferred as well using UPS. Our proof of concept photoelectrochemical measurements showed a strong increase in photocurrent as compared to non-dye-functionalized B:NCD films.

In Chapter 4, donor-acceptor type light-harvesting molecular dyes are covalently attached to B:NCD surfaces via a combination of diazonium electrografting and Suzuki cross-coupling. In order to achieve a high coupling yield for the Suzuki reaction, various catalytic systems were compared with respect to their imposed surface coverage. We found that when combining 2-dicyclohexylphosphino-2’,6’-dimethoxybiphenyl (SPhos) and Pd(0), the diamond coverage improved considerably (by 98%) as compared to the standard tetrakis(triphenylphosphino)palladium(0) (Pd(PPh_3)$_4$) catalyst. From UPS measurements, we found that the highest occupied molecular orbital (HOMO) level of the molecular dyes aligns well with the valence band maximum (VBM) of

B:NCD. It is concluded that this should favor hole injection from the molecular dyes to the B:NCD during photoexcitation.

In Chapter 5, we report a straightforward protocol for the covalent functionalization of BDD electrodes with either ferrocene or single-stranded deoxyribonucleic acid (ss-DNA). An azide-terminated organic layer was first electrografted on the diamond surface by electrochemical reduction of 4-azidophenyldiazonium chloride. The azidophenyl-modified surface then reacts rapidly and efficiently with molecules bearing a terminal alkyne moiety by means of a Cu(I)-catalyzed alkyne-azide cycloaddition. Covalent attachment of the ferrocene moieties was analyzed by means of XPS and CV, whereas impedance spectroscopy was applied for the characterization of the immobilized DNA.

Nederlandse Samenvatting

In deze thesis werd bijgedragen aan de ontwikkeling van specifieke oppervlaktefunctionaliseringsmethoden voor de introductie van verschillende organische (bio)moleculen op voornamelijk B-gedoteerde (BDD) diamantoppervlakken. Deze methodes zijn gebaseerd op zowel elektrochemische als chemische concepten. Het gefunctionaliseerd diamant werd uiteindelijk getest op zijn toepassingen.

In hoofdstuk 1 wordt eerst een algemene beschrijving gegeven van de classificering van diamant, gevolgd door een korte introductie over de groei van B-gedoteerd diamant. Daarna worden de oppervlakte-eigenschappen van diamant en de elektrochemische eigenschappen van B-gedoteerd diamant beschreven. Het laatste deel van dit hoofdstuk focust op de oppervlaktechemie van diamant.

In hoofdstuk 2 wordt een algemene introductie gegeven tot de karakteriseringstechnieken, zoals X-stralen Foto-elektronen Spectroscopie (XPS), Ultraviolet Foto-elektronen Spectroscopie (UPS), Near-Edge X-ray Absorption Fine Structure Spectroscopie (NEXAFS), Cyclische Voltammetrie (CV) en Impedantie Spectroscopie, die gebruikt werden voor dit werk.

In hoofdstuk 3 wordt aangetoond dat N3 dye molecule [*cis*-*bis*(isothiocyanato)-*bis*(2,2'-bipyridyl-4,4'-dicarboxylato)-ruthenium(II)] covalent kan binden op B-gedoteerde dunne diamantfilms door een combinatie van chemische koppelingen, d.w.z. diazonium, Suzuki en EDC-NHS. Spectroscopische technieken zoals XPS, UPS en NEXAFS werden gebruikt om de covalente koppeling van het dye molecule op het B-gedoteerde diamant te verifiëren. Deze spectroscopische resultaten bevestigen de aanwezigheid van een dense N3 chromofoorlaag op het B:NCD oppervlak. Ook de positie van de grensorbitalen ten opzichte van de valentieband van de B:NCD film werd bepaald met behulp van UPS. Foto-elektrochemische metingen toonden een sterke stijging in fotostroom aan in vergelijking met niet-gefunctionaliseerde B:NCD films.

In hoofdstuk 4 werden donor-acceptor type light-harvesting moleculaire draden covalent gebonden op B:NCD oppervlakken met behulp van een combinatie van diazonium elektrografting en Suzuki-koppeling. Om een zo hoog mogelijke opbrengst te behalen voor de Suzuki-koppeling werden verschillende katalytische systemen vergeleken op basis van de behaalde oppervlaktebedekking. Bij een combinatie van 2-dicyclohexylfosfino-2’,6’-dimethoxybifenyl (SPhos) en Pd(0) neemt de bedekking van het diamantword oppervlak aanzienlijk toe (met 98%) in vergelijking met de standaard tetrakis(trifenylfosfine)palladium(0) ($Pd(PPh_3)_4$) katalysator. Uit de UPS metingen volgde dat het niveau van de ‘highest occupied molecular orbital’ (HOMO) overlapt met het maximum van de valentieband van B:NCD. We concluderen hieruit dat de injectie van protonen van de moleculaire draden naar het B:NCD vergemakkelijkt wordt tijdens de foto-excitatie.

In hoofdstuk 5 rapporteren we een eenvoudig protocol voor de covalente functionalisering van BDD elektrodes met enerzijds ferroceen en anderzijds enkelstrengs deoxyribonucleïnezuur (ss-DNA). Een azide-getermineerde organische laag werd eerst gehecht op het diamantoppervlak met behulp van elektrografting door de elektrochemische reductie van 4-azidofenyldiazonium chloride. Het azidofenyl-gemodificeerde oppervlak kan daarna met behulp van de Cu(I)-gekatalyseerde alkyn-azide cycloadditie snel en efficiënt reageren met moleculen die een eindstandige alkyngroep dragen. De covalente binding van ferroceengroepen werd geanalyseerd met behulp van XPS en CV, terwijl het geïmmobiliseerde DNA werd gekarakteriseerd aan de hand van impedantie spectroscopie.

List of Figures

List of Tables

List of Abbreviations and Symbols

A	Adenine
AC	Alternating Current
AEY	Auger Electron Yield
AFM	Atomic Force Microscopy
Al Kα	Aluminium Kα X-ray
Ar	Aryl
B/C	Boron/Carbon Ratio
BDD	Boron-Doped Diamond
B:MCD	Boron-Doped Microcrystalline Diamond
B:NCD	Boron-Doped Nanocrystalline Diamond
Br-BT-Rho	(*Z*)-2-{5-[(5'-bromo-[2,2'-bithiophen]-5-yl)methylene]-4-oxo-2-thioxothiazolidin-3-yl}acetic acid
Br-CPDT-Fur	(*E*)-2-{4-[2-(6-bromo-4,4-diethyl-4*H*-cyclopenta[1,2-*b*:5,4-*b*']dithiophen-2-yl)vinyl]-3-cyano-5,5-dimethylfuran-2(5*H*)-ylidene}malononitrile
4BrPD	4-Bromophenyl Diazonium Salt
t-BuOH	*tert*-butanol
C	Cytosine
C	Capacitance
C_2	Molecular Layer Capacitance
C_3	Space Charge Layer Capacitance
C60	Fullerene-C60
CBM	Conduction Band Minimum
CE	Counter Electrode
CPDT	Cyclopentadithiophene
CuAAC	Copper(I)-Catalyzed Azide-Alkyne Cycloaddition
CV	Cyclic Voltammetry
CVD	Chemical Vapour Deposition
d_C	Molecular Bond Length
DC	Direct Current

DIPEA	*N*,*N*-Diisopropylethylamine
DMF	Dimethylformamide
DMSO	Dimethylsulfoxide
DND	Detonation Nanodiamond
DNA	Deoxyribonucleic Acid
dsDNA	Double-Stranded Deoxyribonucleic Acid
DSSC	Dye-Sensitized Solar Cell
$\mathrm{E_B}$	Binding Energy
$\mathrm{E_{cutoff}}$	Secondary Energy Cutoff
ECR	Electron Cyclotron Resonance
EDC-NHS	1-Ethyl-3-[3-Dimethylaminopropyl]-Carbodiimide-*N*-hydroxysuccinimide
EEDQ	*N*-Ethoxycarbonyl-2-ethoxy-1,2-dihydroquinoline
$\mathrm{E_F}$	Fermi Level
$\mathrm{E_g}$	Bandgap
EIS	Electrochemical Impedance Spectroscopy
$\mathrm{E_{kin}}$	Kinetic Energy of the Emitted Electron
E_{ox}	Oxidation Potential
E_{pa}	Anodic Peak Potential
E_{pc}	Cathodic Peak Potential
E_{red}	Reduction Potential
eV	Electron Volt
$\mathrm{E_{vac}}$	Vacuum Level
EY	Electron Yield
FAM	6-Carboxyfluorescein
2FBB	2-Fluorobiphenyl Boronic Acid
FTO	Fluorine Tin Oxide
FWHM	Full Width Half Maximum
FY	Fluoresce Yield
G	Guanine
He I	Helium 1α Line
He II	Helium ($\mathrm{He^+}$) line
HOMO	Highest Occupied Molecular Orbital
HPHT	High Pressure High Temperature

HPLC	High Pressure Liquid Chromatography
IP	Ionization Potential
ITO	Indium Tin Oxide
K	First electron shell, *K* shell
KE	Kinetic Energy
L	Second electron shell, *L* shell
L-AA	L-Ascorbic Acid
LED	Light Emitting Diode
LUMO	Lowest Unoccupied Molecular Orbital
MCP	Multi-Channeltron Plate
MeCN	Acetonitrile
MeOH	Methanol
Mg Kα	Magnesium Kα Line
ML	Monolayer
m.p.	Melting Point
MV^{2+}	Methyl Viologen
MW	Microwave
MW-PECVD	Microwave Plasma-Enhanced Chemical Vapour Deposition
N3	[*cis*-*bis*(isothiocyanato)-*bis*(2,2'-bipyridyl-4,4'-dicarboxylato)-ruthenium(II)]
NBu_4PF_6	Tetrabutylammonium Hexafluorophosphate
NBS	*N*-bromosuccinimide
NEXAFS	Near Edge X-Ray Absorption Fine Structure
NEA	Negative Electron Affinity
p-NiO	p-Doped Nickel Oxide
NMR	Nuclear Magnetic Resonance
OLED	Organic Light Emitting Diode
PBS	Phosphate Buffered Saline
PCR	Polymerase Chain Reaction
ppm	Parts Per Million
$Pd(dppf)Cl_2$	[1,1′-Bis(diphenylphosphino)ferrocene]dichloropalladium(II)
$Pd(PPh_3)_4$	Tetrakis(triphenylphosphino)palladium(0)
PEA	Positive Electron Affinity
PEY	Partial Electron Yield

P(*o*-tol)$_3$	tri(*o*-tolyl)phosphine
R	Resistance
R_1	Solution Resistance
R_2	Molecular Layer Resistance
R_3	Space Charge Layer Resistance
RCA	Substrate Cleaning Method developed at Radio Corporation of American
RE	Reference Electrode
RF	Radio Frequency
Rs	Sheet Resistance
$Ru(bpy)_3^{2+}$	Tris(bipyridine)ruthenium(II)
$Ru(tpy)_2^{2+}$	Bis(terpyridine)ruthenium (II)
SAM	Self-Assembled Monolayer
SCE	Saturated Calomel Electrode
SEM	Scanning Electron Microscopy
SPhos	2-Dicyclohexylphosphino-2',6'-dimethoxybiphenyl
SSC	Saline Sodium Citrate
ss-DNA	Single-Stranded Deoxyribonucleic Acid
SWCNT	Single Wall Carbon Nanotube
T	Thymine
TAMRA	Carboxytetramethylrhodamine
$TBAPF_6$	Tetrabutylammonium Hexafluorophosphate
TBTA	Tris(benzyltriazolylmethyl)amine
2TC60	Bithiophene-Fullerene
$2T(CN)_2$	Bithiophene-dicyano
TEY	Total Electron Yield
THF	Tetrahydrofuran
u-NCD:H	Hydrogen-Terminated Undoped Nanocrystalline Diamond
u-NCD:O	Oxygen-Terminated Undoped Nanocrystalline Diamond
UNCD	Ultrananocrystalline Diamond
UPS	Ultra-violet Photoelectron Spectroscopy
UV	Ultra-violet
UV-Vis	Ultra-violet Visible
UV-Vis-NIR	Ultra-violet Visible Near Infrared

W	Width
WE	Working Electrode
XPhos	2-Dicyclohexylphosphino-2',4',6'-triisopropylbiphenyl
XPS	X-Ray Photoelectron Spectroscopy
$Y_{imaginary}$	Imaginary Admittance
Y_{real}	Real Admittance
Z	Impedance
Z	Atomic Number
A	Area
ε	Extinction Coefficient
e^-	Electron
E	Voltage
$E°$	Formal Reduction Potential
ΔE_p	Peak Separation
F	Faraday Constant
$h\nu$	Photon
I	Current
i_{pa}	Anodic Peak
i_{pc}	Cathodic Peak
j	$\sqrt{-1}$
λ	Wavelength
n	Number of Electrons
χ	Electron Affinity
μ_e	Chemical Potential
ω	Phase Shift
Φ	Work Function

Chapter 1

Introduction

For most people, diamond is just a well-known gemstone and it is considered as one of many precious possessions. Diamond comes from the Greek word “adamas”, meaning unconquerable. The word diamond presents wealth, status, and prosperity. Natural diamond was first discovered in India in 500 BC. The Chinese were the first to apply diamond for industrial purposes, stemming from its combination of supreme hardness and wear resistance. For scientists, diamond possesses other superior properties - optical, thermal, electrochemical, chemical, and electronic - that outclass competing materials such as silicon and germanium. When these setlines are combined, diamond offers us an engineering material with tremendous potential. It could offer solutions that can shift performance to new levels or enable completely new approaches to solve challenging problems.

The interest in chemical modification of the diamond surface is due to the current trend that is connecting technology to nanotechnology in various fields, which makes surface properties predominating over bulk ones. One of many approaches originating from diamond surface modification involves the construction of hybrid organic diamond devices, based on organic molecules covalently grafted onto a diamond surface, for applications such as solution gate field-effect transistors (“more Moore”), molecular electronics (“beyond Moore”), sensors and micro-electromechanical systems (“more than Moore”). Diamond is generally considered to have a poor reactivity, so its functionalization with organic moieties is still a challenging issue and worthwhile to study.

This chapter first covers some general properties of diamond, classification of diamond, and methods to grow synthetic diamonds. Next, some interesting phenomena arising from diamond surface termination and electrochemical properties of p-type diamond are discussed. Finally, surface and coupling chemistries dedicated to functionalize diamond for its application in diamond-based devices are reviewed and discussed, emphasizing the underlying chemistry.

1.1 General Properties of Diamond

Diamond is one of the allotropes of carbon. It is composed of the single element carbon. The carbon atoms in diamond are arranged in a face-centered cubic structure (diamond lattice). Under standard state conditions, diamond is the second most stable form of carbon after graphite. At normal temperatures and pressures, there is no easy mechanism to convert diamond into graphite due to the large activation barrier for such conversion. However, diamond can be transformed into graphite at temperatures above 1700 °C in vacuum. In air, transformation starts at ~ 700 °C [1].

Unlike graphite sp^2 planar structure, the diamond structural network is formed by sp^3-hybridized carbon atoms, with each carbon atom is covalently bonded to four neighboring carbon atoms in a tetrahedral coordination. This gives diamond a lattice constant of a = 3.567 Å and the distance between the nearest carbon atoms is 1.545 Å. The basic structure can be viewed as two carbon atoms commonly placed at positions [0, 0, 0] and [¼, ¼, ¼] of the cubic unit cell, as shown in Figure 1.1. The strong covalent binding and inflexible three dimensional network present in the diamond lattice give diamond an extraordinary hardness with Young's modulus of 4.4×10^{11} Nm^{-2}, which is about four times harder than Si (0.98×10^{11} Nm^{-2}) [2]. Diamond is the hardest natural material according to Mohs scale [3].

Diamond is a wide band gap material [4, 5] with a band gap of 5.47 eV. Undoped diamond is an electrical insulator with a resistivity in the order of 10^{20} Ohm. However, similar to other Group 14 materials, diamond can be made conductive by doping. In order to increase its electrical conductivity, diamond can be doped with boron at certain concentrations during the synthetic growing process to transform it into a p-type semiconductor. At low doping levels, the diamond acts as an extrinsic semiconductor. At high doping levels, diamond with metallic-like conductivity can be obtained. Typical and useful boron concentrations in diamond are between 500 ppm to about 10, 000 ppm [6]. The boron atoms are single substitutionally inserted into the diamond lattice to replace carbon atoms. These boron atoms function as electron acceptors and contribute to the formation of free-charge carriers, i.e. holes [7].

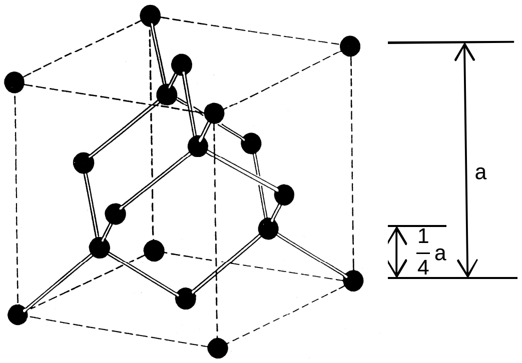

Figure 1.1 Schematic diagram of a diamond unit cell.

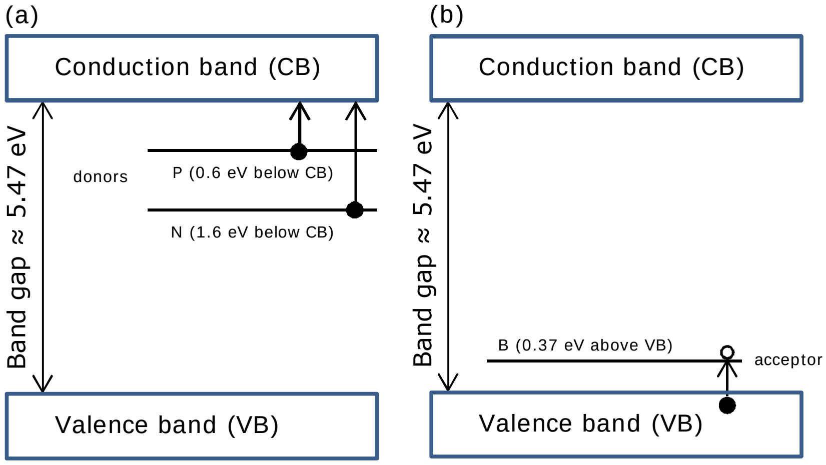

Figure 1.2 Band diagram for (a) n-type diamond and (b) p-type diamond.

Like boron doping, nitrogen [8] or phosphorus [9] doping increases diamond's conductivity this time by turning it into an n-type semiconductor. Here, the nitrogen or phosphorus atoms function as electron donors and the free-charge carriers are free electrons. Band diagrams for p-type and n-type semiconductor diamond are illustrated in Figure 1.2.

1.2 Diamond Classification

In this section, the classification of diamonds is first done by the type and the concentration of impurities. The second classification is based on crystallinity, which is derived from the crystallite size in polycrystalline diamonds.

1.2.1 Classification by Impurities

This classification is based principally on the optical absorption of nitrogen, boron, and hydrogen-related defects [10].

- Type Ia: Most natural diamonds are of this type. The nitrogen impurities are present in type Ia diamond as non-paramagnetic aggregates. The typical nitrogen concentration in natural type Ia diamond is between 500 to 3000 ppm.

- Type Ib: Most synthetic nitrogen-containing diamonds are of this type. The nitrogen impurities are present in type Ib diamond as paramagnetic single substitutional nitrogen atoms. The typical nitrogen concentration in synthetic type Ib diamond is between 10^{18} to 10^{19} atoms cm^{-3}.

- Type IIa: Very rare in nature, these diamonds contain very little nitrogen (< 5 ppm). Type IIa diamonds are the most optically transparent diamonds. This diamond does not show any specific IR optical absorption related to boron and hydrogen impurities in the one-phonon region. The electrical conductivity of type IIa diamond is 10^{16} Ω.cm. High-quality CVD diamond films always fall into this category.

- Type IIb: Extremely rare in nature. These diamonds have a very low concentration of nitrogen (even lower than type IIa). Type IIb diamond shows optical absorption due to boron impurities. It is a p-type semiconductor due to the uncompensated boron acceptor impurities. Synthetic type IIb diamonds can be doped with boron up to 10^{21} atoms cm^{-3}. Most of the works in this thesis used the heavily boron-doped synthetic diamonds.

1.2.2 Polycrystalline Diamond

Diamond on the one hand, can be a single continuous crystal (single crystal) or it can composed of many smaller crystals (polycrystal). Polycrystalline diamond consists of a large number of single crystal diamonds (grains), held together by thin layers of amorphous solid called the grain boundaries [11]. The grain boundaries induce disorder, hence influencing the polycrystalline diamond properties significantly. For instance, polycrystalline diamond has a lower chemical stability compared to single crystal diamond due to the presence of these grain boundaries, as they contain sp^2 carbon, which in most cases is more reactive than sp^3 carbon.

Depending on the growth parameters such as the gas mixture, temperature and substrate seeding, CVD growth can produce microcrystalline, nanocrystalline, and ultrananocrystalline diamond.

When the average grain size of polycrystalline diamond exceeds the value of 500 nm, it is classified as microcrystalline diamond (MCD) [12]. The grain boundaries and crystal defects in MCD have shown to reduce electron and holes mobilities and degrade the electronic performance of MCD [13]. Therefore, only limited success has been reported using MCD in the production of electronic devices. Figure 1.3 shows a SEM image of a MCD sample.

When the average grain size of polycrystalline diamond is less than 500 nm, it falls into the class of nanocrystalline diamond (NCD) [14]. Diamond films with the smallest grains are called ultrananocrystalline diamond (UNCD) [15]. UNCD has a typical grain size below 10 nm. Figure 1.4 displays SEM images of (a) a 150 nm thick B:NCD thin film and (b) a 100 nm thick UNCD thin film. NCD has been shown to function as an excellent electrode for electrochemical applications due to its large electrochemical potential window and low background current [16, 17].

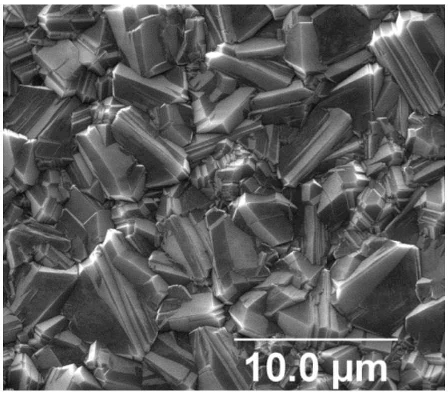

Figure 1.3 SEM image of a boron-doped MCD film grown at IMO.

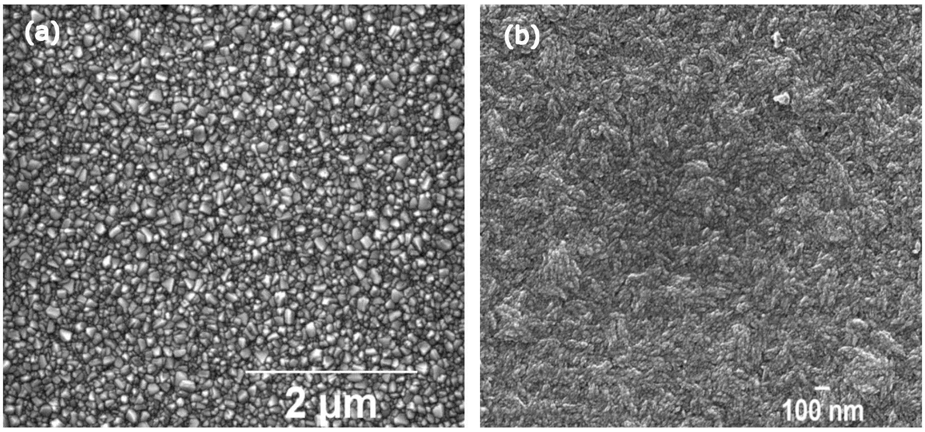

Figure 1.4 Typical SEM images of (a) B:NCD and (b) UNCD films.

1.3 Growth of Doped Diamond

Due to its high cost, natural diamond is seldomly used in research. Instead, synthetic diamond is widely used because of its low cost and reproducible properties. Undoped diamond, due to its large bandgap (> 5 eV), is electrically insulating and cannot be used as an electrode material. Nevertheless, like some other wide band gap materials, diamond can be made conductive by doping it with certain elements during its growth. Currently, in most cases boron is used as a dopant, resulting in p-type semiconducting properties. This section briefly discusses two methods used to produce synthetic boron-doped diamond.

1.3.1 High Pressure and High Temperature (HPHT)

Natural diamond is believed to form at depths of around 200 km in the earth's mantle. This corresponds to pressures and temperatures of 7–8 GPa and 1400–1600 °C, respectively [18]. In contrast to natural genesis, the first industrialized HPHT method used a pressure of 5 GPa and a temperature of 1500 °C to produce synthetic diamond [19]. As shown in Figure 1.5, HPHT diamond is produced in the thermodynamically stable regime from a locally carbon-rich melt. A catalytic amount of a solvent metal, such as Fe, Co or Ni, was found to be essential for a practical process [20]. Most HPHT diamonds produced by this method lead to small crystals of type Ib and are used in grinding and other abrasive applications. The production of p-type diamond particles by the HPHT method has also been reported [21, 22]. The major drawback of the HPHT method is that it can only produce very small single crystal diamond, ranging in the size from nanometers to millimeters, which limits its applications.

1.3.2 Chemical Vapor Deposition (CVD)

Currently most of the boron-doped diamond electrodes in use are produced by the CVD method [23]. Figure 1.5 shows a region where diamond can be produced via the CVD method. In this region, diamond films can be deposited on substrates at lower pressures (10 mtorr to 769 torr) and at lower temperatures (~700 °C to 1200 °C). In the early stages of research concerning CVD diamond films, the major focus was on the formation of the diamond film itself. Although diamond films could be formed, they were of little technological or commercial importance due to several drawbacks such as extremely low growth rate, lack of substrate selectivity, and the formation of graphite. Not until 1982, a major breakthrough in diamond CVD technology was made by the use of a hot filament [24]. Since then, various gas phase activation methods such as direct current (DC)-plasma [25], radio frequency (RF)-plasma [26], microwave (MW)-plasma

[27], electron cyclotron resonance (ECR)-microwave plasma [28], and so on, were developed.

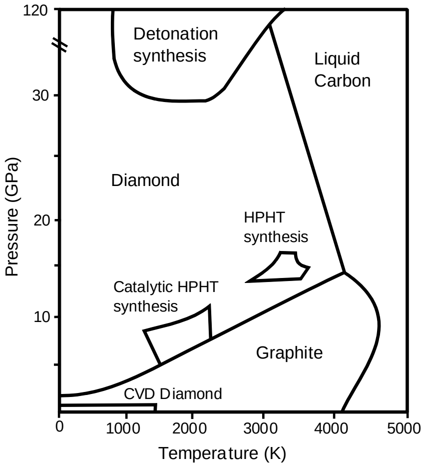

Figure 1.5 Phase diagram for carbon, indicating the main regions of pressure–temperature space in which diamond growth occurs (after [23].)

In general, most CVD techniques can be classified into two groups: hot filament assisted CVD and plasma-assisted CVD. This means that the gaseous source needed for the deposition is activated either thermally [6, 29, 30] or by plasma radiation [31–33]. In both cases, the gas phase (about 10 to 50 mbar) typically consists of hydrogen as the carrier gas and methane (0.5–3% CH_4 in H_2) [32] or an acetone/methane mixture [34] as the carbon source. To introduce boron into the diamond lattice during the film growth, a boron containing substance is added to the deposition gas mixture. Two commonly used boron precursors are diborane (B_2H_6) [34] and trimethyl borane ($B(CH_3)_3$) [32]. This gaseous source is first activated thermally or by plasma. Molecular hydrogen is then dissociated into atomic hydrogen. Atomic hydrogen subsequently reacts with hydrocarbon species [35]. The reacted hydrocarbon species then form hydrocarbon radical species. The flow of molecular hydrogen and hydrocarbon radicals to the surface of already existing diamond seed initiates the diamond growth. Due to the presence of atomic hydrogen during the deposition, graphite is etched away simultaneously, which in turn lead to higher diamond growth rates. The diamond seed which is used to initiate the growth is either a natural diamond, or a HPHT diamond, or diamond nanoparticles produced by detonation synthesis.

As mentioned earlier, before diamond deposition the substrate has to be pre-treated properly [34]. One pre-treatment step is the activation of the substrate with nanoscale diamond particles. This is, however, not the case if the substrate itself is a HPHT or natural single crystal diamond. The nanoscale diamond crystallites act as the nucleation sites for the growth of the thin diamond film during the CVD process. With such pre-treatment, nucleation densities are enhanced to more than 10^{11} cm^{-2} [10]. This surface activation step or seeding-pretreatment can be done in several ways such as (i) scratching the substrate surface with diamond powders (10 nm – 10 μm), (ii) immersing the substrate into a slurry of micron-size diamond powders accompanied by ultrasonication, or (iii) immersing the substrate into a seeding suspension made of detonation nanodiamond powders [32]. At IMO, method (iii) is used frequently.

The substrate temperature during diamond film production is usually maintained at about 700 to 900 °C but temperature as low as 250 °C have also been reported using pulsed linear antenna microwave plasma systems [36]. Typical growth rates are between 0.2 to 0.3 µm/h [32]. Various sizes and thicknesses of diamond films can be deposited. Substrates used to deposit p-doped diamond films are usually either p-doped silicon (both single-crystalline or polycrystalline) or self-passivating metals such as titanium, tantalum, tungsten, molybdenum, and niobium [33]. The use of silicon as a substrate leads to a more perfect pore-free film. Free-standing p-doped diamond films can also be produced by first depositing a relatively thick conductive diamond film on silicon or other substrates and subsequent removal of the substrate, e.g. by chemical etching. The production of single-crystalline doped diamond by CVD is also possible. To do this, a natural or HPHT single crystal diamond is used as a substrate for the CVD thin film deposition [37].

The boron-doped nanocrystalline diamond thin films used in Chapter 3 and 4 in this thesis were grown on fused-silica substrates [38] to meet their final applications. In order to grow a uniform diamond layer, the fused silica is first seeded with detonation nanodiamond particles to increase the nucleation densities [39], as discussed earlier.

1.4 Electrochemical Properties of Boron-Doped Diamond Electrodes

Currently, boron-doped diamond (BDD) electrodes receive much attention [40a]. Electrochemists are fascinated by BDD electrodes as they show a number of outstanding electrochemical properties compared to either conventional carbon based electrodes such as glassy carbon, pyrolytic graphite, and carbon paste or metal electrodes such as platinum and gold [40b]. BDD electrodes have: (i) low capacitance and low background current in aqueous and non-aqueous media, which are desirable for a material to be used as electrode in electroanalytical and sensor applications [40-42]; (ii) very high overpotentials for both oxygen and hydrogen evolution giving rise to a very wide potential range in aqueous media in which the rate of water electrolysis is negligible [43]. This is interesting because within the potential window of water stability, other electrochemical reactions could be observed, which are important for sensor applications; (iii) high stability even at high temperatures and current densities (0.1–10 Acm^{-2}), enabling operation under harsh experimental conditions such as in 85% H_3PO_4 solution [44]; (iv) long term response stability; (v) high sensitivity, rapidity, and selectivity to determine several redox species concurrently in aqueous or non-aqueous solutions without any pretreatment, resulting in direct electrochemical detection and eliminating mediated reagents [45, 46]; (vi) weak adsorption of polar molecules, resulting in improved resistance to electrode deactivation and fouling; (vii) high transparency even when doped, permitting its use as a transparent electrode for spectroelectrochemical measurements [47].

There are several factors affecting the electrochemical response of BDD electrodes such as the doping level, the presence of non-diamond carbon impurities, and the surface chemistry. In order to have sufficient electrical conductivity for electrochemical measurements (< 0.1 Ωcm^{-1}), the boron dopant concentration within diamond films should be maintained at 1 X 10^{19} atoms cm^{-3} or greater [40]. Also it was found that electrochemical reaction rates are higher at the (111) face compared to the (110) face and lowest at the (100) face. This is because the (111) face can incorporate more boron and hence approaches metallic behavior [40]. Rectifying effects are observed in moderately doped diamond but not in heavily doped diamond. Moderately doped diamond is a p-type semiconductor and its anodic current is found to increase with increasing positive overpotential. A hole accumulation region is formed in moderately doped diamond at a potential more positive than its flatband potential [48]. At positive overpotential (rectifying effect), the behavior of a semiconductor electrode is similar to that of a metallic electrode because there is an excess of charge carriers available for charge transfer. On the other hand, heavily doped diamond shows metallic behavior rather than rectifying. This is because at a high level of doping, the Fermi level lies within the valence band and narrows the depletion region. This allows the positive holes in the valence band to tunnel into the electrolyte [48].

The presence of graphitic impurities (sp^2-carbon) was reported to narrow the potential window of water decomposition. These non-diamond carbon impurities were found to shunt the currents that passed through the electrode and short-circuited the electrochemical process that occurred on the diamond electrode [41]. In contrast, several groups reported that sp^2-carbon forms more active sites at diamond surfaces and can cause certain electrochemical reactions to be more active and reversible [49–51]. Thus, leaving the question of stability open, we may still conclude that the non-diamond impurities in BDD could favor electrode electroactivity to some extent.

Surface cleanliness greatly influences the electrode’s response as adsorbed contaminants can either block the active sites of the electrode, thus inhibiting surface-sensitive redox reactions, or increase the electron tunneling distance for redox species, thereby decreasing the rate of electron transfer. Because BDD is grown in a hydrogen-rich atmosphere, as-grown diamond surfaces are hydrogen-terminated. This leads the diamonds to be hydrogen-terminated, and therefore hydrophobic and with a low surface energy. As a result, the hydrogen-terminated BDD surface is inert and not as susceptible to contamination as other carbon electrodes are. The hydrogen-terminated surface of BDD can be easily restored by rehydrogenation in hydrogen microwave plasma after the diamond electrodes are cleaned thoroughly with chemical treatment in *aqua regia* (HNO_3 + 3HCl)) and piranha solution (H_2O_2 + $3H_2SO_4$) [52].

1.5 Diamond Surface Properties

Due to its large bandgap, the conduction band minimum of diamond is close to the vacuum level. This fundamental aspect makes diamond having some unique surface properties that govern subsequent reaction mechanisms of diamond surface functionalization.

1.5.1 Negative Electron Affinity (NEA)

The electron affinity χ of a semiconductor material is defined as the energy gained when an additional electron is brought out of the vacuum into the conduction band minimum (CBM). Thus, it is identical to the energy difference between the vacuum level (E_{vac}) and the CBM of the semiconductor. Most materials usually exhibit positive electron affinity (PEA) which implies that these materials have their CBM below E_{vac}. On the other hand, wide bandgap materials such as diamond have its CBM close to E_{vac} which can potentially lead to NEA. There are two types of NEA: true NEA and effective NEA, and Bell has clearly differentiated between them [53]. Figure 1.6a shows the diagram of true NEA. As E_{vac} is lying below the CBM at the surface, electrons that are excited to the conduction band can be thermalized down to the CBM at the surface and have enough energy to escape to the vacuum. Figure 1.6b shows the diagram of effective NEA. In this case, E_{vac} is located above the CBM at the surface but below the CBM in the bulk. As such, electrons which thermalize to the surface CBM will remain bound to the solid and only those electrons that tunnel ballistically across the depletion region from the bulk CBM to the surface can have enough energy to escape to the vacuum.

True NEA was first reported on a H-terminated diamond (111) surface by Himpsel et al. [54] and on a (100) surface by Van der Weide et al. [55] When a diamond surface is hydrogen-terminated, the C-H bonds at the terminal surface create a surface dipole layer that lowers the electron affinity, which can indeed lead to a negative value as low as -1.3 eV [56]. On the contrary, the H-free clean diamond surface and the O-terminated diamond surface show PEA. The oxygen termination increases the electron affinity due to the large electronegativity of oxygen. Moreover, one can change the NEA on diamond to PEA and vice versa by changing the surface dipole or by depositing electropositive metallic layers onto the diamond surface [57]. Maier et al. [57a] reported that when H-terminated and O-terminated diamond were slowly annealed in vacuum, the electron affinity changed from -1.3 eV to +0.5 eV and from +1.7 eV to +0.5 eV, respectively. Also, when a thin layer of titanium [58] or lithium [59] was covered on O-terminated diamond, NEA was observed.

Besides surface dipoles, there are other factors affecting the NEA. For example, Diederich et al. [60] reported no NEA effect was observed on an N-doped hydrogenated (100) diamond surface due to the strong upward band bending.

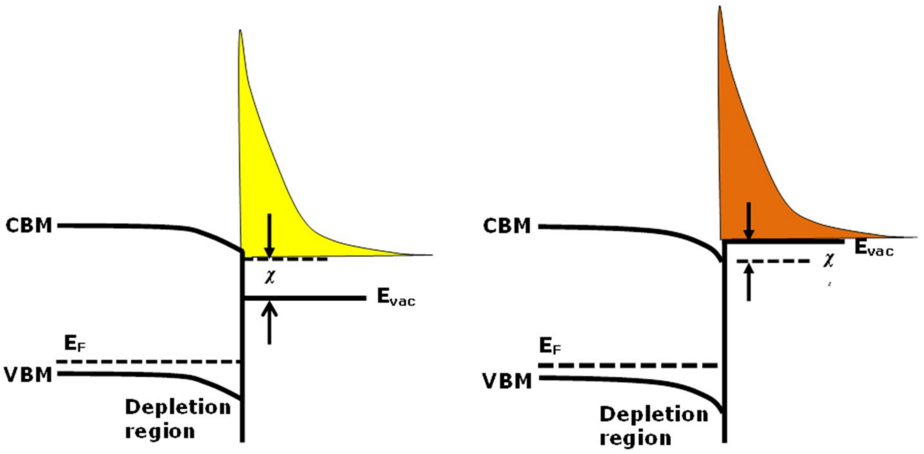

(a) (b)

Figure 1.6 Band diagrams showing (a) true NEA and (b) effective NEA of p-type diamond. (CBM= conduction band minimum; VBM= valence band maximum).

Furthermore, Diels-Alder cycloaddition reactions of unsaturated organic molecules on H-free clean diamond have shown to lower the electron affinity of diamond. Hossain et al. [61] and Wang et al. [62] were among the first few groups that investigated the chemisorption of 1,3-butadiene on H-free clean diamond C(100) 2 x 1 by Diels-Alder [4+2] cycloadditions. However, at that time, focus was mainly put on showing the possibility of using Diels-Alder reactions to chemically functionalize the diamond surfaces. The effect produced by this adsorbed hydrocarbon on the electron affinity was not documented. Not until 2006, Ouyang et al. reported the observed lowering of diamond electron affinity through [2+2] cycloaddition of acetylene and [4+2] cycloaddition of 1,3-butadiene on H-free clean diamond [63]. The adsorbed molecules were found to play the same role as surface hydrogen in inducing NEA conditions on the H-free clean diamond. Figure 1.7 shows the [4+2] cycloaddition reaction for 1,3-butadiene (a) and [2+2] cycloaddition for acetylene (b) on H-free clean diamond C(100) 2 x 1 surfaces.

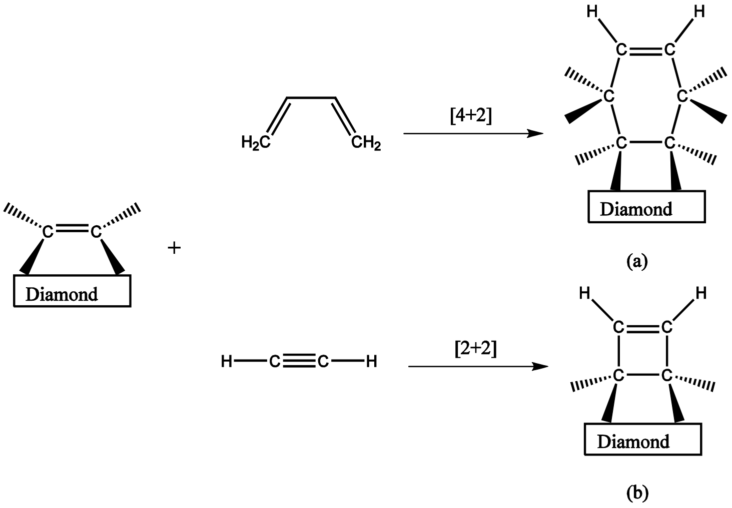

Figure 1.7 [4+2] Cycloaddition reaction for 1,3-butadiene (a) and [2+2] cycloaddition for acetylene (b) on H-free clean diamond C(100) 2 x 1 surfaces [63].

However, the authors also found that the change in electron affinity does not scale linearly with the coverage of the organic molecules [63]. As explained by the authors, this is because the predominant effects on the change of surface charge density are on the spatial profile of the C-H dipoles as well as the orientation of the molecules on the surface [64]. The NEA and low ionization potential of H-terminated diamond surfaces are found to be unique and interesting for certain applications.

1.5.2 Surface Transfer Doping

Undoped diamond with its large bandgap of 5.47 eV is undoubtedly an insulator. However, in 1989, Ravi and Landstrass observed p-type surface conductivity on H-terminated undoped diamond when exposed to air [65]. Subsequent research, initially by Ri et al. [66–68], started to disclose the reasons behind the conductivity. Ri showed that the conductivity increased with exposure to a Lewis acidic gas such as NO_2, but decreased in the presence of a Lewis basic gas such as NH_3 [66, 67] and the sheet concentration of holes was as high as 7×10^{13} cm^{-2} [67]. Ri proposed that this phenomenon was due to the holes arising from the oxidation of the terminal hydrogen atoms by the hydronium ions, H_3O^+ [68]. Ri's explanation was among the several that were put forward to explain the surface conductivity, including the presence of acceptor sites arising from subsurface hydrogen [65].

In 2000, Maier et al. [69] showed that H-termination is not the only required condition for the observed surface conductivity on undoped diamond and they proposed a more convincing p-type surface transfer doping mechanism based on atmospheric surface acceptors in the surface wetting layer.

When diamond is terminated with hydrogen, the C-H bonds at the terminated surface create a dipole layer that not only induces NEA but also a concurrent lowering of the ionization energy to 4.2 eV [56]. When this happens, it facilitates electron transfer from the valence band into an appropriate adsorbed layer on diamond. The hydrogen termination passivates the surface by removing interfering surface states from the gap that would otherwise accept the transferred charge [69]. This creates a subsurface hole accumulation layer that extends a few nanometers into the diamond surface and a corresponding upward band bending. The transfer doping proceeds until the Fermi level of diamond equilibrates with the chemical potential (μ_e) of the surface acceptors [68, 69]. Figure 1.8 shows the accumulation of holes and band bending at the surface of hydrogen-terminated diamond occuring as a consequence of charge transfer into an adsorbed water layer when exposed to air.

Strobel et al. showed that p-type surface doping could also be achieved with fullerene (C_{60}) and its fluorinated derivatives [70, 71]. In this case, charge is transferred from the diamond valence band into the lowest unoccupied molecular orbital (LUMO) of the fullerene which acts as a surface acceptor. Despite providing further supporting evidence for the surface transfer doping mechanism as being responsible for the charge accumulation at the surface of diamond, their work has also shown for the first time the possibility of using other molecular species beside water molecules as surface acceptors on the hydrogenated diamond surface.

Later, surface transfer doping of diamond with other molecular species such as 7,7,8,8-tetracyanoquinodimethane and its fluorinated derivatives [72], and molecular heterolayers have also been demonstrated [73]. Very recently, Russell et al. [74a] and Tordjman et al. [74b] extended this work to include the use of the transition metal oxide MoO_3 as a surface electron acceptor material, which may offer improved stability and performance in diamond devices. Even though the use of organic acceptors to induce surface conductivity in diamond is still in its early stage, there is considerable potential to create new functional devices based on this type of platform.

The surface conductivity in diamond induced by transfer doping has been applied in metal-semiconductor field-effect transistors [75, 76], solution-gate field-effect transistors [77], ion-sensitive field-effect transistors [78], etc. The application of diamond surface conductivity to diamond electronic devices is still an ongoing and active research field and one can expect this trend to continue in the future.

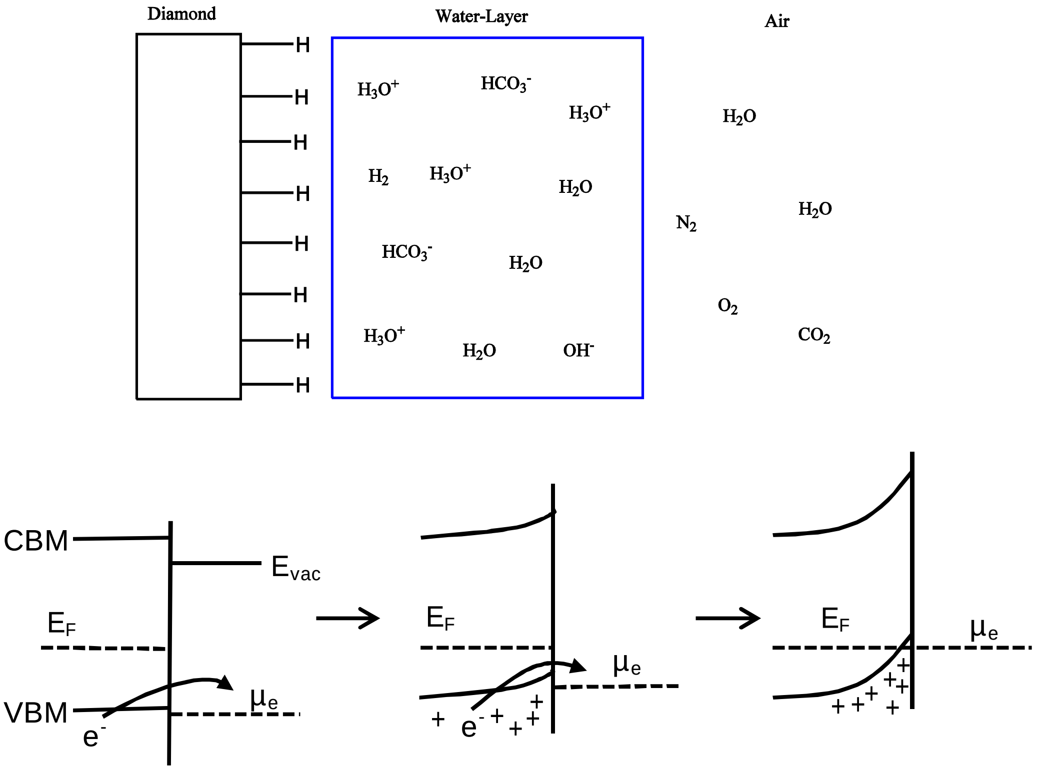

Figure 1.8 Schematic picture of the hydrogenated diamond surface in contact with a water layer as it forms in air. Bottom: Evolution of band bending during the electron transfer process at the interface between diamond and the water layer [68].

1.6 Surface Chemistry of Diamond

Chemically modified solid surfaces with (bio)molecules have recently become an immensely attractive subject due to their potential applications as molecular components in electronic and photonic devices. For molecular photovoltaic and biosensing applications, functionalization of the electrode surface is usually needed, and that is where suitable chemical reactions have to be performed on the electrode surface. Diamond is a particularly attractive electrode material for its outstanding properties. It is chemically stable, with a surface that can be modified with various chemical routes in order to achieve a surface termination toward highest possible performance. There are many different functionalization strategies for diamond surfaces that have been developed over the years and have been reviewed by Szunerits and Boukherroub [79], Stutzman et al. [80], Nebel et al. [81], and Zhong et al. [82]. In almost all cases, the diamonds are first functionalized with linker molecules. This can be done via UV photochemical and aryldiazonium salt reduction reactions on hydrogen-terminated surfaces or silanization and esterification on oxygen-terminated surfaces. Covalent attachment of various functional molecules to the linker molecules can then be carried out using proper coupling chemistries such as EDC-NHS, Cu(I)-catalyzed azide-alkyne cycloaddition click reactions, Suzuki coupling, etc. In this section, aryldiazonium grafting, surface Suzuki coupling, and surface Cu(I)-catalyzed azide-alkyne cycloaddition click reaction will be further discussed as these three methods are used to attach functional molecules on diamond in this thesis.

1.6.1 Reduction of Aryldiazonium Salts

The interface between a grafted organic layer and an electrode is usually the weakest link in a molecular device. A dense organic film interface will prevent hydrolysis or oxidative cleavage of the interfacial bonds due to infiltration of water or oxygen. In this case, aryldiazonium grafting [82] has advantages over the UV photochemical grafting of diamond with terminal alkenes [79]. The presence of π-π stacking in aryl compounds offers denser packing of the monolayer compared to an alkyl monolayer. Moreover, the delocalized electrons in aryl linkers might afford a greater efficiency in charge transfer compared to alkyl linkers, which is important if diamond is to be used as electrode in organic electronics.

The electrochemical reduction of aryldiazonium cations at a BDD electrode to form a covalently modified surface was first reported by Kuo et al. [83] in 1999 and was recently reviewed [84-86]. This method is popular because diazonium reagents with a wide range of functional groups (carboxylic, bromo, nitro, etc.) are commercially available and can be introduced onto the electrode surface in one step. Moreover, diazonium salts can be easily prepared from aromatic amines, widening their application scope. Two unique characteristics of aryldiazonium cations are the strong electron withdrawing effect of the N_2^+ group and the high stability of the dinitrogen leaving group (evolution of N_2 gas) [85]. The formation of C-C bonds between BDD surfaces and phenyl radicals generated by diazonium reduction is shown in Figure 1.9. It is clear that the electroreduction of aryldiazonium cations proceeds through a concerted mechanism. One equivalent of an electrogenerated radical is required to abstract a hydrogen atom from the H-terminated BDD surface. After that, a second radical can couple with the surface radical to form the final C-C bond [86].

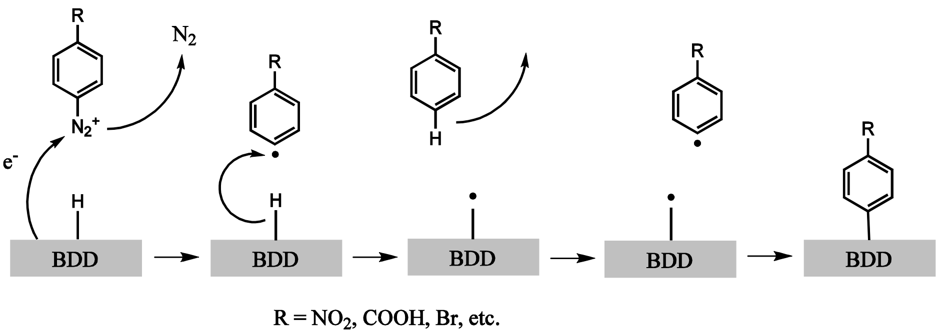

Figure 1.9 Electrografting of organic layers through reduction of aryldiazonium cations.

Diazonium grafting has two specific features that make it particularly attractive for surface modification [86]. Since the reactive radical is made electrochemically, it is generated precisely where it is most likely to react with the electrode surface [86]. Moreover, the C-C bond that is formed between the phenyl radical and the electrode surface is strong.

Whilst the electrochemical aryldiazonium reduction method is a convienient way for the derivatization of diamond surfaces, precise control to limit the reaction to a monolayer, is however, not a straightforward task. The formation of multilayers is possible due to the aggressive reactions of electrogenerated radicals [87, 88]. A radical generated at an unmodified electrode surface can attack an adjacent surface of bound molecules instead of the electrode surface itself [86]. Monolayer formation can only be achieved through careful control of the grafting parameters such as the charge consumed during the electrografting process and the concentration of aryldiazonium salts [84]. For instance, Nebel and coworkers compared the electrografted organic layer of 4-nitrobenzene on diamond using cyclic voltammetry and constant potential attachment with AFM measurements [89]. They found that the cyclic voltammetry attachment formed a thick organic layer of up to 80 Å. On the contrary, by employing the constant potential attachment, the organic layer that formed was denser and only 25 Å thick. Besides, the reactivity of the aryldiazonium salts controls the extent of the reaction. The presence of a strong electron-withdrawing group activates the N_2^+ leaving group. As an example, a monolayer of 4-bromobenzene can be achieved by the constant potential method, but the same conditions produce a 25 Å thick layer of 4-nitrobenzene [89].

One more possible way to overcome the problem of multilayer formation using the electrochemical grafting process is the use of spontaneous grafting (chemical grafting), as shown first by Lud et al. [90] and further confirmed by Zhong et al. [91]. Zhong made a comparison of 4-nitrobenzene layers grafted on diamond by cyclic voltammetry, constant potential, and spontaneous grafting. They found that the spontaneous grafting method resulted in a self-limiting monolayer formation. More significantly, they also found that the spontaneous grafting method is applicable to undoped H-terminated diamond, but not to undoped oxygenated diamond. They claimed that the reaction on undoped H-terminated diamond could occur possibly due to the spontaneous electron transfer from the H-terminated diamond to the aryldiazonium cation, which is facilitated by the NEA of H-terminated diamond, as shown in Figure 1.10. This spontaneous grafting is attractive as it does not require expensive electrochemical equipment or doped diamond films.

The principle interest in diamond diazonium coupling is that the diamond-tethered functional groups can be used for the covalent linking of various (bio)molecules. In this thesis, we showed that we are able to functionalize 4-bromophenyl, 4-aminophenyl boronic esters, and 4-azidophenyl groups on B:NCD surfaces with aryldiazonium grafting. The 4-aminophenyl boronic ester layer is particularly important for the covalent coupling of novel donor-acceptor light harvesting molecules to B:NCD via Suzuki coupling. In the same way, Click reactions were demonstrated on 4-azidophenyl-functionalized B:NCD surfaces with a terminal alkyne redox probe and DNA.

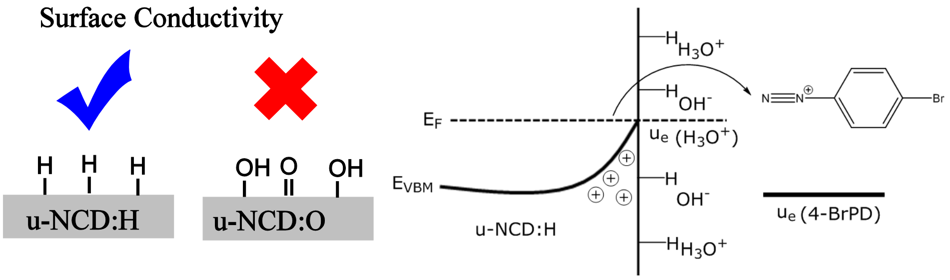

Figure 1.10 Schematic description of spontaneous reduction of 4-bromophenyldiazonium tetrafluoroborate (4BrPD) on undoped H-terminated NCD (u-NCD:H). The reaction is facilitated by a surface conductive layer induced by acidic water (0.1M HCl) [91].

1.6.2 Surface Suzuki Coupling

The Suzuki coupling reaction is a transition metal catalyzed cross coupling between aryl halides and aryl boronic acids to form biaryls. The most common catalyst used is a palladium complex. This reaction has emerged as an extremely powerful tool in organic synthesis for C-C coupling [92]. This Pd-catalyzed cross-coupling reaction has been applied for the preparation of a huge variety of conjugated aromatic compounds, for example to be used for organic light-emitting diodes (OLEDs) [93], polymer LEDs [94], organic photovoltaics [95], and nonlinear optical materials [96]. The first application of the Suzuki cross-coupling on a solid surface was by Cheng and Adronov [96]. In 2006, they used iodophenyl pre-functionalized single-walled carbon nanotubes (SWCNTs) as synthons for Suzuki coupling. They successfully functionalized these SWCNTs with porphyrins, fluorene, and bithiophene. Subsequently, in 2008, Loh and coworkers at the National University of Singapore published a paper that demonstrated the Suzuki coupling on diamond [91]. The authors investigated the optimal conditions for the generation of bromophenyl and arylboronic ester functional groups on a diamond surface, to be used as a solid platform for surface Suzuki cross-coupling to the respective arylboronic ester and bromobenzene. They showed that 2-fluorobiphenyl boronic acid (2FBB) can be coupled to the bromophenyl functionalized surface with a high coupling yield (of 87%) by monitoring the bromine and fluorine markers from XPS. Also, from AFM measurements, they found that the thickness of the 2FBB adlayer on single crystal diamond agrees well with the height of the grafted 2FBB molecules, suggesting that surface Suzuki coupling eliminates any possible multilayer film formation and proving that the Suzuki coupled mesogenic molecules are standing upright on the diamond surface [91].

The practical application of this versatile surface Suzuki coupling was further demonstrated by the same group in their subsequent paper with the coupling of various conjugated “donor-acceptor” molecular dyes on arylboronic ester-functionalized diamond surfaces [98], as shown in Figure 1.11. They found that the interface between diamond and the coupled molecules is highly stable, as evident from the higher photostability exhibited for the dye-coupled diamond compared to the dye coupled to conventional transparent conductive oxide electrodes such as indium tin oxide (ITO) and fluorine-doped tin oxide (FTO).

In the same way, Suzuki coupling of pyrene-boronic acid to bromophenyl-functionalized detonation nanodiamond (DND) was demonstrated [99]. The pyrene-functionalized DND show a fluorescent effect under UV light. Despite showing all the advantages of surface Suzuki coupling, some aspects such as variations in apparent surface coverage and optimum conditions were not properly addressed. For example, the authors claimed that 2FBB can be coupled to bromophenyl-functionalized diamond with 87% yield. However, the reported surface coverage of 2-(dicyanovinyl)-5-iodobithiophene was as low as 0.41 monolayer, relative to a high quality reference monolayer of dodecanethiol on gold, as determined by XPS.

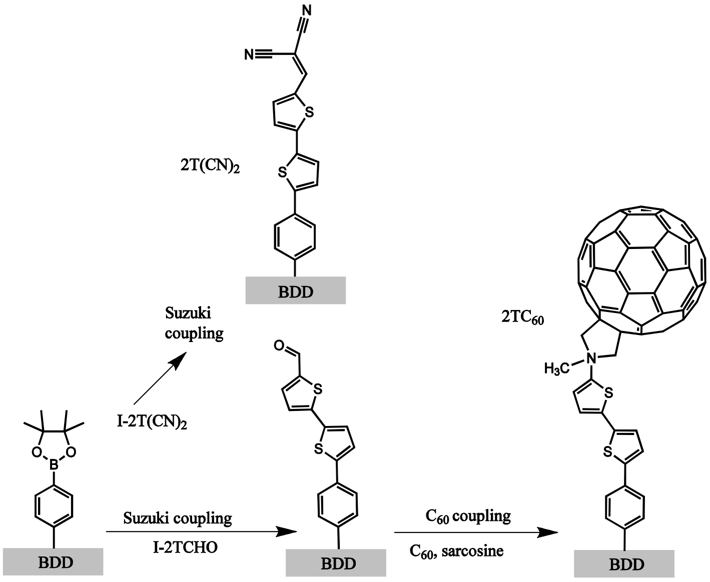

Figure 1.11 Schematic drawing of surface functionalization of arylboronic ester-functionalized diamond with bithiophene-C60 (2TC60) and bithiophene-dicyano (2T(CN)$_2$) on a BDD thin film [97].

As the selection of an efficient catalytic system is of great importance in transition metal catalyzed cross-couplings [92], in this thesis work, we have investigated the optimum conditions for Suzuki coupling reactions to achieve high coupling yield.

1.6.3 Surface Cu(I)-Catalyzed Azide-Alkyne Cycloaddition (CuAAC) Click Reaction

According to Sharpless' definition, click reactions are characterized by high yields, mild reaction conditions, and tolerance to a broad range of functional groups [100]. Click chemistry is not limited to a specific type of reaction, but comprises a range of reactions, with different reaction mechanisms yet common reaction paths. The copper(I)-catalyzed Huisgen 1,3-dipolar cycloaddition of azides and terminal alkynes (CuAAC) is arguably the most prominent example of a click reaction [101]. This heterogenous coupling strategy was found to be fast, reproducible, with a minimum of side reactions, and highly tolerant to diverse reaction conditions. This reaction is catalyzed by Cu(I) and an organic azide and a terminal alkyne are united to afford 1,4-regioisomers of 1,2,3-triazoles as the sole products as shown in Figure 1.12. Due to the orthogonal nature of the CuAAC reaction, it holds great promise for surface immobilization of complex molecules in their unprotected and functional form. The CuAAC reaction has already been tested on various surfaces such as polystyrene, polyethylene, glass, silica (gels), gold, etc. [102]. Virtually any material to which an alkyne or azide can be attached, can be functionalized by CuAAC. For example, Arnold et al. recently demonstrated the clicking of 5-azidofluorescein to 4-(trimethylsilyl) ethynylstyrene polymer brushes that were grown on a silicon surface [103]. Grabosch et al. presented a 'dual click' strategy for the fabrication of bioselective glycosylated self-assembled monolayers as glycocalyx models [104].

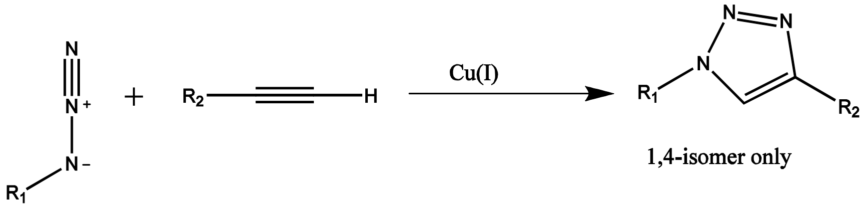

Figure 1.12 Schematic diagram showing the CuAAC reaction.

Szunerits and her colleagues published a series of papers that demonstrated the CuAAC reaction on either polycrystalline diamond or on DND. Among the molecules they have attached are ferrocene [105], carbohydrates [106], thiophene [107], decyne and pyrene [108]. They showed that their click reaction provides a rather mild surface immobilization with excellent coupling yields, versatility, regioselectivity, functional group tolerance, and stability of the catalytic process in different solvents. In one particular paper, Szunerits and coworkers “clicked” an alkynl-terminated BDD surfaces with azide-terminated mono- and disaccharides by a CuAAC reaction using $CuSO_4$/sodium ascorbate for the construction of a glycan-modified diamond. The measurement of the affinity of the sugar to different lectins could be followed by impedance spectroscopy [106].

Electrocatalytic active molecules that are tethered on conductive substrates offer highly efficient conversion of electrical energy to chemical energy, high stability, and low catalyst loadings. Metalloporphyrins containing earth-abundant metals such as cobalt are of particular interest for CO_2 reduction, and Hamers and coworkers have demonstrated the functionalization of a BDD surfaces with a cobalt(II) porphyrin via surface CuAAC reaction for CO_2 reduction studies [109]. The BDD surface was functionalized with azide groups and then the cobalt(II) porphyrin complexes bearing four alkyne groups were “clicked” to the azide-functionalized BDD surface via a CuAAC reaction using $Cu(BF_4)_2$/DIPEA, as shown in Figure 1.13. The catalyst-modified BDD was used as “smart” electrode for the electrochemical reduction of CO_2 to CO in acetonitrile solution. Besides showing good electrocatalytic activity, the modified BDD electrode exhibited good stability owing to the extremely stable surface-immobilized catalytic system.

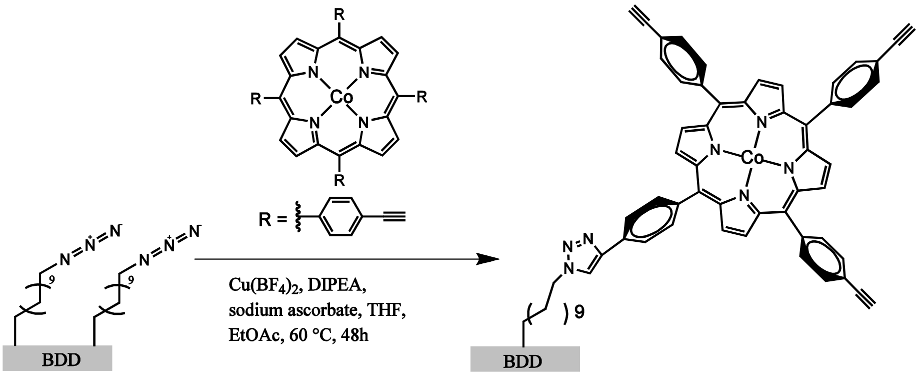

Figure 1.13 Attachment of a cobalt porphyrin onto an azide-functionalized diamond surface by a CuAAC reaction [109].

Another interesting report by Meinhardt et al. [110] describes an elegant double-functionalization of DND. An Oregon-Green dye and a TAMRA dye were functionalized onto the same DND surfaces. sp^2-graphitized DND was first functionalized with alkyne and carboxylic groups using a mixture of the respective anilines via diazonium coupling. Next, the Oregon-Green dye bearing an amino functional group was coupled to the carboxylic acid group using the zero-length cross linker EEDQ (*N*-ethoxycarbonyl-2-ethoxy-1,2-dihydroquinoline). Finally, the second dye TAMRA bearing an azide functional group, was “clicked” to the alkyne group on the DND surface. This functionality is not affected by the first functionalization due to its orthogonal nature (Figure 1.14). This procedure, as claimed by the authors, produces a multifunctional surface on DND.

In Chapter 5, we report on a straightforward protocol for the covalent functionalization of BDD with either ferrocene or single-stranded deoxyribonucleic acid (ss-DNA). An azide-terminated organic layer is first electrografted on the diamond surface by electrochemical reduction of 4-azidophenyldiazonium chloride. The azidophenyl-modified surface then reacts rapidly and efficiently with ferrocene and ss-DNA bearing a terminal alkyne moiety by means of a CuAAC reaction.

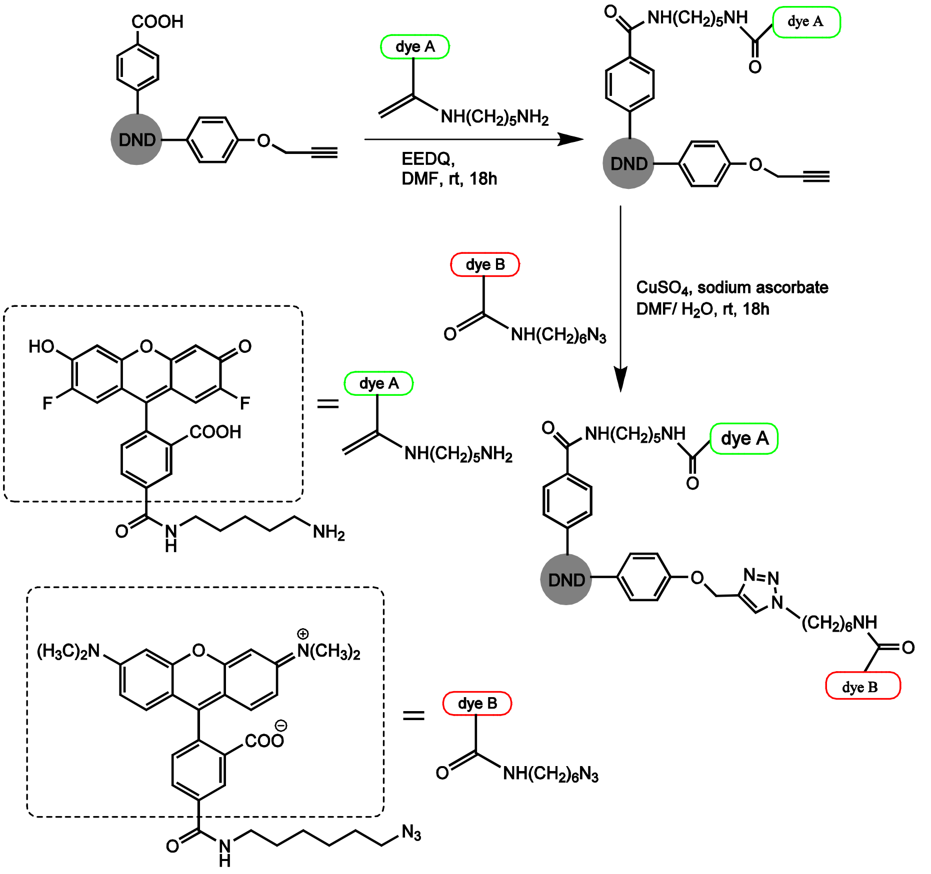

Figure 1.14 Orthogonal functionalization of DND with alkyne and COOH groups enables the specific grafting of two dyes with different terminal groups [110].

1.7 Scope of This Study

In this thesis work, several methods were applied to functionalize diamond with a view toward its application in the area of photoelectrochemistry and biosensing. Various surface and spectroscopic techniques were employed to characterize the functionalized diamond surfaces. The underlying theory of various techniques used will be discussed in Chapter 2. Detailed introduction, experimental setups and results of the different topics will be given in chapter 3, chapter 4 and chapter 5, respectively.

1.8 References

1. John, P.; Polwart, N.; Troupe, C. E.; Wilson, J. I. B., The Oxidation of (100) Textured Diamond. *Diam. Relat. Mater.* **2002**, *11*, 861.

2. Field, J. E. *Science of Hard Materials*; Adam Hilger Ltd: England; **1986**; pp 181-183.

3. *Mohs Scale of Mineral Hardness*, American Federation of Mineralogical Societies.

4. van der Weide, J.; Zhang, Z.; Baumann, P. K.; Wensel, M. G.; Berholc, J.; Nemanich, R. J., Negative-Electron-Affinity Effects on the Diamond (100) Surface. *Phys. Rev. B* **1994**, *50*, 5803.

5. Roberts, R. A.; Walker, W. C., Optical Study of the Electronic Structure of Diamond. *Phys. Rev.* **1967**, *161*, 730.

6. Fryda, M.; Matthée, Th.; Mulcahy, S.; Hampel, A.; Schäfer, L.; Tröster, I., Fabrication and Application of Diachem^R Electrodes. *Diam. Relat. Mater.* **2003**, *12,* 1950.

7. Mamin, R. F.; Inushima, T., Conductivity in Boron-Doped Diamond. *Phys. Rev. B* **2001**, *63*, 033201.

8. Nesladek, M., Conventional n-Type Doping in Diamond: State of the Art and Recent Progress. *Semicond. Technol.* **2005**, *20*, R19.

9. (a) Kalish, R., Doping of Diamond. *Carbon* **1999**, 37, 781; (b) Janssen, W.; Turner, S.; Sakr, G.; Jomard, F.; Barjon, J.; Degutis, G.; Lu, Y.-G.; D'Haen, J.; Hardy, A.; Bael, M. V.; Verbeeck, J.; Tendeloo, G. V.; Haenen, K., Substitutional Phosphorus Incorporation in Nanocrystalline CVD Diamond Thin Films. *Phys. Status Solidi RRL*, **2014**, *8*, 705.

10. Zaitsev, A. M., Optical Properties of Diamond: A Data Handbook; Springer: USA, **2010**.

11. Eto, H.; Tamou, Y.; Ohsawa, Y.; Kikuchi, N., TEM Observations of Diamond Films Prepared by Microwave Plasma CVD. *Diam. Relat. Mater.* **1992**, *1*, 373.

12. Lu, C.; Tian, S. B.; Gu, C. Z.; Li, J. J., Grain Boundary Effect on the Superconducting Transition of Microcrystalline Boron-Doped diamond Films. *Diam. Relat. Mater*. **2011**, *20*, 217.

13. Janssens, S. D. Morphological and Electronic Properties of Strongly Boron-Doped Diamond Films Prepared by Chemical Vapor Deposition. Ph.D. Thesis, Hasselt University, June **2011**.

14. Williams, O. A.; Daenen, M.; D'Haen, J.; Haenen, K.; Maes, J.; V.V. Moshchalkov, V. V.,Nesladek, M; Gruen, D. M., Comparison of The Growth and Properties of Ultrananocrystalline Diamond and Nanocrystalline Diamond. *Diam. Relat. Mater*. **2006**, *15*, 654.

15. (a) Saravanan, A,; Huang, B.; Sangkaran, J. K.; Kunuku, S.; Dong, C.; Leou, K.; Tai, N.; Lin, I., Bias-Enhanced Nucleation and Growth Processes for Ultrananocrystalline Diamond Films in Ar/CH_4 Plasma and Their Enhanced Plasma Illumination Properties. *ACS Apply. Mater. Interfaces* **2014**, *6*, 10566; (b) Asmussen, J.; Grotjohn, T. A.; Schuelke, T., Advances in Plasma Synthesis of UNCD Films. In *Ultrananocrystalline Diamond. Synthesis, Properties, and Application of UNCD*; Shenderova, O.; Gruen, D., Eds.; Elsevier: Amsterdam, **2012**; pp 53-83.

16. Show, Y.; Witek, M. A.; Sonthalia, P.; Swain, G. M., Characterization and Electrochemical Responsiveness of Boron-Doped Nanocrystalline Diamond Thin-Film Electrodes. *Chem. Mater.* **2003**, *15*, 879.

17. Chen, Q.; Gruen, D. M.; Krauss, A. R.; Corrigon, T. D.; Witek, M.; Swain, G. M., The Structure and Electrochemical Behavior of Nitrogen-Containing Nanocrystalline Diamond Films Deposited from CH_4/N_2/Ar Mixtures. *J. Electrochem. Soc.* **2001**, *148*, E44.

18. Finnerty, A. A.; Boyd, F. R., Evaluation of Thermobarometers for Garnet Peridotites. *Geochim. Cosmochim. Acta* **1984**, *48*, 15.

19. Bundy, F. P.; Hall, H. T.; Strong, H. M.; Wentorf Jun, R. H., Man-Made Diamonds. *Nature* **1955**, *176,* 51.

20. Bundy, F. P., Direct Conversion of Graphite to Diamond in Static Pressure Apparatus. *J. Chem. Phys.* **1963**, *38*, 631.

21. Dubrovinskaia, N.; Dubrovinsky, L.; Miyajima, N.; Langenhorst, F.; Crichton, W. A.; Braun, H. F., High-pressure/High-temperature Synthesis and Characterization of Boron-doped Diamond. *Z. Naturforsh* **2006**, *61b*, 1561.

22. Zhang, H.; Zang, C.; Li, X.; Ma, H.; Li, S.; Zhou, S.; Guo, W.; Jia, X., HPHT Synthesis of Micron Grade Boron-Doped Diamond Single Crystal in Fe-Ni-C-B Systems. *Chin. Phys. Lett.* **2008**, *25*, 2667.

23. Balmer, R. S.; Brandon, J. R.; Clewes, S. L.; Dhillon, H. K.; Dodson, J. M.; Friel, I.; Inglis, P. N.; Madgwick, T. D.; Markham, M. L.; Mollart, T. P.; Perkins, N.; Scarsbrook, G. A.; Twitchen, D. J.; Whitehead, A. J.; Wilman, J. J.; Woollard, S. M., Chemical Vapour Deposition Synthetic Diamond: Materials, Technology and Applications. *J. Phys. Condens. Matter* **2009**, *21*, 364221.

24. Matsumoto, S.; Sato, Y.; Kamo, M.; Setaka, N., Vapor Deposition of Diamond Particles from Methane. *Jpn. J. Appl. Phys*. **1982**, *21*, L183.

25. Lee, J.; Baik, Y.; Eun, K. Y.; Park, J., Properties of Diamond Films Deposited by Multi-Cathode Direct Current Plasma Assisted CVD Method. *Diam. Relat. Mater*. **2001**, *10*, 552.

26. Meyer, D. E.; Dillon, R. O.; Woollam, J. A., Radio-Frequency Plasma Chemical Vapor Deposition Growth of Diamond. *J. Vac. Sci. Technol. A* **1987**, *7*, 2325.

27. (a) Lee, J.; Hong, B.; Collins, R. W., Nucleation and Bulk Film Growth Kinetics of Nanocrystalline Diamond Prepared by Microwave Plasma-Enhanced Chemical Vapor Deposition on Silicon Substrates. *Appl. Phys. Lett*. **1996**, *69*, 12, 1716; (b) Zhou, D.; McCauley, T. G.; Gruen, D. M., Synthesis of Nanocrystalline

Diamond Thin Films From An Ar-CH_4 Microwave Plasma. *J. Appl. Phys.* **1998**, *83*, 540; (c) Ye, H.; Sun, C. Q.; Wei, J., Nucleation and Growth Dynamics of Diamond Films by Microwave Plasma-Enhanced Chemical Vapor Deposition (MPECVD). *Surf. Coat. Tech.* **2000**, *123*, 129.

28. Chiang, M. J.; Lung, B. H.; Hon, M. H., Low-Pressure Deposition of Diamond by Electron Cyclotron Resonance Microwave Plasma Chemical Vapor Deposition. *J. Cryst. Growth* **2000**, *211*, 216.

29. Haubner, R.; Lux, B., Diamond Growth by Hot-Filament Chemical Vapor Deposition: State of the Art. *Diam. Relat. Mater.* **1993**, *2,* 1277.

30. Schäfer, L.; Höfer, M.; Kröger, R., The Versatility of Hot-Filament Activated Chemical Vapor Deposition. *Thin Solid Films* **2006**, *515,* 1017.

31. Williams, O. A.; Nesladek, M.; Daenen, M.; Michaelson, S.; Hoffman, A.; Osawa, E.; Haenen, K.; Jackman, R. B., Growth, Electronic Properties and Applications of Nanodiamond. *Diam. Relat. Mater.* **2008**, *17,* 1080.

32. Janssens, S. D.; Pobedinskas, P.; Vacik, J.; Petrakova, V.; Ruttens, B.; D'Haen, J.; Nesladek, M.; Haenen, K.; Wagner, P. Separation of Intra- and Intergranular Magnetotransport Properties in Nanocrystalline Diamond Films on The Metallic Side of The Metal-Insulator Transition. *New J. Phys.* **2011**, *13*, 083008.

33. Williams, O.; Nesladek, M.; Mares, J. J.; Hubik, P. Growth and Properties of Nanocrystalline Diamond Films. In: *Physics and Applications of CVD Diamond*; Koizumi, S.; Nebel, C.; Nesladek, M., Eds.; Wiley-VCH: Weinheim, Germany, **2008**; pp 13-27.

34. Ramamurti, R.; Becker, M.; Schuelke, T.; Grotjohn, T.; Reinhard, D.; Swain, G.; Asmussen, J., Boron Doped Diamond Deposited by Microwave Plasma-Assisted CVD at Low and High Pressures. *Diam. Relat. Mater.* **2008**, *17,* 481.

35. Butler, J. E.; Woodin, R. L., Thin Film Diamond Growth Mechanisms. *Phil. Trans. R. Soc. A* **1993**, *342*, 209.

36. Izak, T.; Babchenko, O.; Varga, M.; Potocky, S.; Kromka, A., Low Temperature Diamond Growth by Linear Antenna Plasma CVD Over Large Area. *Phys. Status Solidi B* **2012**, *249*, 2600.

37. Achard, J.; Issaoui, R.; Tallaire, A.; Silva, F.; Barjon, J.; Jomard, F.; Gicquel, A., Freestanding CVD Boron Doped Diamond Single Crystals: A Substrate for Vertical Power Electronic Devices. *Phys. Status Solidi A* **2012**, *209*, 1651.

38. Daenen, M.; Williams, O. A.; D'Haen, J.; Haenen, K.; Nesládek, M., Seeding, Growth and Characterization of Nanocrystalline Diamond Films on Various Substrates. *Phys. Status Solidi A* **2006**, *203*, 3005.

39. Williams, O. A.; Douhéret, O.; Daenen, M.; Haenen, K.; Ōsawa, E.; Takahashi, M., Enhanced Diamond Nucleation on Monodispersed Nanocrystalline Diamond. *Chem. Phys. Lett.* **2007**, *445*, 255.

40. (a) Macpherson, J. V., A Practical Guide to Using Boron Doped Diamond in Electrochemical Research. *Phys. Chem. Chem. Phys.* **2014**, DOI: 10.1039/C4CP04022H, (b) Fujishima, A.; Einaga, Y.; Rao, T. N.; Tryk, D. A., Fundamental and Applied Aspects of Diamond Electrodes. In *Diamond Electrochemistry*; Fujishima, A.; Einaga, Y.; Rao, T. N.; Tryk, D. A., Eds.; Elsevier: Amsterdam, **2005**; pp 556-574.

41. Swain, G. M., Ramesham, R., The Electrochemical Activity of Boron-Doped Polycrystalline Diamond Thin Film Electrodes. *Anal Chem.* **1993**, *65*, 345.

42. Swain, G. M., The Use of CVD Diamond Thin Films in Electrochemical Systems. *Adv. Mater.* **1994**, *6*, 388.

43. Martin, H. B.; Argoitia, A.; Landau, U.; Anderson, A. B.; Angus, J. C., Hydrogen and Oxygen Evolution on Boron-Doped Diamond Electrodes. *J. Electrochem. Soc.* **1996**, *143*, L133.

44. Goeting, C. H.; Jones, F.; Foord, J. S.; Eklund, J. C.; Marken, F.; Compton, R. G.; Chalker, P. R.; Johnston, C., Electrochemistry at Boron-Doped Diamond Films Grown on Graphite Substrates: Redox-, Adsorption and Deposition Processes. *J. Electroanal. Chem.* **1998**, *442*, 207.

45. Suzuki, A,; Ivandini, T. A.; Kamiya, A.; Nomura, S.; Yamanuki, M.; Matsumoto, K.; Fujishima, A.; Einaga, Y., Direct Electrochemical Detection of Sodium Azide in Physiological Saline Buffers Using Highly Boron-Doped Diamond Electrodes. *Sensor Actuat. B-CHEM*. **2007**, *120*, 500.

46. Pop, A.; Manea, F.; Radovan, C.; Dascalu, D.; Vaszilcsin, N.; Schoonman, J., Non-Enzymatic Electrochemical Detection of Glycerol on Boron-Doped Diamond Electrode. *Analyst* **2012**, *137*, 641.

47. Hupert, M.; Muck, A.; Wang, J.; Stotter, J.; Cvackova, Z.; Haymond, S.; Show, Y.; Swain, G. M., Conductive Diamond Thin-Films in Electrochemistry. *Diam. Relat. Mater.* **2003**, 12, 1940.

48. Zhang, Z.; Yates, J. T., Band Bending in Semiconductors: Chemical and Physical Consequences at Surfaces and Interfaces. *Chem. Rev*. **2012**, *112*, 5520.

49. Mahé, E.; Devilliers, D.; Comninellis, C., Electrochemical Reactivity at Graphitic Micro-Domains on Polycrystalline Boron Doped Diamond Thin-Films Electrodes. *Electrochim. Acta* **2005**, *50*, 2263.

50. Duo, I.; Fujishima, A.; Comninellis, C., Electron Transfer Kinetics on Composite Diamond (sp^3)-graphite (sp^2) Electrodes. *Electrochim. Commun*. **2003**, *5*, 695.

51. Reuben, C.; Galun, E.; Cohen, H.; Tenne, R.; Kalish, R.; Muraki, Y.; Hashimoto, H.; Fujishima, A.; Butler, J. F.; Levy-Clement, C., Efficient Reduction of Nitrite and Nitrate to Ammonia Using Thin-Film B-Doped Diamond Electrodes. *J. Electroanal. Chem*. **1995**, *396*, 233.

52. Granger, M. C.; Witek, M.; Xu, J.; Wang, J.; Hupert, M.; Hanks, A.; Koppang, M.; Butler, J. E.; Lucazeau, G.; Mermoux, M.; Strojek, J. W.; Swain, G. M., Standard Electrochemical Behavior of High-Quality, Boron-Doped Polycrystalline Diamond Thin-Film Electrodes. *Anal. Chem.* **2000**, 72, 3793.

53. Bell, R. L., Negative Electron Affinity Devices; Clarendon Press: Oxford, **1973**; pp 1-145.

54. Himpsel, F. J.; Knapp, J. A.; VanVechten, J. A.; Eastmann, D. E., Quantum Photoyield of Diamond (111)—A Stable Negative-Affinity Emitter. *Phys. Rev. B* **1979**, *20*, 624.

55. Van der Weide, J.; Zhang, Z.; Baumann, P. K.; Wensell, M. G.; Bernholc, J.; Nemanich, R. J., Negative-Electron-Affinity Effects on the Diamond (100) Surface. *Phys. Rev. B* **1994**, *50*, 5803.

56. Cui, J. B.; Ristein, J.; Ley, L., Electron Affinity of the Bare and Hydrogen Covered Single Crystal Diamond (111) Surface. *Phys. Rev. Lett.* **1998**, *81*, 429.

57. (a) Maier, F.; Ristein, J.; Ley, L., Electron Affinity of Plasma-Hydrogenated and Chemically Oxidized Diamond (100) Surfaces. *Phys. Rev. B* **2001**, *64*, 165411; (b) Nemanich, R. J.; Baumann, P. K.; Benjamin, M. C.; King, S. W.; Van der Weide, J.; Davis, R. F., Negative Electron Affinity Surfaces of Aluminum Nitride and Diamond. *Diam. Relat. Mater.* **1996**, *5*, 790; (c) Diederich, L.; Küttel, O. M.; Aebi, P.; Maillard-Schaller, E.; Fasel, R.; Schlapbach, L. Photoelectron Emission from the Negative Electron Affinity Caesiated Natural Diamond (100) surface. *Diam. Relat. Mater.* **1998**, *7*, 660; (d) Loh, K. P.; Egdell, R. G.; Jackman, R. B.; Foord, J. S. Tuning The Electron Affinity of CVD Diamond with Adsorbed Caesium and Oxygen Layers. *Diam. Relat. Mater.* **1997**, *6*, 874; (e) Foord, J. S.; Goeting, C. H., Electrochemically Controlled Modification of CVD Diamond Surfaces. *Diam. Relat. Mater.* **2004**, *13*, 1054.

58. Van der Weide, J.; Nemanich, R. J., Schottky Barrier Height and Negative Electron Affinity of Titanium on (111) Diamond. *J. Vac. Sci. Technol. B* **1992**, *10*, 1940.

59. O’ Donnell, K.; Edmunds, M.; Ristein, J.; Tadich, A.; Thomsen, L.; Wu, Q.; Pakes, C. I.; Ley, L., Diamond Surfaces with Air-Stable Negative Electron Affinity and Giant Electron Yield Enhancement. *Adv. Funct. Mater.* **2013**, *23*, 5608.

60. Diederich, L.; Küttel, O. M.; Aebi, P.; Schlapbach, L., Electron Affinity and Work Function of Differently Oriented and Doped Diamond Surfaces Determined by Photoelectron Spectroscopy. *Surf. Sci.* **1998**, *418*, 219.

61. Hossain, M. Z.; Aruga, T.; Takagi, N.; Tsuno, T.; Fujimori, N.; Ando, T.; Nishijima, M., Diels-Alder Reaction on the Clean Diamond (100) 2×1 Surface. *Jpn. J. Appl. Phys.* **1999**, *38*, L1496.

62. Wang, G. T.; Bent, S. F.; Russell, J. N.; Butler, J. E.; D'Evelyn, M. P., Functionalization of Diamond(100) by Diels−Alder Chemistry. *J. Am. Chem. Soc.* **2000**, *122*, 744.

63. Ouyang, T.; Gao, X.; Qi, D.; Wee, A. T. S.; Loh, K. P., Cycloadditions on Diamond (100) 2 × 1: Observation of Lowered Electron Affinity due to Hydrocarbon Adsorption. *J. Phys. Chem. B,* **2006**, *110*, 5611.

64. Hoh, H. Y., Loh, K. P., Sullivan, M. B. and Wu, P., Spatial Effect of C-H Dipoles on the Electron Affinity of Diamond (100)-2×1 Adsorbed with Organic Molecules. *ChemPhysChem*, **2009**, *9*, 1338.

65. (a) Landstrass, M. I.; Ravi, K. V., Resistivity of Chemical Vapor Deposited Diamond Films. *Appl. Phys. Lett.* **1989**, *55*, 975; (b) Landstrass, M. I.; Ravi, K. V., Hydrogen Passivation of Electrically Active Defects in Diamond. *Appl. Phys. Lett.* **1989**, *55*, 1391.

66. Ri, S. G.; Ishikawa, T.; Tanaka, S.; Kimura, T.; Akiba, Y.; Iida, M., Possibility of Realizing a Gas Sensor Using Surface Conductive Layer on Diamond Films. *Jpn. J. Appl. Phys*. **1997**, *36*, 2057.

67. Ri, S. G.; Tashiro, K.; Tanaka, S.; Fujisawa, T.; Kimura, H.; Kurosu, T.; Iida, M., Hall Effect Measurements of Surface Conductive Layer on Undoped Diamond Films in NO_2 and NH_3 Atmospheres. *Jpn. J. Appl. Phys*. **1999**, *38*, 3492.

68. Ri, S. G.; Mizumasa, T.; Akiba, Y.; Hirose, Y.; Kurosu, T.; Iida, M., Formation Mechanism of p-Type Surface Conductive Layer on Deposited Diamond Films. *Jpn. J. Appl. Phys*. **1995**, *34*, 5550.

69. Maier, F.; Reidel, M.; Mantel, B.; Ristein, J.; Ley, L., Origin of Surface Conductivity in Diamond. *Phys. Rev. Lett*. **2000**, *85*, 3472.

70. Strobel, P.; Riedel, M.; Ristein, J.; Ley, L., Surface Transfer Doping of Diamond. *Nature*, **2004**, *430*, 439.

71. Strobel, P.; Riedel, M.; Ristein, J.; Ley, L.; Boltalina, O., Surface Transfer Doping of Diamond by Fullerene. *Diam. Relat. Mater.* **2005**, *14*, 451.

72. Chen, W.; Qi, D.; Gao, X.; Wee, A. T. S., Surface Transfer Doping of Semiconductors. *Prog. Surf. Sci.* **2009**, *84*, 279.

73. Langley, D.; Smets, Y.; Stark, C. B.; Edmonds, M. T.; Tadich, A.; Rietwyk, K. J.; Schenk, A.; Wanke, M.; Wu, Q.; Barnard, P.; Ley, L.; Pakes, P. I., Surface Transfer Doping of Diamond with A Molecular Heterojunction. *Appl. Phys. Lett.* **2012**, *100*, 032103.

74. (a) Russell, S. A. O.; Cao, L.; Qi, D.; Tallaire, A.; Crawford, K. G.; Wee, A. T. S.; Moran, D. A., Surface Transfer Doping of Diamond by MoO_3: A Combined Spectroscopic and Hall Measurement Study. *Appl. Phys. Lett.* **2013**, *103*, 202112; (b) Tordjman, M.; Saguy, C.; Bolker, A.; Kalish, R., Superior Surface Transfer Doping of Diamond with MoO_3. *Adv. Mater. Interfaces* **2014**, *1*, 1300155.

75. Kawarada, H.; Aoki, M.; Itoh, I., Enhancement Mode Metal-Semiconductor Field Effect Transistors Using Homoepitaxial Diamonds. *Appl. Phys. Lett.* **1995**, *65*, 1563.

76. Itoh, H.; Kawarada, H., Fabrication and Characterization of Metal-Semiconductor Field-Effect Transistor Utilizing Diamond Surface-Conductive Layer. *Jpn. J. Appl. Phys.* **1995**, *34*, 4677.

77. Dankerl, M.; Lippert, A.; Birner, S.; Stuetzel, E. U.; Stutzmann, M.; Garrido, J. A., Hydrophobic Interaction and Charge Accumulation at the Diamond-Electrolyte Interface. *Phys. Rev. Lett.* **2011**, *106*, 196103.

78. Kawarada, H.; Araki, Y.; Sakai, T.; Ogawa, T.; Umezawa, H., Electrolyte-Solution-Gate FETs Using Diamond Surface for Biocompatible Ion Sensors. *Phys. Stat. Sol. A* **2001**, *185*, 79.

79. Szunerits, S.; Boukherroub, R., Different Strategies for Functionalization of Diamond Surfaces. *J. Solid State Electrochem.* **2008**, *12*, 1205.

80. Stutzmann, M.; Garrido, J. A.; Eickhoff, M.; Brandt, M. S., Direct Biofunctionalization of Semiconductors: A Survey. *Phys. Stat. Sol. A* **2006**, *203*, 3424.

81. (a) Nebel, C. E., Shin, D.; Rezek, B.; Tokuda, N.; Uetsuka, H.; Watanabe, H., Diamond and Biology. *J. R. Soc., Interface* **2007**, *4*, 439; (b) Nebel, C. E.; Rezek, B.; Shin, D.; Uetsuka, H.; Yang, N., Diamond for Bio-Sensor Applications. *J. Phys. D: Appl. Phys*. **2007**, *40*, 6443.

82. Zhong, Y. L; Loh, K. P., The Chemistry of C-H Bond Activation on Diamond. *Chem. Asian J.* **2010**, *5*, 1532.

83. Kuo, T. C.; McCreery, R. L.; Swain, G. M., Electrochemical Modification of Boron-Doped Chemical Vapor Deposited Diamond Surfaces with Covalently Bonded Monolayers. *Electrochem. Solid-State Lett.* **1999**, *2*, 288.

84. Pinson, J.; Podvorica, F., Attachment of Organic Layers to Conductive or Semiconductive Surfaces by Reduction of Diazonium Salts. *Chem. Soc. Rev*., **2005**, *34*, 429.

85. Belanger, D.; Pinson, J., Electrografting: A Powerful Method for Surface Modification. *Chem. Soc. Rev.* **2011**, *40*, 3995.

86. McCreery, R. L., Advanced Carbon Electrode Materials for Molecular Electrochemistry. *Chem. Soc. Rev*. **2008**, *108*, 2646.

87. Kariuki, J. K.; McDermott, M. T., Formation of Multilayers on Glassy Carbon Electrodes via the Reduction of Diazonium Salts. *Langmuir* **2001**, *17*, 5947.

88. Combellas, C.; Kanoufi, F.; Pinson, J.; Podvorica, F., Time-of-Flight Secondary Ion Mass Spectroscopy Characterization of the Covalent Bonding between a Carbon Surface and Aryl Groups. *Langmuir* **2005**, *21*, 280.

89. Uetsuka, H.; Shin, D.; Tokuda, N.; Saeki, K.; Nebel, C. E., Electrochemical Grafting of Boron-Doped Single-Crystalline Chemical Vapor Deposition Diamond with Nitrophenyl Molecules. *Langmuir* **2007**, *23*, 3466.

90. Lud, S. Q.; Steenackers, M.; Jordan, R.; Bruno, P.; Gruen, D. M.; Feulner, P.; Garrido, J. A.; Stutzmann, M. Chemical Grafting of Biphenyl Self-Assembled Monolayers on Ultrananocrystalline Diamond. *J. Am. Chem. Soc.* **2006**, *128*, 16884.

91. Zhong, Y. L.; Loh, K. P.; Midya, A.; Chen, Z. K., Suzuki Coupling of Aryl Organics on Diamond. *Chem. Mater.* **2008**, *20*, 3137.

92. Miyaura, N.; Suzuki, A., Palladium-Catalyzed Cross-Coupling Reactions of Organoboron Compounds. *Chem. Rev*. **1995**, 95, 2457.

93. Bujak, P.; Kulszewicz-Bajer, I.; Zagorska, M.; Maurel, V.; Wielgus, I.; Pron, A., Polymers for electronics and spintronics. *Chem. Soc. Rev.* **2013**, *42*, 8895.

94. Pron, A.; Gawrys, P.; Zagorska, M.; Djurado, D.; Demadrille, R., Electroactive Materials for Organic Electronics: Preparation, Strategies, Structural Aspects and Characterization Techniques. *Chem. Soc. Rev.* **2010**, *39*, 2577.

95. (a) Bijleveld, J. C.; Shahid, M.; Gilot, J.; Wienk, M. M.; Janssen, R. A. J., Copolymers of Cyclopentadithiophene and Electron-Deficient Aromatic Units Designed for Photovoltaic Applications. *Adv. Funct. Mater.* **2009**, 19, 3262; (b) Watters, D. C.; Yi, H.; Pearson, A. J.; Kingsley, J.; Iraqi, A.; Lidzey, D., Fluorene-Based Co-polymer with High Hole Mobility and Device Performance in Bulk Heterojunction Organic Solar Cells. *Macromol. Rapid Commun*. **2013**, 34, 1157.

96. Wu, W.; Huang, L.; Xiao, L.; Huang, Q.; Tang, R.; Ye, C.; Qin, J.; Li, Z., New Second-Order Nonlinear Optical (NLO) Hyperbranched Polymers Containing Isolation Chromophore Moieties Derived from One-Pot "A(2)+B-4" Approach via Suzuki Coupling Reaction. *RSC Adv.* **2012**, *2*, 6520.

97. Cheng, F.; Adronov, A., Suzuki Coupling Reactions for the Surface Functionalization of Single-Walled Carbon Nanotubes. *Chem. Mater.* **2006**, *18*, 5389.

98. Zhong, Y. L.; Midya, A.; Ng, Z.; Chen, Z.; Daenen, M.; Nesladek, M.; Loh, K. P., Diamond-Based Molecular Platform for Photoelectrochemistry. *J. Am. Chem. Soc.* **2008**, *130*, 17218.

99. Yeap, W. S.; Chen, S.; Loh, K. P., Detonation Nanodiamond: An Organic Platform for the Suzuki Coupling of Organic Molecules. *Langmuir* **2009**, 25, 185.

100. Kolb, H. C.; Finn, M. G.; Sharpless, K. B., Click Chemistry: Diverse Chemical Function from a Few Good Reactions. *Angew. Chem. Int. Ed.* **2001**, *40*, 2004.

101. Lahann. J., Click Chemistry: A Universal Ligation Strategy for Biotechnology and Materials Science. In *Click Chemistry for Biotechnology and Materials Science;* Lahann, J., Eds.; John Wiley & Sons Ltd: West Sussex, **2009**; pp 1-8.

102. Meldal, M.; Tornøe, C. W., Cu-Catalyzed Azide-Alkyne Cycloaddition. *Chem. Rev.* **2008**, *108,* 2952.

103. Arnold, R. M.; Locklin, J., Self-Sorting Click Reactions That Generate Spatially Controlled Chemical Functionality on Surfaces. *Langmuir* **2013**, *29*, 5920.

104. Grabosch, C.; Kind, M.; Gies, Y.; Schweighöfer, F.; Terfort, A.; Lindhorst, T. K., A 'Dual Click' Strategy for the Fabrication of Bioselective, Glycosylated Self-Assembled Monolayers as Glycocalyx Models. *Org. Biomol. Chem.* **2013**, 28, 4006.

105. Das, M. R.; Wang, M.; Szunerits, S.; Gengembre, L.; Boukherroub, R., Clicking Ferrocene Groups to Boron-doped Diamond Electrodes. *Chem. Commun.* **2009**, *19*, 2753.

106. Szunerits, S.; Niedziǒłka-Jönsson, J.; Boukherroub, R.; Woisel, P.; Baumann, J.; Siriwardena, A., Label-Free Detection of Lectins on Carbohydrate-Modified Boron-Doped Diamond Surfaces. *Anal. Chem.*, **2010**, *82*, 8203.

107. Wang, M.; Das, M. R.; Li, M. S.; Boukherroub, R.; Szunerits, S., "Clicking" Thiophene on Diamond Interfaces. Preparation of a Conducting Polythiophene/ Diamond Hybrid Material. *J. Phys. Chem. C* **2009**, *113*, 17082.

108. Barras, A.; Szunerits, S.; Marcon, L.; Monfilliette-Dupont, N.; Boukherroub, R., Functionalization of Diamond Nanoparticles Using “Click” Chemistry. *Langmuir* **2010**, *26*, 13168.

109. Yao, S. A.; Ruther, R. E.; Zhang, L.; Franking, R. A.; Hamers, R. J.; Berry, J. F., Covalent Attachment of Catalyst Molecules to Conductive Diamond: CO_2 Reduction Using “Smart” Electrodes. *J. Am. Chem. Soc.* **2012**, *134*, 15632.

110. Meinhardt, T.; Lang, D.; Dill, H.; Krueger, A., Pushing the Functionality of Diamond Nanoparticles to New Horizons - Orthogonally Functionalized Nanodiamond Using Click Chemistry. *Adv. Funct. Mater.* **2011**, *21*, 494.

Chapter 2

Experimental

2.1 Introduction

This chapter presents the principles of the various surface techniques used for the characterization of the physical and chemical properties of the functionalized boron-doped diamond films. The boron-doped diamonds were derivatized with various functional groups and covalently linked to (bio)molecules. A wide range of analytical techniques were used to analyze the composition of the resulting diamond-(bio)molecule hybrids.

2.2 X-ray Photoelectron Spectroscopy (XPS)

All solid materials interact with their surroundings through their surfaces. The physical and chemical compositions of these surfaces determine the nature of the interactions. Surfaces therefore influence many important properties of the solids. X-ray photoelectron spectroscopy (XPS) (Figure 2.1) has become one of the widely used techniques in the area of surface analysis [1], as it can determine (i) the elemental composition, (ii) the chemical state and chemical empirical formula, and (iii) electronic states of the elements that exists within a material. If the material is present as a thin film at the surface, XPS can measure the thickness and determine how uniform the chemical composition of the thin film is [2]. XPS uses highly focused monochromatic soft X-rays to irradiate the sample surface under ultra-high vacuum conditions (10^{-8} to 10^{-10} mbar). The two commonly used X-ray sources for XPS are Al Kα (1486.6 eV) and Mg Kα (1253.6 eV). These two X-ray sources produce photons with few satellite peaks, resulting in relatively narrow line widths, and consequently better chemical state information [1].

The process of photoemission is shown schematically in Figure 2.2. An X-ray photon is absorbed by an atom on or near the surface, leading to the photoionization and the emission of core shell electrons to the vacuum. Those electrons which are excited and escape without energy loss contribute to the characteristic peaks in the spectrum; those which undergo inelastic scattering and suffer energy loss contribute to the background of the spectrum. Once the photoelectron has been emitted, the ionized atom relaxes either by emission of an X-ray photon, known as X-ray fluorescence or by ejection of an Auger electron [1].

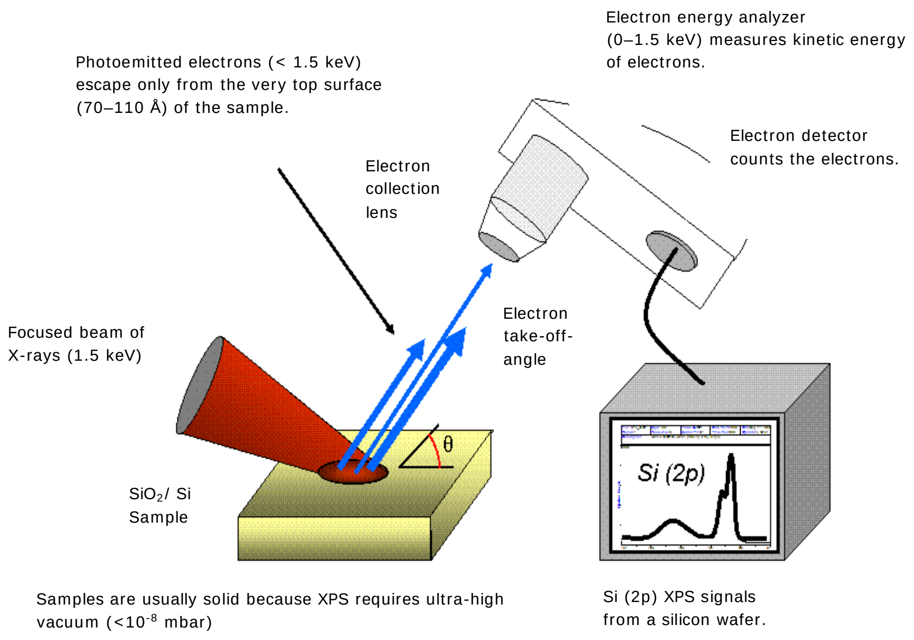

Figure 2.1 Schematic drawing of the basic components of an XPS system [2b].

The kinetic energy of the emitted electron can be measured by using an electron energy analyzer. The binding energy (E_B) is calculated as

$$E_B = h\nu - E_{kin} - \Phi \qquad \text{(Equation 2.1)}$$

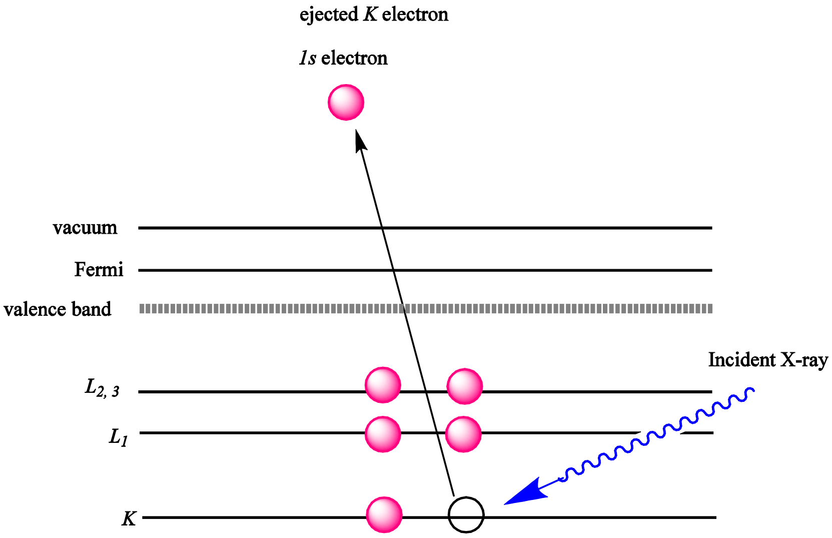

Figure 2.2 Schematic diagram of the XPS process, showing photoionization of an atom followed by ejection of a 1s electron.

where Φ is the work function of the spectrometer, E_B is the binding energy with respect to the Fermi level, and E_{kin} is the kinetic energy of the emitted electron. Each photoexcited atom will exhibit a characteristic binding energy of the core-level electron, and this varies with different chemical environments such as oxidation states and molecular environments. This results in a chemical shift in the spectrum of up to a few eV, providing useful information for the investigation of surface changes before and after modification.

2.3 Ultra-violet Photoelectron Spectroscopy (UPS)

The first ultra-violet photoelectron spectroscopy (UPS) measurements were developed to study the photoelectron spectra of free molecules in the gas phase by Tuner and coworkers in 1964 [3]. Today UPS is regarded as the most powerful and versatile technique to study the electronic structure of the valence bands in solid materials and HOMO levels of molecules [4]. Two sources of photons often used in UPS are He I ($h\nu$ = 21.2 eV) and He II ($h\nu$ = 40.8 eV).

During the UPS experiment, the helium lamp is used to excite electrons from the valence band of the sample. Although valence band structures can also be obtained from XPS studies, UPS has two advantages over XPS in such experiments [5]. First, UPS gives higher photoionization cross-section for electrons in the valence region; second, helium lines give photon sources with higher energy resolution for a full-width of half-maximum (FWHM) of ~30 meV .

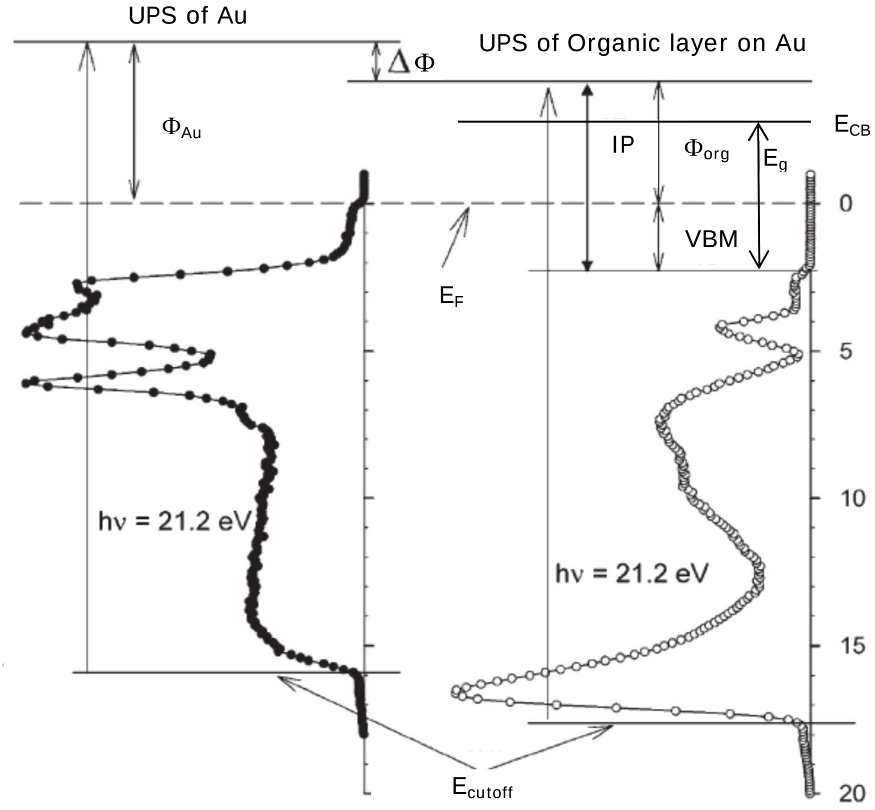

Figure 2.3 Schematic drawing of important parameters from UPS and energy alignment between a gold substrate and its overlying organic layer [5].

As shown in Figure 2.3, UPS spectra can provide valuable information such as:

(i) The work function, Φ, of the sample through the equation:

$$\Phi = h\nu - W \qquad \text{(Equation 2.2)}$$

Where $h\nu$ is the UV light energy and W is the spectrum width, which is the energy difference between the Fermi level, E_F, and the secondary electron cut-off (E_{cutoff}).

(ii) The ionization potential, IP, of the sample through the equation:

$$IP = -VBM + \Phi \qquad \text{(Equation 2.3)}$$

Where VBM is the valence band maximum or HOMO.

(iii) If the bandgap, E_g, of the sample is known, the conduction band minimum (CBM)/ LUMO can be deduced by:

$$CBM = E_g + VBM \qquad \text{(Equation 2.4)}$$

In this thesis work, UPS is used to probe the valence band structures of hydrogen terminated B:NCD and dye-functionalized B:NCD in order to obtain first insights whether dyes-functionalized B:NCD could be employed as a hole conductor in dye-sensitized solar cells.

2.4 Near-Edge X-ray Absorption Fine Structure (NEXAFS) Spectroscopy

With the continuous efforts to improve synchrotron sources throughout the years, today's synchrotron facilities are fully optimized to give a beam of radiation with a small beam cross section and higher degree of collimation using special aid devices called wigglers and undulators [6]. As a result, many synchrotron-based techniques have been developed that allow detailed exploration of the properties of various materials. One of these synchrotron-based techniques is near edge X-ray absorption fine structure (NEXAFS). It was devised in the 1980s, mainly to study the structure of low-Z molecules (molecules that consist of 'light' atoms such as carbon, nitrogen, oxygen, and fluorine) bonded to surfaces [7, 8]. Since then, it has been applied to many other molecules [9] and materials [10-12]. NEXAFS spectroscopy requires a high intensity and tunable monochromatic light source with smooth characteristics within the energy regions of interest. Synchrotron radiation sources are therefore well suited for NEXAFS spectroscopy [13]. NEXAFS spectroscopy is a surface sensitive technique that enables to probe the unoccupied electronic states as well as providing information on chemical and structural properties of adsorbates that are present on a solid surface [14-17].

During a NEXAFS measurement, the sample is irradiated with monochromatic X-rays. The X-ray photon energy is varied around a core-level absorption edge, and the absorbed X-ray intensity is measured by probing the excitation of the core electron to unoccupied states. NEXAFS refers to the absorption fine structure close to an absorption edge, approximately the first 30 eV above the actual edge (e.g. K-edge). This region usually exhibits strong and distinctive features in the X-ray absorption coefficient and is often dominated by intense narrow resonances [13].

NEXAFS measurements proceed via a two-step process. At first the X-ray photon excites a core electron to an unoccupied state, hence leaving a core hole, and in the second step the recombination process of the core hole takes place [13]. There are two main channels for the core-hole to recombine (Figure 2.4): the radiative type, with the emission of photons (fluorescence), or the non-radiative type (Auger-like transitions), with the emission of electrons, which can be collected from the surface with suitable detectors such as a channeltron or energy analyzer [13]. In our experiment, the latter type was measured.

There are two kinds of Auger-like transitions in this case: participator decay, in which the excited electron participates in the core-hole decay process, and spectator decay, in which the excited electron remains in the normally unoccupied level and two valence electrons are removed. The number of generated Auger electrons is directly proportional to the X-ray absorption cross section [7].

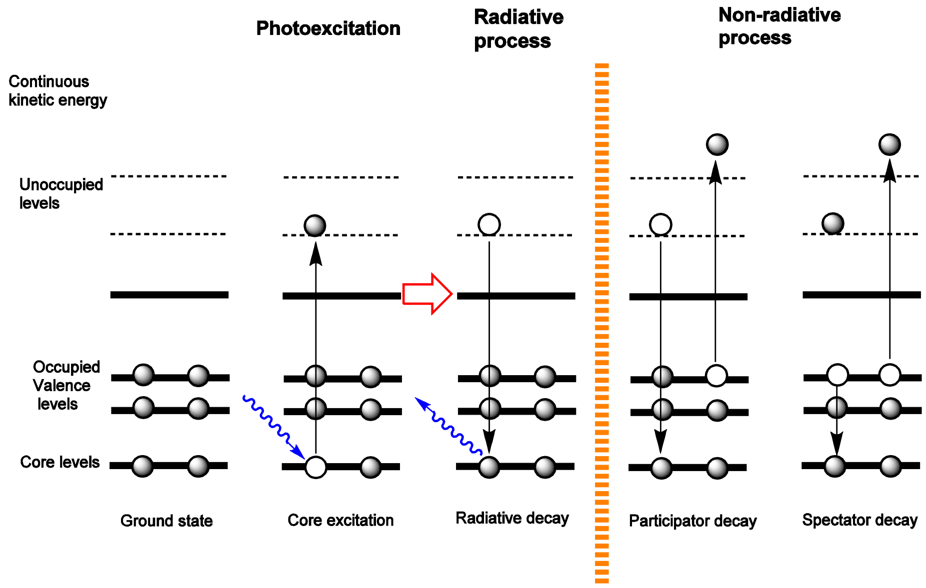

Figure 2.4 Schematic diagram of photoexcitation and recombination processes during a NEXAFS experiment. The photogenerated core hole is filled by an electron from a higher shell, either radiatively by emission of a photon, or non-radiatively by emission of an Auger electron.

Photoabsorption can be detected by the fluorescence yield (FY) or the electron yield (EY) [13]. For bulk materials, FY detection is more frequently used. On the other hand, EY is popular for the investigation of adsorbates on surfaces [13]. There are three ways to perform EY measurements: total electron yield (TEY), partial electron yield (PEY) or Auger electron yield (AEY). In the TEY method, all Auger electrons and photoelectrons are measured. This results in a high signal rate but a very small signal-to-noise ratio. In the PEY method, the surface sensitivity is enhanced by placing a retarding voltage in front of the electron detector to suppress electrons with lower kinetic energy. This way, only those electrons that emerge from the outer most regions (≈ 3 nm) are detected [13]. Due to the flexibility in choosing the retarding voltage, one can avoid the interference from the low kinetic energy electrons, thus increasing the signal-to noise ratio. A further method, the AEY method, measures only the elastically scattered Auger electrons by setting the energy analyzer at a specific Auger transition energy [13]. This method offers the largest signal-to-noise ratio of all the electron-yield techniques, but the smallest signal rate. In this thesis work, the PEY method was employed.

2.5 Electrochemistry: Controlled-Potential Techniques

Controlled-potential (potentiostatic) techniques deal with the study of charge transfer processes at the electrode-solution interfaces and are based on non-zero-current situations. In potentiostatic techniques, the electrode potential is used to drive an electron transfer reaction and the resulting current is measured. Among the well-known potentiostatic techniques are DC polarography, AC polarography, chronoamperometry, cyclic voltammetry and stripping voltammetry [18].

2.5.1 Cyclic Voltammetry (CV)

Cyclic voltammetry (CV) is perhaps the most versatile electroanalytical technique for the study of electroactive species [18,19]. Its versatility combined with the ease of measurements has resulted in extensive use of CV in the field of electrochemistry, inorganic chemistry, organic chemistry, biochemistry, etc. Most of the CV experiments now are done with a potentiostat in the three-electrode configuration (Figure 2.5) [19b]. This method uses a reference electrode (RE), a working electrode (WE), and a counter electrode (CE). CV consists of cycling the potential of the WE, which is immersed in an unstirred solution, and measuring the resulting current. The potential of this WE is controlled by the potentiostat versus the RE and the CE closes the electrical circuit for the current to flow [19]. The potential applied across the WE and RE electrodes can be considered as an excitation signal [18]. The excitation signal for CV is a linear potential scan with a triangular waveform. During the measurement, CV sweeps the potential of the electrode between two values, known as switching potentials [18]. The sweeping rate is known as the scan rate (Vs^{-1}). Single or multiple cycles can be used. Modern instrument allows switching potentials and scan rates to be easily modified [19]. During the CV experiments, the current at the WE is measured and plotted versus the applied voltage and a cyclic voltammogram is obtained [18, 19]. The resulting current can be considered as the response signal to the potential excitation signal. During the forward scan, the current will increase as the potential reaches the electrochemical potential of the analyte in the solution, but soon decreases as the concentration of the analyte is substantially diminished at the electrode surface. If the redox analyte is electrochemically reversible, it will be oxidized (if it is reduced in the forward scan) or reduced (if it is oxidized in the forward scan) back in the reverse scan. In order for the oxidation/reduction peak to be observed, the redox analyte must be redox active within the electrochemical window of the WE and the electrolyte solution [18, 19].

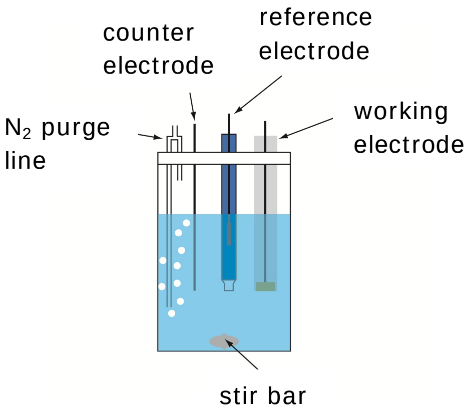

Figure 2.5 Three electrode electrochemical cell for cyclic voltammetry [19b].

The important parameters of a cyclic voltammogram are the magnitude of the anodic peak (i_{pa}) and cathodic peak current (i_{pc}), and the anodic (E_{pa}) and cathodic peak potential (E_{pc}) [18, 19]. For an ideal reversible redox system, the relationship between the oxidation (E_{ox}) and reduction (E_{red}) potential can be described by Equation 2.5.

$$\Delta E_p = E_{pa} - E_{pc} \cong \frac{0.059}{n} \qquad \text{(Equation 2.5)}$$

Where n is the number of electrons transferred in the electrode reaction for a reversible couple and ΔE_p is the peak separation. The ideal reversible redox system will obey the equation and show a peak separation of 59 mV in a cyclic voltammogram. In contrast, slow electron transfer at the electrode surface causes the peak separation to increase.

2.5.2 Chronoamperometry

Chronoamperometry is one of the potential-controlled techniques. As shown in Figure 2.6, during a single potential step chronoamperometry experiment, the applied potential is changed instantaneously from the initial potential to the first step potential, and it is held at this value for the first step time. In a double potential step experiment, the potential is changed to the second step potential after the first step time, and it is then held at this value for the second step time. The resulting current from the faradic process at the working electrode is then recorded as a function of time [20]. In this thesis work, chronoamperometry is used in Chapter 3 and Chapter 4 to measure the photocurrent generation by the molecular dye-functionalized B:NCD electrodes. An electron mediator (acceptor) is added during the measurements.

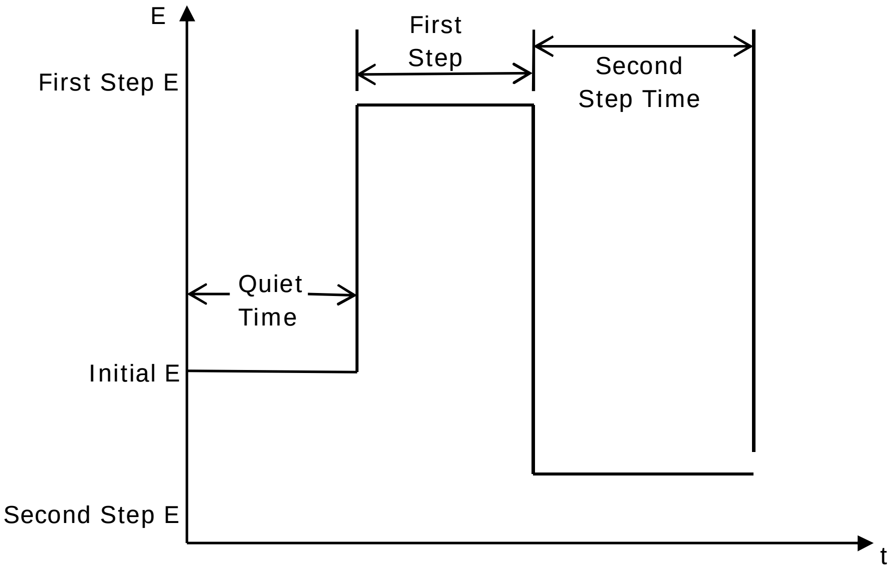

Figure 2.6 Potential waves from a chronoamperometry experiment.

2.6 Eletrochemical Impedance spectroscopy (EIS)

Most, if not all, classical electrochemical experiments involve large amplitude electrical perturbations of the electrode-solution interface. In a typical voltammetric experiment for example, the electrode is subjected to a potential ramp often spanning several hundred millivolts. As a consequence, the current-potential response is nonlinear. Electrochemical impedance spectroscopy (EIS) is another methodology which applies very small amplitude periodic (usually sinusoidal) electrical perturbations to an electrochemical cell and measures its impedance over a range of frequencies [21]. These applied perturbations are sufficiently small.

EIS experiments comprise the following steps: (1) a small ac voltage of between 5 to 50 mV is applied to a system over a range of frequencies of 1 mHz to 100 kHz; (2) its ac signal is then acquired and analyzed as a sum of sinusoidal functions (sinusoid at the same frequency but shifted in phase); (3) an equivalent electrical circuit is worked out; (4) components of the equivalent circuit are related to key physical and chemical characteristics of the electrochemical system. Data obtained from EIS is plotted graphically in a Bode plot or Nyquist plot. Each of the circuit elements of the electrochemical system in the solution can be represented by an equivalent circuit model.

An EIS instrument records both the real and imaginary components of the impedance response. Similar to resistance, impedance is a measurement of the ability of a circuit to resist the flow of electrical current. For an electrode that behaves like a pure resistor, the relation between current and potential follows Ohm’s law. This is actually not the case for the ac behavior of the real electrode, but instead reactive elements (capacitive elements) appear which give a more complex behavior [20]. Hence, impedance is used instead of resistance. Table 2.1 compares a resistor and a capacitor and the equation for their current versus voltage and impedance relationship. The impedance of a resistor is independent of frequency and has only a real component. As there is no imaginary impedance, the current passing through a resistor is always in phase with the voltage. On the other hand, the impedance of a capacitor is dependent on the frequency and consists of real and imaginary components as described by parameter *j*.

Table 2.1 Comparison between a resistor and a capacitor.

Component	Current vs. Voltage	Impedance
Resistor	$E = IR$	$Z = R$
Capacitor	$I = C\, \mathrm{d}E/\mathrm{d}t$	$Z = 1/j\omega C$

EIS has grown tremendously over the past few years and it is now widely used in various scientific fields, such as fuel cell testing [22, 23] and biomolecular interactions [24, 25]. In Chapter 5, non-faradaic impedance detection is applied to follow the surface modification and to record the changes in resistance or capacitance of the interface which are induced by the DNA hybridization events.

2.7 References

1. Watts, J. F.; Wolstenholme, J. *An Introduction to Surface Analysis by XPS and AES*; John Wiley: West Sussex, **2003**; pp 1-182.

2. (a) Ratner, B.; Castner, D. G. Electron Spectroscopy for Chemical Analysis. In *Surface Analysis-The Principle Technique*; Vickerman, J. C.; Gilmore, I. A., Eds.; John Wiley & Sons Ltd: West Sussex, **2003**; pp 47-109; (b) Crist, B. V. XPS International LLC, **2005**; pp 1-2.

3. Turner, D. W.; Baker, C.; Baker, A. D.; Brundle, C. R. *Molecular Photoelectron Spectroscopy*; John Wiley & Sons Ltd: London, **2003**.

4. Ellis, A. M.; Feher, M.; Wright, T. G., Electronic and Photoelectron Spectroscopy. Fundamentals and Case Studies; Cambridge University Press: New York, **2005**; pp 102-112.

5. Braun, S.; Salaneck, W. R.; Fahlman, M., Energy-Level Alignment at Organic/ Metal and Organic/ Organic Interfaces. *Adv. Mater*. **2009**, *21*, 1450.

6. Conte, M.; Mackey, W. M. *An Introduction to the Physcis of Particle Accelerators*; World Scientific Publishing Co. Pte. Ltd: Singapore, **2008**; pp 164-183.

7. Stöhr, J. *NEXAFS Spectroscopy*; Springer-Verlag: USA, **2003**; pp 1-7.

8. Stöhr, J.; Baberschke, K.; Jaeger, R.; Treichler, R.; Brennan, S., Orientation of Chemisorbed Molecules from Surface-Absorption Fine Structure Measurements – CO and NO on Ni(100). *Phys. Rev. Lett.* **1981**, *47*, 381.

9. Hitchcock, A. P.; Morin, C.; Zhang, X. R.; Araki, T.; Dynes, J.; Stover, H.; Brash, J.; Lawrence, J. R.; Leppard, G. G., Soft X-ray Spectromicroscopy of Biological and Synthetic Polymer Systems. *J. Electron Spectrosc. Relat. Phenom.* **2005**, *144*, 259.

10. Schöll, A.; Fink, R.; Umbach, E.; Mitchell, G. E.; Urquhart, S. G.; Ade, H., Towards A Detailed Understanding of NEXAFS Spectra of Bulk Polyethylene Copolymers and Related Alkanes. *Chem. Phys. Lett.* **2003**, *370*, 834.

11. Yang, Q.; Yang, S.; Li, Y. S.; Lu, X.; Hirose, A., NEXAFS Characterization of Nanocrystalline Diamond Thin Films Synthesized with High Methane Concentrations. *Diam. Relat. Mater.* **2007**, *16*, 730.

12. Rodriguez, J. A.; Hanson, J. C.; Frenkel, A. I.; Kim, J. Y.; Pérez, M., Experimental and Theoretical Studies on the Reaction of H2 with NiO: Role of O Vacancies and Mechanism for Oxide Reduction. *J. Am. Chem. Soc.* **2002**, *124*, 346.

13. Hähner, G., Near Edge X-ray Absorption Fine Structure Spectroscopy as a Tool to Probe Electronic and Structural Properties of Thin Organic Films and Liquids. *Chem. Soc. Rev.* **2006**, *35*, 1244.

14. Hähner, G.; Zwahlen, M.; Caseri, W., Chain Length Dependance of the Conformational Order in Self-Assembled Dialkylammonium Monolayers on Mica Studied by Soft X-ray Absorption. *Langmuir* **2005**, *21*, 1424.

15. Zubavichus, Y.; Zharnikov, M.; Yang, Y. J.; Fuchs, O.; Umbach, E.; Heske, C.; Ulman, A.; Grunze, M., X-ray Photoelectron Spectroscopy and Near-Edge X-

ray Absorption Fine Structure Study of Water Adsorption on Pyridine-Terminated Thiolate Self-Assembled Monolayers. *Langmuir* **2004**, *20*, 11022.

16. Lud, S. Q.; Steenackers, M.; Jordan, R.; Bruno, P.; Gruen, D. M.; Feulner, P.; Garrido, J. A.; Stutzmann, M., Chemical Grafting of Biphenyl Self-Assembled Monolayers on Ultrananocrystalline Diamond. *J. Am. Chem. Soc.* **2006**, *128*, 16884.

17. Zegkinoglou, I.; Cook, P. L.; Johnson, P. S.; Yang, W. L.; Guo, J. H.; Pickup, D.; Gonzalez-Moreno, R.; Rogero, C.; Ruther, R. E.; Rigsby, M. L.; Ortega, J. E.; Hamers, R. J.; Himpsel, F. J. Electronic Structure of Diamond Surfaces Functionalized by Ru(tpy)$_2$. *J. Phys. Chem. C* **2012**, *116*, 13877.

18. Bard, A. L.; Faulkner, L. R. *Electrochemical Methods: Fundamentals and Applications*, John Wiley & Sons Inc: New York, **2001**.

19. (a) Kissinger, P. T.; Heineman, W. R., Cyclic Voltammetry. *J. Chem. Ed.* **1983**, *60*, 702; (b) UCDavis ChemWiki. http://ChemWiki.ucdavis.edu (accessed Jan 8, 2015).

20. Bagotsky, V. S. *Fundamentals of Electrochemistry*; John Wiley & Sons Inc: New Jersey, **2006**; pp 387-404.

21. Macdonald, J. R.; Johnson, W. B. Fundamental of Impedance Spectroscopy. In *Impedance Spectroscopy Theory, Experiment, and Applications*; Barsoukov, E. and Macdonald, J. R., Eds.; John Wiley & Sons Inc.: New Jersey, **2005**; pp 1-26.

22. Easton, E. B. and Pickup, P. G., An Electrochemical Impedance Spectroscopy Study of Fuel Cell Electrodes. *Electrochim. Acta* **2005**, *50*, 2469.

23. Brunetto, C.; Moschetto, A.; Tina, G., PEM Fuel Cell Testing by Electrochemical Impedance Spectroscopy. *Electr. Pow. Syst. Res.* **2009**, *79*, 17.

24. Katz, E. and Willner, I., Probing Biomolecular Interactions at Conductive and Semiconductive Surfaces by Impedance Spectroscopy: Routes to Impedimetric Immunosensors, DNA-Sensors, and Enzyme Biosensors. *Electroanalysis* **2003**, *15*, 913.

25. Park, J-Y. and Park, S-M., DNA Hybridization Sensors Based on Electrochemical Impedance Spectroscopy as a Detection Tool. *Sensors* **2009**, *9*, 9513.

Chapter 3

Functionalization of Boron-Doped Nanocrystalline Diamond with N3 Dye Molecules

Published in *ACS Appl. Mater. Interfaces*, **6**, 10322–10329 (2014)

W.S. Yeap,[1] X. Liu,[2] D. Bevk,[1,3] A. Pasquarelli,[4] L. Lutsen,[3] M. Fahlman,[2]

W. Maes,[1,3] and K. Haenen[1,3]

[1] Hasselt University, Institute for Materials Research (IMO), B-3590 Diepenbeek, Belgium

[2] Linköping University, Department of Physics, Chemistry and Biology, S-58183 Linköping, Sweden

[3] IMEC vzw, IMOMEC, B-3590 Diepenbeek, Belgium

[4] Ulm University, Institute of Electron Devices and Circuits, 89069 Ulm, Germany

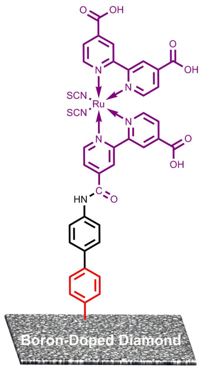

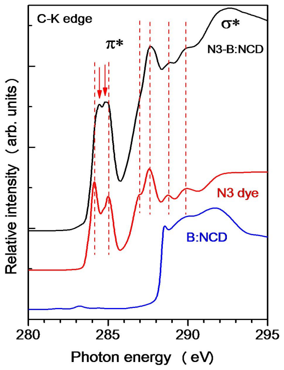

3.1 Abstract

N3 dye molecules [*cis*-*bis*(isothiocyanato)-*bis*(2,2'-bipyridyl-4,4'-dicarboxylato)-ruthenium(II)] are covalently attached onto B:NCD thin films through a combination of coupling chemistries, i.e. diazonium, Suzuki and EDC-NHS. XPS, UPS, and NEXAFS are used to verify the covalent bonding of the dye on the B:NCD surface (as compared to a hydrogen-terminated reference). The spectroscopic results confirm the presence of a dense N3 chromophore layer and the positions of the frontier orbitals of the dye relative to the band edge of the B:NCD thin film are inferred as well. Proof of concept photoelectrochemical measurements show a strong increase in photocurrent as compared to non-dye-functionalized B:NCD films. This study opens up the possibility to apply N3-sensitized B:NCD thin films as hole conductors in dye-sensitized solar cells.

Keywords: boron-doped diamond, diazonium coupling, Suzuki cross-coupling, N3 dye, spectroscopy surface characterization, photocurrent

3.2 Introduction

Diamond is an extraordinary material with excellent properties such as high optical transparency, corrosive resistance, a wide electrochemical potential window and biocompatibility. With recent advanced technologies such as microwave plasma-enhanced chemical vapor deposition (MW-PECVD), nanocrystalline diamond (NCD) thin films can be grown on various substrates at lower temperatures and pressures and reduced costs from cheap hydrocarbon precursors [1, 2]. Furthermore, the films can show p-type conductivity by doping with boron. High boron doping ratios afford metallic conductivity with a specific resistivity as low as 0.005 Ω.cm. This has opened up various technological applications for boron-doped nanocrystalline diamond (B:NCD) thin films. They have for instance been used as efficient transducers for sensors [3-7]. B:NCD thin film electrodes decorated with metal nanoparticles have shown catalytic effects in the reduction of CO_2 and alkenes [8], the oxidation of methanol [9], and the degradation of environmental pollutants [10]. Recently, boron-doped diamond nanoparticles have been produced from CVD diamond films [11]. These nanoparticles not only are conductive due to boron doping but also have high surface-to-volume ratio owing to their very small size. This new interesting diamond material may be applied for a broad range of applications. Despite these advantages, the major downside of diamond is the low reactivity of its surface, which makes the direct attachment of functional organic molecules quite challenging. This difficulty can be overcome by using photochemical attachment techniques [11, 12], diazonium coupling [13–15] or plasma treatment [16]. Post-modification of the diamond surface with (other) organic moieties can then be carried out employing various efficient chemical reactions [14, 15, 17–19].

The first report on dye sensitization of p-type semiconductive diamond electrodes was published in 1999 by Fujishima et al. [20] Photocurrent was observed when a synthetic semiconductive p-type diamond electrode was photosensitized by the $Ru(bpy)_3^{2+}$ (bpy = 2,2'-bipyridine) molecule in an electrolyte solution. More recently, robust covalent linking of $Ru(tpy)_2$ (tpy = 2,2':6',2"-terpyridine) dye molecules onto a boron-doped diamond (BDD) surface has been demonstrated [18]. The electronic structure of the obtained films was systematically probed by spectroscopic techniques [21]. The HOMO level of the $Ru(tpy)_2$ dye was found to be 0.9 eV lower than the valence band maximum (VBM) of BDD, prompting the authors to suggest a possible facile hole transfer from $Ru(tpy)_2$ to BDD. This result could pave the way to employ dye-sensitized BDD as an electrode in dye-sensitized solar cells (DSSCs).

The N3 dye [*cis*-*bis*(isothiocyanato)-*bis*(2,2'-bipyridyl-4,4'-dicarboxylato)-ruthenium(II)] (Figure 3.1) is one of the most efficient sensitizers used in DSSCs [21]. The dye has a large molar extinction coefficient in the visible region and is more widely used than $Ru(tpy)_2$ and $Ru(bpy)_3^{2+}$. Sensitization of the N3 dye with n-type semiconductors has been reported before [22–25]. Dye-sensitized tandem solar cells have also been made using p-type semiconductors such as p-NiO in combination with N3 dye molecules. This p-type semiconductor co-deposited onto titania acted both as a light absorber and hole conductor [26]. B:NCD possesses several advantages over NiO. B:NCD is highly transparent [27] in the visible range, whereas NiO absorbs a significant amount of light [28]. NiO also has a lower hole mobility (4×10^{-8} $cm^2V^{-1}s^{-1}$) [29] as compared to B:NCD (0.77 $cm^2V^{-1}s^{-1}$) [30]. B:NCD is known to be very chemically stable as well [1]. In DSSCs, p-doped diamond electrodes might be employed as hole conductors to replace the traditional highly corrosive tri-iodide electrolyte [21] Moreover, as shown previously by Zhong et al. [14], a highly stable photocurrent conversion could be observed for molecular dye-functionalized B:NCD, which was attributed to strong interfacial C-C covalent bonding. To the best of our knowledge, covalent attachment of the N3 dye on p-doped B:NCD thin films has not been performed so far. To obtain insights whether B:NCD could be a possible hole conductor when sensitized with N3 molecules, first of all covalent attachment of the N3 dye on a B:NCD surface has to be established.

Herein we report a strategy to covalently attach the N3 dye on B:NCD thin films using a combination of coupling chemistries. The B:NCD surface is first functionalized with 4-bromophenyl groups by diazonium coupling. Suzuki cross-coupling is then applied to couple 4-aminophenylboronic pinacol ester to the bromophenyl moieties to obtain (1,1'-biphenyl)-4-amine groups on the B:NCD surface, and finally the amine functions are used to attach the N3 dye through

EDC-NHS coupling. Wet chemical functionalization in solution is preferred here over physical plasma treatment to obtain a more homogeneous surface. Moreover, the use of this method can easily be extended to functionalized particles, including the nano-sized boron-doped diamond mentioned above [11]. After each functionalization step the surface composition is analyzed by X-ray photoelectron spectroscopy (XPS). Ultraviolet photoelectron spectroscopy (UPS) and near-edge X-ray absorption fine structure spectroscopy (NEXAFS) are used to investigate the HOMO and LUMO levels, respectively, of the N3 dye relative to the band edges of diamond. Photoelectrochemical measurements are performed to evaluate photocurrent generation by the functionalized B:NCD films. The results obtained might open up new possibilities in solar energy research by demonstrating the suitability of dye-sensitized B:NCD thin films as hole conductors in DSSCs.

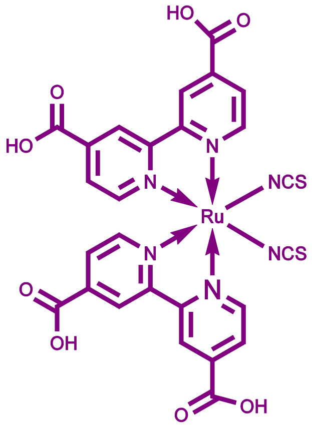

Figure 3.1 Chemical structure of the N3 dye.

3.3 Experimental

3.3.1 Chemical Reagents

Commercially available chemicals were purchased in the purest grades available and used without further purification. *N*-hydroxysuccinimide (NHS), cesium acetate, palladium(II) acetate, 4-aminophenylboronic acid pinacol ester, 4-

bromobenzenediazonium tetrafluoroborate, methyl viologen dichloride hydrate, sodium sulphate and tri(*o*-tolyl)phosphine were purchased from Sigma-Aldrich. The N3 dye was purchased from DYESOL. 1-Ethyl-3-[3-(dimethylamino)propyl]carbodiimide hydrochloride (EDC) was purchased from Thermo Scientific. All solvents used for reactions and rinsing were of HPLC grade, unless otherwise stated. Water used for reactions and rinsing was prepared with a Type 1 Ultrapure water by Sartorius stedium Biotech.

3.3.2 Diamond Growth

Heavily boron-doped nanocrystalline diamond thin films (150 nm) were grown by microwave plasma-enhanced chemical vapor deposition from methane/hydrogen mixtures (1% CH_4) in an ASTeX 6500 reactor. The substrates used were 1 × 1 cm fused silica. The growth conditions were as follows: substrate temperature 700–900 °C, total gas flow 500 sccm, total pressure in the reactor 30 Torr, microwave power 3500 W. Trimethylborane gas was added during the growth with a ratio of 10000 ppm B/C (with respect to CH_4) to ensure good electrical conductivity [30]. Sheet resistance (Rs), as measured by a four-point probe measurement, was 207 Ω sq^{-1}, which agrees well with the typical value for boron-doped NCD grown at this conditions [27, 30]. Prior to the diamond growth, the fused silica substrates were cleaned for 15 min each in RCA 1 (30% NH_3 + 30% H_2O_2 + H_2O; 1:1:5) and RCA 2 (37% HCl + 30% H_2O_2 + H_2O; 1:1:5) solutions at 90 °C. Following this, the cleaned fused silica substrates were seeded with nanodiamond powder in water to improve the nucleation density. After deposition, the diamond samples were allowed to cool down in the reactor for 30 min under vacuum. To remove any graphitic layers, the as-deposited diamond films were boiled in an acid mixture of 99% H_2SO_4 + 30% HNO_3 (3:1) at 90 °C for 30 min. After rinsing and sonicating with plenty of deionized water, the diamond samples were subjected to hydrogenation. Figure 3.2 displays a scanning electron microscopy (SEM) image of a typical as-grown B:NCD thin film.

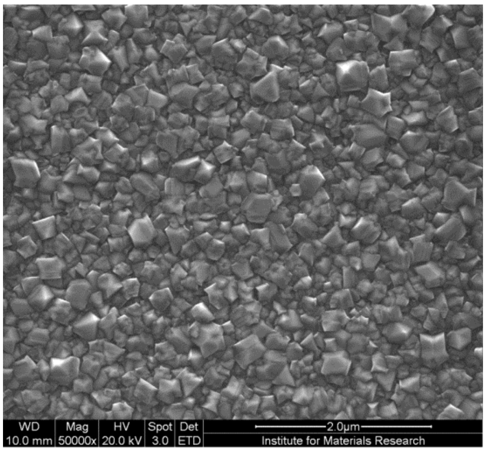

Figure 3.2 SEM image of a typical as-grown B:NCD thin film.

3.3.3 Hydrogenation

Hydrogenation was performed using the same PECVD reactor (ASTeX 6500). To create a hydrogen-terminated surface, all diamond samples were treated with hydrogen plasma under the following conditions: i. 500 sccm of hydrogen flux, 30 Torr reactor pressure with 3500 W microwave power for 2 min; ii. 500 sccm of hydrogen flux, 15 Torr reactor pressure with 2500 W microwave power for 5 min. At the end of the plasma treatment, the microwave power was switched off and the samples were allowed to cool down under hydrogen flux for 40 min.

3.3.4 Diamond Surface Functionalization

Functionalization of the diamond surface with 4-bromophenyl groups was carried out by simply immersing the hydrogenated B:NCD samples into a solution of 4-bromobenzenediazonium tetrafluoroborate (5 mM) in 0.1 M HCl for 120 min [14]. After surface modification, the substrates were sequentially rinsed and sonicated in ultrapure water, THF and *n*-hexane to remove any physisorbed molecules.

All preparations for the Suzuki cross-coupling reactions were performed in a glovebox. A 15 mL ACE pressure tube (Sigma Aldrich) containing a magnetic stirring bar and 4-bromophenyl-functionalized B:NCD was charged with 4-aminophenylboronic acid pinacol ester (20 mg, 100 µmol), 10 mol% tri(*o*-tolyl)phosphine (3.1 mg, 10 µmol), cesium acetate (19 mg, 100 µmol), 5 mol% palladium(II) acetate (1.1 mg, 5 µmol), and 5 mL of THF. The resulting mixture was then heated at 80 °C for 18 h. After the reaction, the substrates were sequentially rinsed and sonicated in methanol, THF and *n*-hexane to remove any physisorbed molecules.

The N3 dye was coupled onto the (1,1'-biphenyl)-4-amine-functionalized B:NCD films through EDC-NHS coupling. To this extent, the N3 dye (37 mg, 50 µmol) was dissolved in 2 mL of absolute ethanol. In a separate vial, EDC (38 mg, 200 µmol) and NHS (58 mg, 500 µmol) were dissolved in 3 mL of ultrapure water. The resulting two solutions were mixed together. The (1,1'-biphenyl)-4-amine-functionalized B:NCD films were then submerged into this solution for 5 h at room temperature. After the reaction, the functionalized diamond samples were sequentially rinsed and sonicated in ethanol and water to remove any physisorbed molecules.

3.3.5 Photoelectron Spectroscopy

Photoemission experiments were carried out using a Scienta ESCA 200 spectrometer in ultrahigh vacuum with a base pressure of 1×10^{-10} mbar. The measurement chamber is equipped with a monochromatic Al Kα X-ray source and He discharged lamp providing photons with 1486.6 eV for XPS and 21.22 eV for UPS, respectively. The XPS experimental conditions were set as such that the full width at half maximum of the clean Au $4f_{7/2}$ line is 0.65 eV. The total-energy resolution of the measurements in UPS, determined by the Fermi edge of clean gold, is about 0.1 eV. All spectra were measured at a photoelectron take-off angle of 0° normal emission. The UPS spectra have been corrected for the contributions from He I satellites radiation.

3.3.6 Near-Edge X-ray Absorption Fine Structure Spectroscopy (NEXAFS)

Polarized X-ray absorption spectroscopy measurements were performed at the beam line D1011 of the MAX-II storage ring, located at the MAX-Laboratory for Synchrotron Radiation Research in Lund, Sweden. The energy resolution was about 100 meV at photon energy close to the C-K edge. The absorption spectrum was collected in the total electron yield mode by measuring the sample current. Simultaneously, the absorption spectrum with partial electron yield was also recorded by a multi-channeltron plate (MCP) detector with a bias of -100 V to screen the electrons with lower kinetic energy. The raw data have been corrected for the energy dependence of the incident X-ray beam and subsequently normalized to have the same absorption edge step well above the threshold.

3.3.7 Photoelectrochemical Measurements

Photoelectrochemical measurements were performed in a N_2-saturated 0.1 M Na_2SO_4 solution containing 5 mM methyl viologen (MV^{2+}) as an electron carrier in a three-electrode glass cell containing B:NCD as a working electrode, a Pt counter electrode and an Ag/AgCl reference electrode. The glass cell was placed in a dark Faraday cage and controlled by a potentiostat (Princeton Applied Research PARSTAT 2273). The cold light light source employed was a 150 W halogen lamp (Mitutoyo Fiber Optic Illuminator). The incident light intensity was focused and calibrated with a photodiode to 150 mW cm^{-2}. The area of the B:NCD samples exposed to light was 0.07 cm^2.

3.4 Results and Discussion

3.4.1 Chemical Functionalization Strategies

The various steps in the chemical functionalization protocol of the B:NCD films are shown in Figure 3.3. The combination of diazonium, Suzuki, and EDC-NHS coupling reactions provides a powerful chemical route to covalently immobilize N3 dye molecules onto a B:NCD surface. After each step, the success of the coupling reaction was monitored by XPS (*vide infra*).

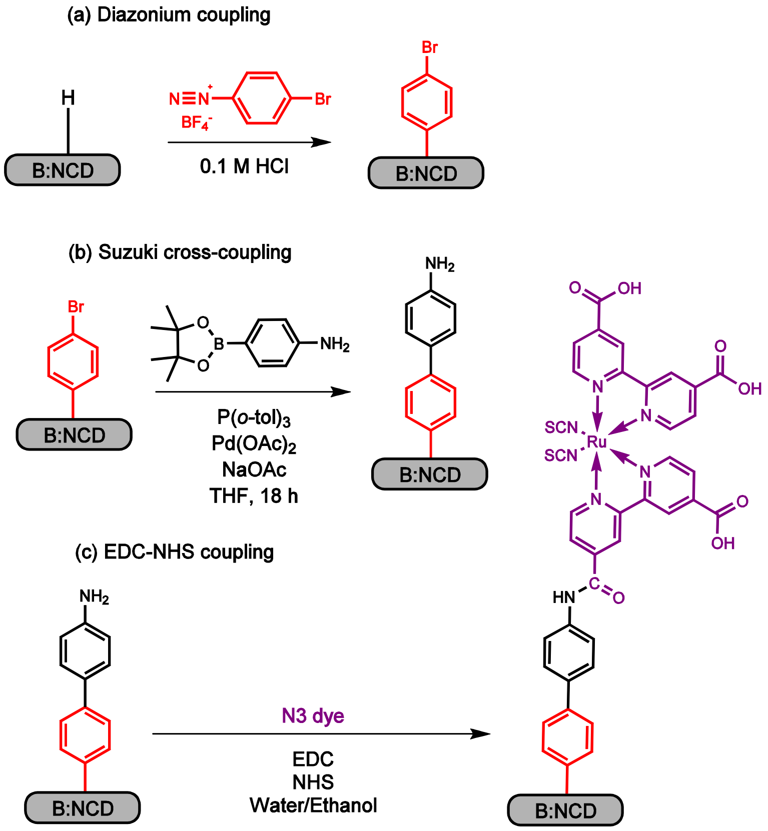

Figure 3.3 Subsequent coupling chemistries employed for the functionalization of B:NCD with N3 dyes.

The surface modification sequence starts with functionalization of the B:NCD surface with 4-bromophenyl groups. These entities can be covalently attached on hydrogenated B:NCD through reaction with the respective diazonium salt. This is done by submerging a hydrogenated B:NCD film into an acidic solution of 4-bromobenzenediazonium tetrafluoroborate for 2 hours. Previous studies have already shown that diazonium salts can be coupled spontaneously to hydrogenated diamond surfaces due to direct charge transfer between the hydrogenated diamond – with negative electron affinity – and the diazonium cations.[14] Spontaneous coupling provides a better control of the thickness of the organic layer compared to electrochemical grafting [31]. A monolayer of 4-bromophenyl groups can be attained by spontaneous coupling [14].

The bromoaryl-functionalized diamond film can then react further via Suzuki reactions [14, 17]. Suzuki-Miyaura cross-coupling of 4-aminophenylboronic acid pinacol ester to the prefunctionalized B:NCD creates a layer of (1,1'-biphenyl)-4-amine groups on the B:NCD surface. The selection of an efficient catalytic system is of great importance to achieve high coupling yields in transition metal catalyzed cross-couplings [32, 33]. Best results were obtained for a $Pd(OAc)_2$-$P(o\text{-tol})_3$ catalytic system compared to other systems using $Pd(PPh_3)_4$ or $Pd(dppf)Cl_2$. Finally, EDC-NHS coupling of the N3 dye to the (1,1'-biphenyl)-4-amine groups was carried out in an ethanol/water mixture.

3.4.2 Surface Composition by X-ray Photoelectron Spectroscopy

After each functionalization step, the variation of the surface components is a key parameter to assess the success of the functionalization process. XPS is a powerful tool to probe the surface composition of materials. Figure 3.4a shows the XPS Br 3p peaks of 4-bromophenyl-functionalized B:NCD. The appearance of the Br 3p signals at 181 and 189 eV clearly indicates that the B:NCD surface is decorated with Br due to 4-bromobenzene functionalization [14]. Furthermore, a (1,1'-biphenyl)-4-amine layer forms after Suzuki coupling of 4-aminophenylboronic acid pinacol ester. Successful cross-coupling was confirmed through the corresponding N 1s spectra, as shown in Figure 3.4b. The N 1s spectrum of the amino groups of (1,1'-biphenyl)-4-amine-functionalized B:NCD exhibits a peak at 400 eV, which is in agreement with earlier reports [31].

Upon final functionalization with the N3 chromophore, new XPS spectral features clearly appear, as indicated in Figure 3.5, consistent with the chemical structure of the dye. The XPS peak at 281 eV, which corresponds to Ru $3d_{5/2}$, can be considered as a fingerprint of the N3 dye, since each dye molecule introduces one Ru atom [35].

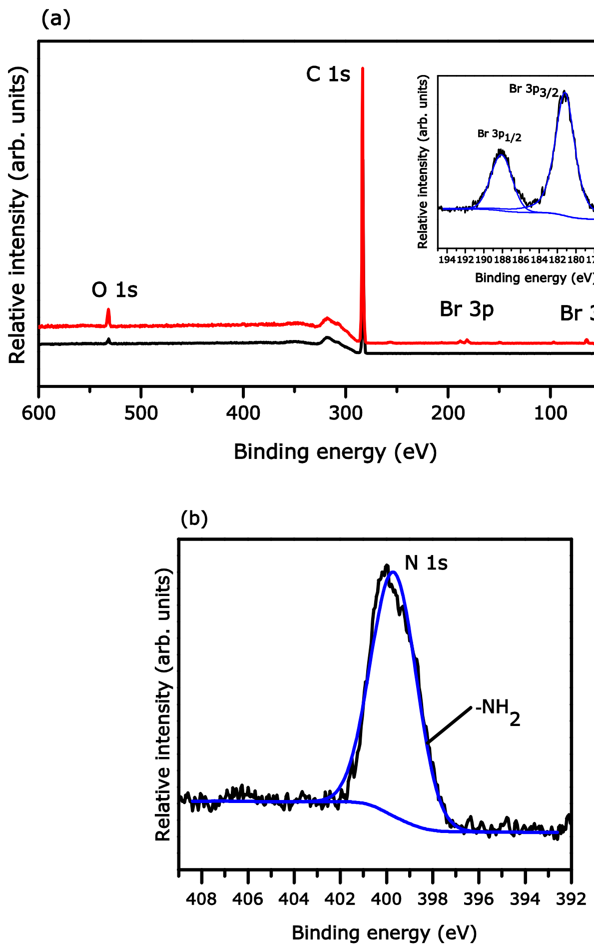

Figure 3.4 (a) XPS survey spectra of a 4-bromophenyl-functionalized B:NCD surface (red line) as compared to a reference sample of hydrogenated B:NCD (black line). Inset: High-resolution Br 3p XPS spectrum of 4-bromophenyl-functionalized B:NCD. (b) High-resolution N 1s XPS spectrum of (1,1'-biphenyl)-4-amine-functionalized B:NCD.

Furthermore, the other elements in the N3 dye with different chemical environment are also clearly demonstrated in the XPS results [36]. For instance, there are two kinds of nitrogen species in the N3 dye, one from the four pyridine groups and another one due to the two isothiocyanate groups [35]. The splitting of the N 1s peak can be clearly observed, with two components included in the N 1s spectral feature. The shoulder at lower binding energy (399 eV) can be assigned to the N=C=S groups [35, 37], whereas the sharp peak at higher binding energy (400 eV) can be attributed to the four pyridine units [35, 36]. Due to the additional contribution to the N 1s signal from the amide linkage to the N3 dye, the spectral weight ratio of the components at higher and lower binding energy is slightly different from the ratio observed in the pure N3 dye. Furthermore, the sulfur atoms of the isothiocyanate groups are also observed at 163 eV (S 2p peak) [35, 36]. The observed broad O 1s peak is due to several oxygen species in the N3 dye and surface adsorption of oxygen from the environment before XPS characterization.

The coverage of the N3 dye on B:NCD after functionalization is crucial for future device applications. The number of N3 dye molecules on the B:NCD surface can be deduced from the XPS results by the areal Ru density. The advantage of using the Ru intensity is that the change of spectral weight is considerably less influenced by impurities and/or contaminants on the functionalized B:NCD thin films compared to other relevant elements such as C, O, and S. Based on the core-level C 1s spectrum with the Ru 3d peak at 281.1 eV, and considering the following assumptions [19]:

1) The Ru 3d photoelectrons at the topmost surface do not experience scattering.

2) Carbon from the initial layer and from underlying NCD can be treated as being equivalent in the contribution of the C 1s signal.

3) The inelastic mean free path of the C 1s photoelectron is 2 nm.

4) The number density of carbon atoms in NCD is 1.66×10^{23} atoms/cm^3.

5) The areal density of carbon is 3.32×10^{16} atoms/cm^2 (NCD mass density ~ 3.3g/cm^3), the XPS area ratio can be expressed as:

$$\frac{A_{\mathrm{Ru\ 3d}_{\frac{5}{2}}}}{A_{\mathrm{C1s}}} = \frac{\mathrm{Ru}\left(\frac{\mathrm{atoms}}{\mathrm{cm}^2}\right)*S_{\mathrm{Ru\ 3d}_{\frac{5}{2}}}}{\mathrm{C}\left(\frac{\mathrm{atoms}}{\mathrm{cm}^2}\right)*S_{\mathrm{C1s}}} \qquad \text{(Equation 3.1)}$$

Taking into account the atomic sensitivity factors of Ru $3d_{5/2}$ and C 1s and the spectral weight of C 1s and Ru 3d, the surface coverage of N3 dyes on the B:NCD thin films was determined to be 3×10^{14} Ru/cm^2. This corresponds to 3 Ru/nm^2, which indicates that the N3 dye forms a quite dense film on the B:NCD surface.

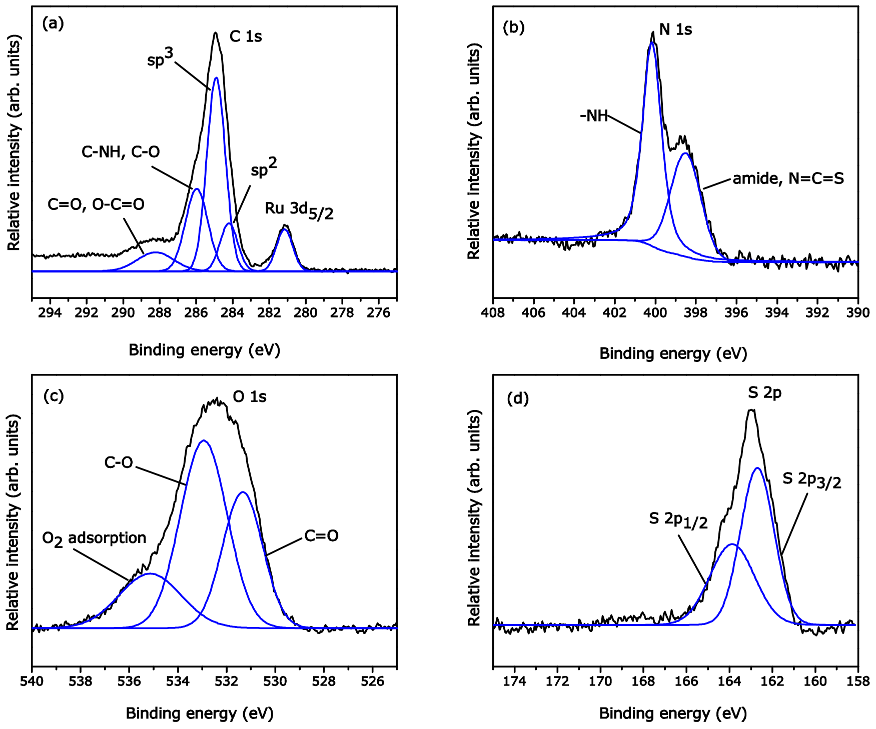

Figure 3.5 XPS spectra after EDC-NHS coupling of the N3 dye to (1,1'-biphenyl)-4-amine-functionalized B:NCD: (a) C 1s, (b) N 1s, (c) O 1s, and (d) S 2p core level spectra.

3.4.3 Ultraviolet Photoelectron Spectroscopy (UPS)

UPS is a powerful tool to directly probe the electronic properties of the valence band of materials. Figure 3.6 illustrates the UPS spectrum of N3 dye-functionalized B:NCD compared to the pure N3 dye. It can clearly be seen that the functionalized B:NCD film reproduces the spectral features of the pure chromophore. When the UPS intensity is plotted on a logarithmic scale, the weak valence band feature can be clearly distinguished. The first valence band peak appears around 2.0 eV in both the functionalized and pure samples. The second peak at ~4 eV was only observed in the functionalized diamond sample, which could be due to the interaction between the dye and the B:NCD substrate.

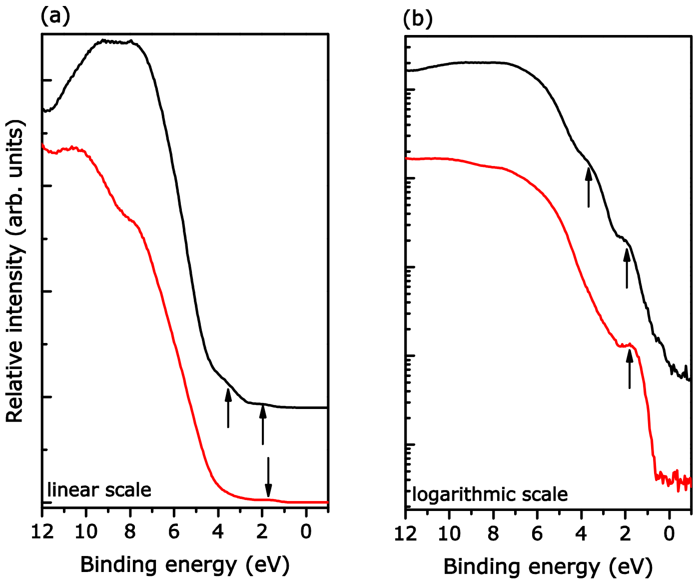

Figure 3.6 Comparison of the UPS spectra of N3 dye-functionalized B:NCD (black line) and the pure N3 dye (drop-casted on a Au substrate) (red line) on a linear (a) and logarithmic (b) scale.

To determine the HOMO energy level of the N3 chromophore, a UPS spectrum of a B:NCD film functionalized with N3 dye molecules was taken (Figure 3.7). The HOMO of the dye is compared to a similar spectrum of a hydrogen-terminated B:NCD thin film. The HOMO level of the N3 dye emerges at 1.1 eV below the Fermi level. Moreover, by linear extrapolation of the hydrogen-terminated

B:NCD thin film UPS data, the position of the VBM of diamond with respect to its Fermi level can be estimated. It is approximately 0.5 eV below the (surface) Fermi level. Accordingly, the HOMO of the N3 dye lies 0.5 eV below the VBM of B:NCD (Figure 3.7).

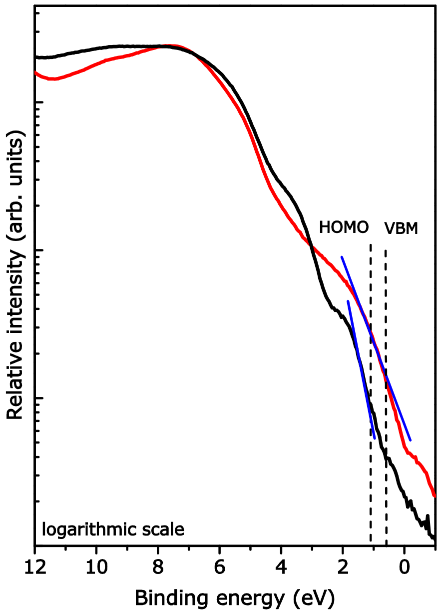

Figure 3.7 Comparison of the UPS spectra of the N3 dye-functionalized B:NCD (black line) and a bare hydrogen-terminated B:NCD film (red line). Linear extrapolation of the valence band edge yields an estimate of the VBM the of B:NCD thin film. The HOMO of the N3 dye lies 0.5 eV below the VBM.

These energy differences have implications on the hole transport between the B:NCD thin film and the appended N3 dye. Based on the principle of charge transfer in DSSCs, upon photogeneration of an exciton, the electron is transferred to an electron acceptor while the hole is transferred from the donor to the working electrode film. Hence, a good match between the HOMO of the donor molecule and the valence band of the electrode is important for efficient hole injection. For B:NCD, the VBM is situated rather close (0.5 eV) to the HOMO of the functionalized N3 dye, which should favor hole injection from the dye to the B:NCD thin film [17, 21].

3.4.4 Near-Edge X-ray Absorption Fine Structure Spectroscopy (NEXAFS)

When we turn to the empty states of the N3 dye-functionalized B:NCD film, as obtained from NEXAFS measurements (Figure 3.8), it can be seen that there are some clear spectral features in the C 1s absorption spectrum. There are two distinguished peaks around 285 eV, a shoulder at ~287 eV, and another three peaks up to a photon energy of 290 eV. As indicated by the XPS data, the N3 dye can form a film on the B:NCD surface with high coverage. The spectral features related to the B:NCD thin film are hence completely suppressed. On the other hand, when compared with the NEXAFS spectrum of the pure N3 dye, the influence of the B:NCD thin film upon the spectral features of the empty states of the N3 molecule can be extracted. The spectral features related to the N3 dye appear at higher photon energy, for instance between 287 and 290 eV (Figure 3.8). All absorption peaks are at approximately the same position in both the functionalized B:NCD sample and the pure N3 dye. A significant change was observed on the empty π* states at lower photon energy, i.e. around 285 eV. The LUMO and LUMO+1 energy levels of the pure N3 dye are observed at around 284.1 and 285.1 eV, respectively, and they are shifted to 284.4 and 284.9 eV for the functionalized B:NCD sample. The change of the LUMO and LUMO+1 positions shows the influence of B:NCD on the functionalized dye on top [21]. To ensure that the (1,1'-biphenyl)-4-amine linker does not significantly distort the result, the spectrum of (1,1'-biphenyl)-4-amine-functionalized B:NCD was taken as well. It contains a single п* peak at 285 eV originating from the biphenyl layer covalently attached onto B:NCD. This peak partially fills the valley between the π* peaks of the N3 dye, without strongly affecting their peak positions.

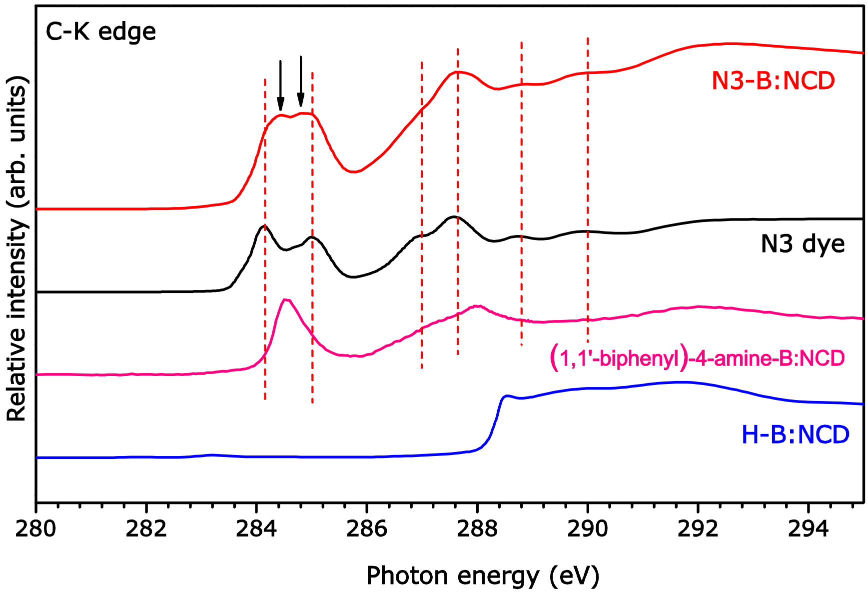

Figure 3.8 Comparison of the C-K edge NEXAFS spectra of N3-functionalized B:NCD, the pure N3 dye, (1,1'-biphenyl)-4-amine-functionalized B:NCD and a hydrogen-terminated B:NCD film.

3.4.5 Photoelectrochemical Measurements

As a proof of concept, photoelectrochemical measurements were performed using either a hydrogen-terminated B:NCD, a (1,1'-biphenyl)-4-amine-functionalized B:NCD or a N3-functionalized B:NCD film as the working electrode in a typical three-electrode electrochemical system. After equilibration in darkness, the light source was switched on and off approximately every 30 s for three cycles. The response curves show a tremendously increased photocurrent intensity for the N3-functionalized B:NCD electrode at -0.1 V bias as compared to both control systems (Figure 3.9). This agrees well with the mechanism that, upon light generation of electron-hole pairs in the N3 dye, the separated electrons flow toward the MV^{2+} (methyl viologen) electron carrier and the holes toward the B:NCD electrode (at negative bias) [14, 17].

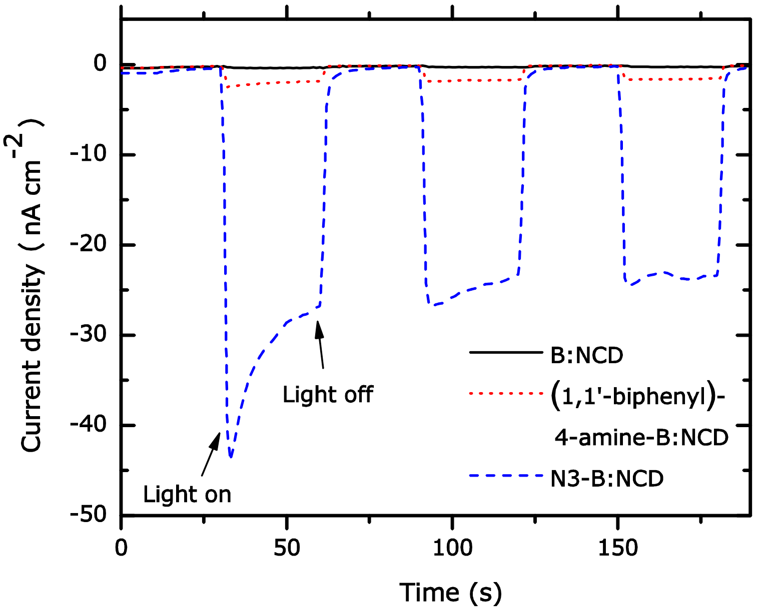

Figure 3.9 Photocurrent response of B:NCD (black solid line), (1,1'-biphenyl)-4-amine-B:NCD (red dotted-line) and N3-functionalized B:NCD (blue dashed-line) electrodes in a 5 mM methyl viologen solution (in 0.1 M Na_2SO_4) at -0.1 V bias (vs Ag/AgCl).

3.5. Conclusions

In conclusion, we have shown that N3 dye molecules can be covalently attached onto boron-doped nanocrystalline diamond thin films. Calculations based upon the Ru presence as analyzed by XPS indicate that a dense layer of chromophore molecules (~3×10^{14} Ru/cm^2) is achieved. UPS and NEXAFS measurements reveal that there is an interaction between the B:NCD thin film and the functionalized N3 dye. As evidenced by UPS measurements – matching of the HOMO level of the N3 dye with the VBM of the B:NCD thin film – holes generated during photoexcitation can possibly transfer from the dye to the B:NCD thin film, which was confirmed by proof of concept photocurrent measurements. This opens up a pathway toward the application of diamond-based dye-sensitized solar energy conversion via systematic energy level alignment. Efforts in this direction are currently ongoing within our groups.

3.6 Acknowledgements

This work was financially supported by the Special Research Fund of Hasselt University, the Research Foundation Flanders (FWO) (G.0555.10N), and the EU FP7 Collaborative Project “MOLESOL” (No. 256617). X. L. acknowledges support from The Swedish Research Council Linnaeus grant LiLi-NFM. We thank P. Robaeys for the four-point probe measurements and Prof. J. D'Haen for the SEM image.

3.7 References

1. Williams, O. A.; Nesladek, M.; Daenen, M.; Michaelson, S.; Hoffman, A.; Osawa, E.; Haenen, K.; Jackman, R. B. Growth, Electronic Properties and Applications of Nanodiamond. *Diam. Relat. Mater.* **2008**, *17*, 1080.

2. Potocky, S.; Kromka, A.; Potmesil, J.; Remes, Z.; Vorlicek, V.; Vanecek, M.; Michalka, M. Investigation of Nanocrystalline Diamond Films Grown on Silicon and Glass at Substrate Temperature Below 400 Degrees C. *Diam. Relat. Mater.* **2007**, *16*, 744.

3. Reitinger, A. A.; Hutter, N. A.; Donner, A.; Steenackers, M.; Williams, O. A.; Stutzmann, M.; Jordan, R.; Garrido, J. A. Functional Polymer Brushes on Diamond as a Platform for Immobilization and Electrical Wiring of Biomolecules. *Adv. Funct. Mater.* **2013**, *23*, 2979.

4. Ishii, Y.; Ivandini, T. A.; Murata, K.; Einaga, Y. Development of Electrolyte-Free Ozone Sensors Using Boron-Doped Diamond Electrodes. *Anal. Chem.* **2013**, *85*, 4284.

5. Subramanian, P.; Motorina, A.; Yeap, W. S.; Haenen, K.; Coffinier, Y.; Zaitsev, V.; Niedziolka-Jonsson, J.; Boukherroub, R., Szunerits, S. An

Impedimetric Immunosensor Based on Diamond Nanowires Decorated with Nickel Nanoparticles. *Analyst* **2014**, *139*, 1726.

6. Kondo, T.; Horitani, M.; Sakamoto, H.; Shitanda, I.; Hoshi, Y.; Itagaki, M.; Yuasa, M. Screen-printed Modified Diamond Electrode for Glucose Detection. *Chem. Lett.* **2013**, *42*, 352.

7. Wang, Q.; Subramanian, P.; Li, M. S.; Yeap, W. S.; Haenen, K.; Coffinier, Y.; Boukherroub, R.; Szunerits, S. Non-enzymatic Glucose Sensing on Long and Short Diamond Nanowire Electrodes. *Electrochem. Commun.* **2013**, *34*, 286.

8. Dhakshinamoorthy, A.; Navalon, S.; Sempere, D.; Alvaro, M.; Garcia, H. Reduction of Alkenes Catalyzed by Copper Nanoparticles Supported on Diamond Nanoparticles. *Chem. Commun.* **2013**, *49*, 2359.

9. Hutton, L. A.; Vidotti, M.; Patel, A. N.; Newton, M. E.; Unwin, P. R.; Macpherson, J. V. Electrodeposition of Nickel Hydroxide Nanoparticles on Boron-Doped Diamond Electrodes for Oxidative Electrocatalysis. *J. Phys. Chem. C* **2011**, *115*, 1649.

10. Toghill, K. E.; Wildgoose, G. G.; Moshar, A.; Mulcahy, C.; Compton, R. G. The Fabrication and Characterization of a Bismuth Nanoparticle Modified Boron Doped Diamond Electrode and Its Application to the Simultaneous Determination of Cadmium(II) and Lead(II). *Electroanal.* **2008**, *20*, 1731.

11. Heyer, S.; Janssen, W.; Turner, S.; Lu, Y.; Yeap, W. S.; Verbeek, J.; Haenen, K.; Krueger, K., Toward Deep Blue Nano Hope Diamonds: Heavily Boron-Doped Diamond Nanoparticles. *ACS Nano* **2014**, 8, 5757.

12. Wang, X. Y.; Landis, E. C.; Franking, R.; Hamers, R. J. Surface Chemistry for Stable and Smart Molecular and Biomolecular Interfaces via Photochemical Grafting of Alkenes. *Acc. Chem. Res.* **2010**, *43*, 1205.

13. Jian, W.; Firestone, M. A.; Auciello, O.; Carlisle, J. A. Surface Functionalization of Ultrananocrystalline Diamond Films by Electrochemical Reduction of Aryldiazonium Salts. *Langmuir* **2004**, *20*, 11450.

14. Zhong, Y. L.; Loh, K. P.; Midya, A.; Chen, Z. K. Suzuki Coupling of Aryl Organics on Diamond. *Chem. Mater.* **2008**, *20*, 3137.

15. Zhong, Y. L.; Ng, W.; Yang, J. X.; Loh, K. P. Electrostatically Self-Assembled Polyoxometalates on Molecular-Dye-Functionalized Diamond. *J. Am. Chem. Soc.* **2009**, *131*, 18293.

16. Nakamura, T.; Ohana, T. Surface Functionalization of Diamond Films by Photoreaction of Elemental Sulfur and Their Surface Properties. *Jpn. J. Appl. Phys.* **2012**, *51*, 085201.

17. Zhong, Y. L.; Midya, A.; Ng, Z.; Chen, Z. K.; Daenen, M.; Nesladek, M.; Loh, K. P. Diamond-Based Molecular Platform for Photoelectrochemistry. *J. Am. Chem. Soc.* **2008**, *130*, 17218.

18. Yao, S. A.; Ruther, R. E.; Zhang, L. H.; Franking, R. A.; Hamers, R. J.; Berry, J. F. Covalent Attachment of Catalyst Molecules to Conductive Diamond: CO_2 Reduction Using "Smart" Electrodes. *J. Am. Chem. Soc.* **2012**, *134*, 15632.

19. Ruther, R. E.; Rigsby, M. L.; Gerken, J. B.; Hogendoorn, S. R.; Landis, E. C.; Stahl, S. S.; Hamers, R. J. Highly Stable Redox-Active Molecular Layers by Covalent Grafting to Conductive Diamond. *J. Am. Chem. Soc.* **2011**, *133*, 5692.

20. Nakabayashi, S.; Ohta, N.; Fujishima, A. Dye Sensitization of Synthetic p-type Diamond Electrode. *Phys. Chem. Chem. Phys.* **1999**, *1*, 3993.

21. Zegkinoglou, I.; Cook, P. L.; Johnson, P. S.; Yang, W. L.; Guo, J. H.; Pickup, D.; Gonzalez-Moreno, R.; Rogero, C.; Ruther, R. E.; Rigsby, M. L.; Ortega, J. E.; Hamers, R. J.; Himpsel, F. J. Electronic Structure of Diamond Surfaces Functionalized by $Ru(tpy)_2$. *J. Phys. Chem. C* **2012**, *116*, 13877.

22. Grätzel, M. Photoelectrochemical Cells. *Nature* **2001**, *414*, 338.

23. Ling, T.; Song, J. G.; Chen, X. Y.; Yang, J.; Qiao, S. Z.; Du, X. W. Comparison of ZnO and TiO_2 Nanowires for Photoanode of Dye-Sensitized Solar Cells. *J. Alloy Compd.* **2013**, *546*, 307.

24. Mali, S. S.; Betty, C. A.; Bhosale, P. N.; Patil, P. S. Eosin-Y and N3-Dye Sensitized Solar Cells (DSSCs) Based on Novel Nanocoral TiO_2: A Comparative Study. *Electrochim. Acta* **2012**, *59*, 113.

25. Mane, R. S.; Pathan, H. M.; Lokhande, C. D.; Han, S. H. An Effective Use of Nanocrystalline CdO Thin Films in Dye-Sensitized Solar Cells. *Sol. Energy* **2006**, *80*, 185.

26. Kalyanasundaram, K. Photochemical and Photoelectrochemical Approaches to Energy Conversion. In *Dye-Sensitized Solar Cells*; Kalyanasundaram, K., Eds.; EPFL Press: Lausanne, **2010**; pp 1–43.

27. Lim, C. H. Y. X.; Zhong, Y. L.; Janssens, S.; Nesladek, M.; Loh, K. P. Oxygen-Terminated Nanocrystalline Diamond Film as an Efficient Anode in Photovoltaics. *Adv. Funct. Mater*. **2010**, *20*, 1313.

28. Nattestad, A.; Mozer, A. J.; Fischer, M. K. R.; Cheng, Y. B.; Mishra, A.; Bauerle, P.; Bach, U. Highly Efficient Photocathodes for Dye-Sensitized Tandem Solar Cells. *Nat. Mater*. **2010**, *9*, 31.

29. Mori, S.; Fukuda, S.; Sumikura, S.; Takeda, Y.; Tamaki, Y.; Suzuki, E.; Abe, T. Charge-Transfer Process in Dye-Sensitized NiO Solar Cells. *J. Phys. Chem. C* **2008**, *112*, 16134.

30. Janssens, S. D.; Pobedinskas, P.; Vacik, J.; Petrakova, V.; Ruttens, B.; D'Haen, J.; Nesladek, M.; Haenen, K.; Wagner, P. Separation of Intra- and Intergranular Magnetotransport Properties in Nanocrystalline Diamond Films on The Metallic Side of The Metal-Insulator Transition. *New J. Phys.* **2011**, *13*, 083008.

31. Lud, S. Q.; Steenackers, M.; Jordan, R.; Bruno, P.; Gruen, D. M.; Feulner, P.; Garrido, J. A.; Stutzmann, M. Chemical Grafting of Biphenyl Self-Assembled Monolayers On Ultrananocrystalline Diamond. *J. Am. Chem. Soc.* **2006**, *128*, 16884.

32. Shen, W. Palladium Catalyzed Coupling of Aryl Chlorides with Arylboronic Acids. *Tetrahedron Lett.* **1997**, *38*, 5575.

33. Barder, T. E.; Walker, S. D.; Martinelli, J. R.; Buchwald, S. L. Catalysts for Suzuki-Miyaura Coupling Processes: Scope and Studies of The Effect of Ligand Structure. *J. Am. Chem. Soc.* **2005**, *127*, 4685.

34. Eck, W.; Stadler, V.; Geyer, W.; Zharnikov, M.; Golzhauser, A.; Grunze, M. Generation of Surface Amino Groups On Aromatic Self-Assembled Monolayers By Low Energy Electron Beams - A First Step Towards Chemical Lithography. *Adv. Mater.* **2000**, *12*, 805.

35. Syres, K. L.; Thomas, A. G.; Cant, D. J. H.; Hardman, S. J. O.; Preobrajenski, A. Pyrocatechol As A Surface Capping Molecule On Raffle TiO_2 (110). *Surf. Sci.* **2012**, *606*, 273.

36. Terasaki, N.; Nitahara, S.; Akiyama, T.; Yamada, S. Structural Characterization and Photocurrent Properties of cis-di(thiocyanato)-bis(4,40-dicarboxy-2,20-bipyridine) Ruthenium(II) Monolayers on the Gold Surfaces. *Jpn. J. Appl. Phys.* **2005**, *44*, 2795.

37. Srinivasan, V.; Walton, R. A. X-ray Photoelectron Spectra of Inorganic Molecules: XX. Observations Concerning the Sulfur 2p Binding Energies in Metal Complexes of Thiourea. *Inorg. Chim. Acta* **1977**, *25*, L85.

Chapter 4

Diamond Functionalization with Light-Harvesting Molecular Dyes: Improved Surface Coverage by Optimized Suzuki Cross-Coupling Conditions

Published in *RSC Advances*, **4**, 42044–42053 (2014)

W.S. Yeap,[1] D. Bevk,[1,2] X. Liu,[3] H. Krysova,[4] A. Pasquarelli,[5] D. Vanderzande,[1,2] L. Lutsen,[1,2] L. Kavan,[4] M. Fahlman,[3] W. Maes,[1,2] and K. Haenen[1,2]

[1] Hasselt University, Institute for Materials Research (IMO), B-3590 Diepenbeek, Belgium

[2] IMEC vzw, IMOMEC, B-3590 Diepenbeek, Belgium

[3] Linköping University, Department of Physics, Chemistry and Biology, S-58183 Linköping, Sweden

[4] Academy of Sciences of the Czech Republic, J. Heyrovský Institute of Physical Chemistry, v.v.i., Dolejškova 3, CZ-182 23 Prague 8, Czech Republic

[5] Ulm University, Institute of Electron Devices and Circuits, 89069 Ulm, Germany

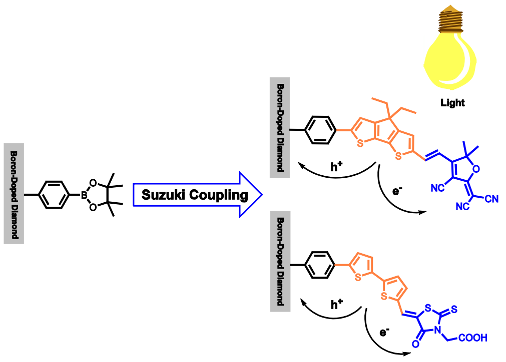

4.1 Abstract

Donor-acceptor type light-harvesting molecular dyes are covalently attached to a boron-doped diamond surface via a combination of diazonium electrografting and Suzuki cross-coupling. For the Suzuki reaction, various catalytic systems are compared with respect to their imposed surface coverage. Combining 2-dicyclohexylphosphino-2',6'-dimethoxybiphenyl (SPhos) and Pd(0), the diamond coverage improves considerably (by 98%) as compared to the standard tetrakis(triphenylphosphine)palladium(0) ($Pd(PPh_3)_4$) catalyst. As the energy levels between the molecular chromophores and the diamond film align well, the sophisticated functionalized diamond surfaces present a first step towards the development of fully carbon-based devices for light to electricity conversion.

Keywords: boron-doped diamond, diazonium coupling, Suzuki cross-coupling, donor-acceptor, spectroscopic surface characterization, photocurrent

4.2 Introduction

In recent years, boron-doped diamond (BDD) has become increasingly important within science and technology [1]. By adding boron, diamond conductivity can be tuned, with values ranging from 1 × 10^{-9} to 100 Ω^{-1} cm^{-1}, the latter resulting in metallic behavior [2]. Boron-doped nanocrystalline diamond (B:NCD) prepared in a thickness of ~150 nm is highly transparent (with a transmission of 70–80%) [3]. Despite its extraordinary physical properties and numerous applications (chemical and biosensors, electrosynthesis etc.) [4], earlier works focused mostly on tailoring the diamond's surface properties. Photochemical modification [5], plasma treatment [6], and diazonium coupling [7] afford a diversity of diamond surface modification schemes, allowing the attachment of various molecular structures. The next challenge, however, is to develop a versatile chemistry that can impart useful sensory, optoelectronic and/or photophysical properties to the B:NCD material.

Next to several click chemistry protocols [8], the Suzuki-Miyaura reaction represents one of the most versatile and powerful carbon-carbon (most often aryl-aryl) bond forming procedures in modern synthetic chemistry [9]. This Pd-catalyzed cross-coupling reaction has been applied for the preparation of a huge variety of conjugated aromatic compounds, for example to be used for organic light-emitting diodes (OLEDs) [10], polymer LEDs [11], organic photovoltaics [12], and nonlinear optical materials [13]. The Suzuki reaction can also be used for (uninterrupted) molecular conjugation of solid surfaces to a large class of organic molecules [14]. This is particularly useful if one wishes to create donor-acceptor type molecular wires on semiconducting substrates for photocurrent/photovoltage generation [15]. However, to the best of our knowledge, there are only three reports so far which address Suzuki cross-coupling reactions on diamond surfaces [16–18]. Zhong *et al.* reported a facile method for the Suzuki coupling of oligothiophene-fullerene and 2-(dicyanovinyl)-5-iodobithiophene molecular wires onto diamond. They showed that this method opens up possibilities for the application of diamond in molecular electronics and photovoltaics. Nonetheless, the reported surface coverage of 2-(dicyanovinyl)-5-iodobithiophene was as low as 0.41 'monolayer' (ML) (relative to a high quality reference monolayer of dodecanethiol on Au, as determined by X-ray photoelectron spectroscopy, XPS) [17].

In this manuscript, we report on the successful decoration of B:NCD with two molecular dye systems, (*Z*)-2-{5-[(5'-bromo-[2,2'-bithiophen]-5-yl)methylene]-4-oxo-2-thioxothiazolidin-3-yl}acetic acid (**Br-BT-Rho**) and (*E*)-2-{4-[2-(6-bromo-4,4-diethyl-4*H*-cyclopenta[1,2-*b*:5,4-*b*']dithiophen-2-yl)vinyl]-3-cyano-5,5-dimethylfuran-2(5*H*)-ylidene}malononitrile (**Br-CPDT-Fur**) (Figure 4.1), via optimized Suzuki cross-coupling reactions.

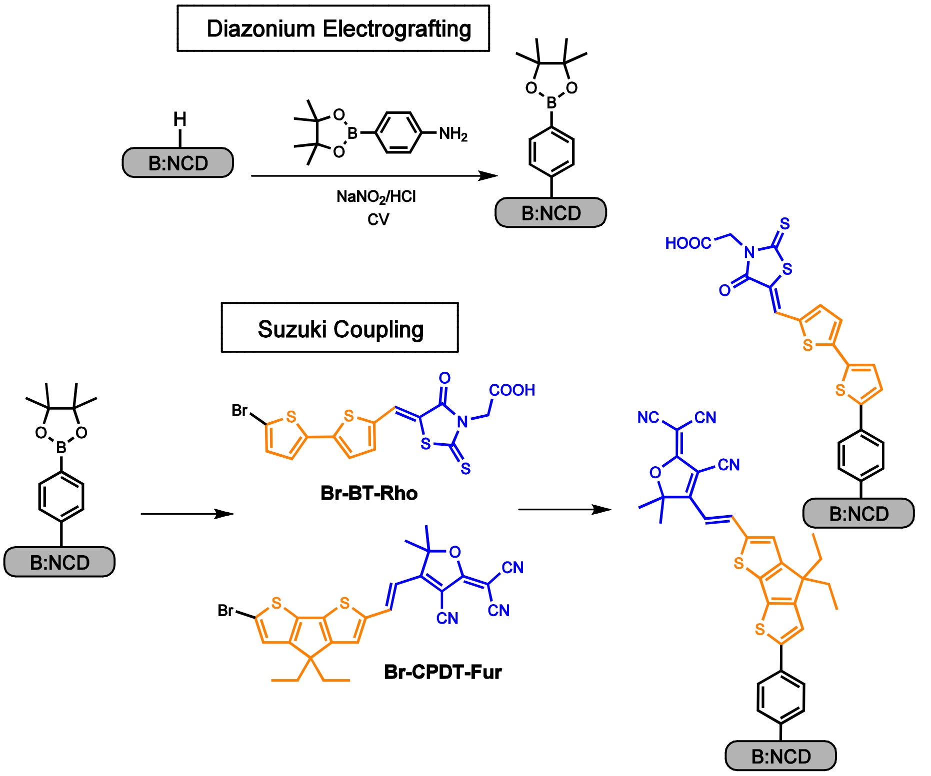

Figure 4.1 Diazonium electrografting and Suzuki cross-coupling towards effective B:NCD functionalization.

Both molecular dyes possess a bromoaryl moiety to enable reaction with an arylboronic ester functionalized B:NCD surface. The most effective catalytic system was pursued to increase the coupling efficiency and hence the surface coverage. Surface functionalization as well as coverage were determined by XPS. The **CPDT-Fur** molecular dye has suitable properties to be used effectively in future molecular photovoltaic systems, i.e. high absorbance, wide absorption and good charge transfer abilities through the π-system [19]. Furthermore, the highest occupied molecular orbital (HOMO) of the dye seems to match well with the valence band of the B:NCD film, as evaluated by ultraviolet photoelectron spectroscopy (UPS), allowing hole injection from the dye to diamond.

4.3 Experimental

4.3.1 Chemical reagents

Commercially available chemicals were purchased in their purest grade available and used without further purification. Sodium nitrite, sodium carbonate, sodium acetate, cesium acetate, cesium fluoride, potassium phosphate, palladium(II) acetate, 4-aminophenylboronic acid pinacol ester, rhodanine-3-acetic acid, tetrakis(triphenylphosphine)palladium(0), and tri(*o*-tolyl)phosphine were purchased from Sigma-Aldrich. 5-Bromo-5'-formyl-2,2'-bithiophene was purchased from TCI Europe N.V. 2-Dicyclohexylphosphino-2’,6’-dimethoxybiphenyl (SPhos) was purchased from Acros Organics. All solvents used for reactions and rinsing were of HPLC grade, unless otherwise stated. Water used for rinsing and electrochemical work was made with Type 1 Ultrapure water by Sartorius stedium Biotech.

4.3.2 Synthesis and characterization

NMR chemical shifts (δ) were determined relative to the residual $CHCl_3$ absorption (7.26 ppm) or the ^{13}C resonance shift of $CDCl_3$ (77.16 ppm). UV-Vis absorption spectra were recorded with an Agilent Cary 500 Scan UV-Vis-NIR spectrometer in a continuous run from 200 to 800 nm at a scan rate of 600 nm min^{-1}. Electrochemical measurements were performed with an Eco Chemie Autolab PGSTAT 30 potentiostat/galvanostat using a three-electrode microcell equipped with a Pt wire working electrode, a Pt wire counter electrode and a Ag/$AgNO_3$ reference electrode (Ag wire dipped in a solution of 0.01 M $AgNO_3$ and 0.1 M NBu_4PF_6 in anhydrous MeCN). Samples were prepared in anhydrous CH_2Cl_2 containing 0.1 M NBu_4PF_6 and ferrocene was used as an internal standard. The respective products were dissolved in the electrolyte solution and degassed with argon prior to each measurement. To prevent air from entering the system, the experiments were carried out under argon. Cyclic voltammograms were recorded at a scan rate of 50 mVs^{-1}. The HOMO-LUMO energy levels of **Br-CPDT-Fur** were determined using CV data. For the conversion of V to eV, the onset potentials of the first oxidation/reduction peaks were used and referenced to ferrocene/ferrocenium, which has an ionization potential of -4.98 eV *vs.* vacuum. This correction factor is based on a value of 0.31 eV for Fc/Fc^+ *vs.* SCE [18a] and a value of 4.68 eV for SCE *vs.* vacuum [20]: $E_{HOMO/LUMO}$ (eV) = -4.98 - $E_{onset\ ox/red}^{Ag/AgNO_3}$ (V) + $E_{onset\ Fc/Fc+}^{Ag/AgNO_3}$ (V). To estimate the optical HOMO-LUMO gap, the wavelength at the intersection of the tangent line drawn at the low energy side of the (solution) absorption spectrum with the x-axis was used (ΔE_{opt} (eV) = 1240/(wavelength in nm)).

4,4-Diethyl-4*H*-cyclopenta[1,2-*b*:5,4-*b'*]dithiophen-2-carboxaldehyde (CPDT-CHO) (2). To a cold solution (0 °C) of 4,4-diethyl-4*H*-cyclopenta[1,2-*b*:5,4-*b*']dithiophene [21a] (**1**) (359 mg, 1.53 mmol) in 1,2-dichloroethane (4.5 mL) and DMF (140 µL), $POCl_3$ (140 µL) was added under nitrogen. After 4 h at this temperature, a saturated NaOAc solution (10 mL) was added. The mixture was stirred at room temperature for 2 h. The crude product was extracted into CH_2Cl_2. The organic layer was washed with water and brine. After drying with $MgSO_4$ and filtration, the solvent was removed to afford the product as colourless oil in a quantitative way (400 mg). ^1H NMR ($CDCl_3$): 0.61 (t, 6H, *J* = 7.4 Hz, $CH_2C\underline{H}_3$), 1.95 (m, 4H, $C\underline{H}_2CH_3$), 7.00 (d, 1H, *J* = 4.8 Hz), 7.43 (d, 1H, *J* = 4.8 Hz), 7.58 (s, 1H), 9.84 (s, 1H, CHO).

6-Bromo-4,4-diethyl-4*H*-cyclopenta[1,2-*b*:5,4-*b'*]dithiophen-2-carboxaldehyde (Br-CPDT-CHO) (3). To a cold solution (0 °C) of CPDT-CHO **2** (410 mg, 1.56 mmol) in THF (50 mL), NBS (345 mg, 1.24 equiv) was added under a nitrogen atmosphere. The reaction mixture was warmed gently to room temperature and stirred further for 5 h. Then, water (50 mL) was added and the product was extracted with CH_2Cl_2. The organic phase was dried ($MgSO_4$) and the solvent was removed to afford the product as a colourless oil in a quantitative way (530 mg). ^{1}H NMR ($CDCl_3$): 0.61 (t, 6H, J = 7.4 Hz, $CH_2C\underline{H}_3$), 1.92 (m, 4H, $C\underline{H}_2CH_3$), 7.02 (s, 1H), 7.57 (s, 1H), 9.84 (s, 1H, CHO).

(*E*)-2-{4-[2-(6-Bromo-4,4-diethyl-4*H*-cyclopenta[1,2-*b*:5,4*b'*]dithiophen-2-yl)vinyl]-3-cyano-5,5-dimethylfuran-2(5*H*)-ylidene}malononitrile (Br-CPDT-Fur). 6-Bromo-4,4-diethyl-4*H*-cyclopenta[1,2-*b*:5,4-*b'*]dithiophene-2-carbaldehyde (**3**) (533 mg, 1.56 mmol) and 2-(3-cyano-4,5,5-trimethylfuran-2(5*H*)-ylidene)malononitrile (**4**) [22] (330 mg, 1.56 mmol) were dissolved in ethanol (10 mL). Piperidine (2 drops) was added and the reaction mixture was heated at reflux overnight. The dark reaction mixture was cooled down to room temperature and a precipitate was formed, which was filtered off and recrystallized from an ethanol/water mixture to give the product as greenish-yellow crystals (dark blue in solution) (478 mg, 58%). m.p. > 250 °C. ^{1}H NMR ($CDCl_3$): 0.61 (t, 6H, J = 7.4 Hz, $CH_2C\underline{H}_3$), 1.74 (s, 6H, CH_3), 1.93 (m, 4H, $C\underline{H}_2CH_3$), 6.59 (d, 1H, J = 15.6 Hz, -CH=CH-), 7.04 (s 1H), 7.34 (s, 1H), 7.90 (d, 1H, J = 15.8 Hz, -CH=CH-). ^{13}C NMR ($CDCl_3$): 9.3, 26.7, 30.3, 56.09, 56.12, 77.4, 95.6, 97.1, 110.5, 111.5, 111.7, 118.2, 125.3, 136.7, 140.6, 141.0, 147.6, 158.8, 161.4, 173.0, 176.1. UV-Vis ($CHCl_3$): λ_{max} = 585 nm, ε = 73100 L mol^{-1} cm^{-1}, ΔE_{opt} = 1.85 eV.

4.3.3 Diamond Growth

Polycrystalline boron-doped nanocrystalline diamond (B:NCD) thin films (150 nm in thickness) were grown by microwave plasma-enhanced chemical vapour deposition (CVD) from methane/hydrogen mixtures (1% CH_4) in an ASTeX 6500 reactor. The substrates used were fused silica (1 cm × 1 cm). The growth conditions used were as follows: substrate temperature 700–900 °C, total gas flow 500 sccm, total pressure in the reactor 30 Torr, microwave power 3500 W. Trimethylborane gas was added during the growth with a ratio of 10000 ppm B/C to CH_4 to ensure good electrical conductivity [1b]. Based on previous experiments [23], this ratio corresponds to a boron film concentration 10^{21} cm^{-3}. Sheet resistance (Rs), as measured by a four-point probe measurement, was 207 Ω/sq, which agrees well with the typical value for B:NCD grown under these conditions [3]. Prior to the diamond growth, the fused silica substrates were cleaned for 15 min each in RCA 1 (30% NH_3 + 30% H_2O_2 + H_2O; 1:1:5) and RCA 2 (37% HCl + 30% H_2O_2 + H_2O; 1:1:5) solutions at 90 °C. Following this, the cleaned fused silica substrates were seeded with nanodiamond powder in water to improve the nucleation density. After deposition, the diamond samples were allowed to cool down in the reactor for 30 min under vacuum. To remove any graphitic layers, the as-deposited diamond films were boiled in an acidic mixture of 99% H_2SO_4 + 30% HNO_3 (3:1) at 90 °C for 30 min. After rinsing and sonicating with plenty of deionized water, the diamond samples were subjected to hydrogenation. Figure 4.2 displays a scanning electron microscopy (SEM) image of a typical as-grown B:NCD thin film.

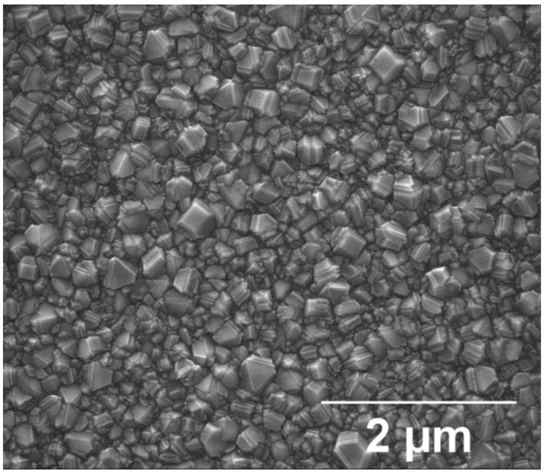

Figure 4.2 Typical SEM image of a B:NCD film.

4.3.4 Hydrogenation

Hydrogenation was performed using the same PECVD reactor (ASTeX 6500). To create a hydrogen terminated surface, all diamond samples were treated with hydrogen plasma under the following conditions: i) 500 sccm hydrogen flux, 30 Torr reactor pressure with a 3500 W microwave power for 2 min, ii) 500 sccm hydrogen flux, 15 Torr reactor pressure with a 2500 W microwave power for 5 min, iii) at the end of the plasma treatment, the microwave power was switched off and the samples were allowed to cool down under hydrogen flux for 40 min.

4.3.5 Diazonium Electrografting

The functionalization of the diamond surfaces started with diazonization of the targeted aniline (4-aminophenylboronic acid pinacol ester) followed by electrochemical reduction of the *in situ* generated diazonium salt by cyclic voltammetry (Figure 4.1) [16] The electrografting reaction was performed with an Autolab PGSTAT30 potentiostat (Eco Chemie B.V.) and controlled by the GPES Program. A one-compartment electrochemical cell with three-electrode configuration was used. The working electrode was a hydrogen-terminated B:NCD film. Platinum wire and Ag/AgCl/KCl$_{(sat)}$ electrodes were used as counter and reference electrodes, respectively. Half of the diamond sample was immersed in the reaction solution for larger area functionalization. As stated above, 5 mM of 4-aminophenylboronic acid pinacol ester was diazotized with an equimolar amount of $NaNO_2$ in a (N_2 gas purged) 0.5 M HCl solution, which was directly used for CV scanning with a potential from +0.5 to -0.8 V (vs Ag/AgCl) at a scan rate of 100 mVs^{-1} for 5 scans [16]. After the modifications, the substrates were sequentially rinsed and sonicated in ultrapure water, THF and *n*-hexane to remove any physisorbed molecules.

4.3.6 Suzuki cross-coupling

All preparations for the Suzuki cross-coupling reactions were performed in a glove box. To achieve the highest possible surface coverage, the most efficient conditions were pursued. In general, a 15 mL ACE pressure tube (Sigma Aldrich) containing a magnetic stirring bar and the functionalized diamond film was charged with the dye (**Br-BT-CHO**/**Br-BT-Rho**/**Br-CPDT**/**Br-CPDT-Fur**), Pd catalyst, base and solvent. The resulting mixture was then heated at 80 °C for 18 h. Detailed information on the catalyst systems is provided in Table 4.1 and 4.2.

4.3.7 X-ray/ultraviolet photoelectron spectroscopy

Photoemission experiments were carried out using a Scienta ESCA 200 spectrometer in ultrahigh vacuum with a base pressure of 1x10^{-10} mbar. The measurement chamber is equipped with a monochromatic Al Kα X-ray source and He discharge lamp providing photons with 1486.6 eV for XPS and 21.22 eV for UPS, respectively. The XPS experimental conditions were set so that the full width at half maximum of the clean Au $4f_{7/2}$ line was 0.65 eV. The total energy resolution of the measurements in UPS, determined by the Fermi edge of clean gold, is about 0.1 eV. All spectra were measured at a photoelectron take-off angle of 0° normal emission. The UPS spectra have been corrected for the contributions from He I satellites radiation.

The surface coverage with the thiophene moieties was estimated using the same method as used in Ref. 17. This is done by calibrating the XPS S 2p signal of the thiophene moieties against the measured XPS S 2p intensity of a dodecanethiol SAM on Au, where the coverage of the latter was assumed to be 100% (1 ML) (Figure 4.3). Several samples of dodecanethiol SAMs were prepared on Au, i.e. at different functionalization times, to make sure the same S 2p signal was obtained by XPS. The S intensity in dodecanethiol has been corrected for the attenuation factor due to the carbon chain.

$$\text{Attenuation factor} = \exp\left(\frac{-nd_c}{\lambda_s\cos\theta}\right) = 0.71 \qquad (4.1)$$

(n = 12 is the number of carbon atoms in the alkyl chain, d_C = 1.1 Å is the length of one methylene group (1.27 Å) at a tilt angle of 30° to the surface normal, θ is the angle made by the electron energy analyzer to the surface normal, and λ_S = 9.0 + 0.022 KE) [24]. All samples were measured with short collection time and on several different spots to avoid any beam damage. However, single-collected S2p data are shown here.

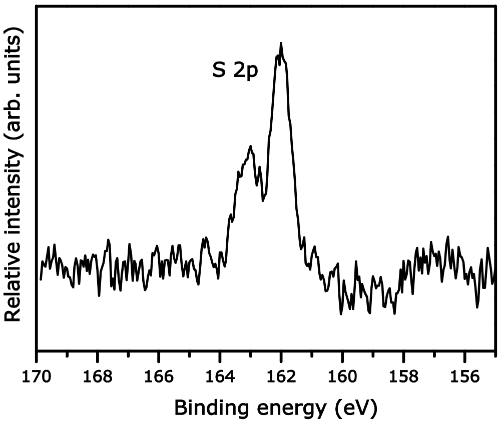

Figure 4.3 XPS spectra showing the S 2p signal of dodecanethiol on a Au surface.

4.3.8 Photoelectrochemical Measurements

Photoelectrochemical measurements were performed in a Ar-saturated 0.1 M Na_2SO_4 solution containing 5 mM methyl viologen (MV^{2+}) as an electron carrier in a three-electrode glass cell equipped with a quartz optical window for illumination of the B:NCD working electrode. The counter electrode was platinum and the reference electrode was Ag/AgCl (sat. KCl). The glass cell was placed in a dark room and controlled by a potentiostat (Autolab, Ecochemie, B.V. with GPES-4 software). The white light source was an Oriel Xenon lamp, model 6269. The incident light intensity was focused and calibrated with a standard Si photodiode (PV Measurements, Inc. USA). The area of the B:NCD samples exposed to light was ca. 0.85 cm^2 and the incident white light intensity was 15 mW/cm^2 (which is roughly 0.15 sun).

4.4 Results and Discussion

4.4.1 Synthesis and characterization

As shown in Figure 4.1, the anchoring of the molecular dyes onto the diamond surface begins with the functionalization of hydrogen-terminated B:NCD with arylboronic ester moieties through diazonium electrografting [16]. Two light-harvesting molecular dyes with a donor-acceptor structure (to increase light-harvesting and enhance charge separation), **Br-BT-Rho** and **Br-CPDT-Fur** (Figure 4.1), were pre-synthesized in solution before undergoing Suzuki coupling to the B:NCD surfaces. Both molecular dyes contain an electron-rich (bridged) bithiophene 'donor' part and an electron-deficient subunit and they carry a reactive arylbromide group on the donor part. As the B:NCD film is finally intended to be used as the hole conductor in photovoltaic devices, the donor part of the chromophores has to be attached to the diamond surface. The **Br-BT-Rho** chromophore was synthesized by reacting commercially available 5-bromo-5'-formyl-2,2'-bithiophene with rhodanine-3-acetic acid in a standard condensation reaction. On the other hand, the **Br-CPDT-Fur** molecule was synthesized according to the procedure outlined in Figure 4.4.

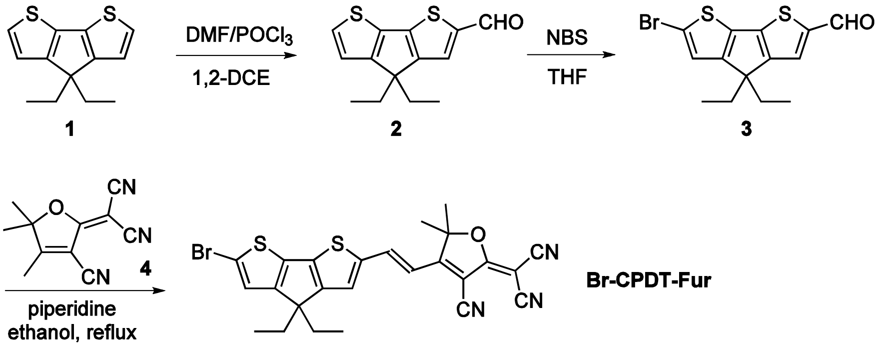

Figure 4.4 Synthetic protocol towards the **Br-CPDT-Fur** molecular wire.

4*H*-Cyclopenta[1,2-*b*:5,4-*b*']dithiophenes (CPDTs) have been proven to be attractive electron donating building blocks for applications in organic electronics due to the planarity of the bridged bithiophene system and the excellent charge transfer capabilities through the molecule [19] For the purpose of B:NCD functionalization, a novel CPDT chromophore has been developed, employing a furan group as the acceptor part attached to the CPDT core via a vinyl bridge. The synthesis of the CPDT core was done according to two different previously published procedures [19a, 21a]. CPDT formylation was performed using a standard Vilsmeier-Haack procedure in 1,2-dichloroethane at 0 °C. This reaction yielded exclusively monoformylated CPDT derivative **2**, which was used in the next step without prior purification. Treatment of CPDT-CHO **2** with *N*-bromosuccinimide (NBS) at room temperature furnished Br-CPDT-CHO derivative **3** in a smooth manner. To attach the furan acceptor, a Knoevenagel condensation reaction was performed in the presence of a catalytic amount of piperidine. The **Br-CPDT-Fur** dye precipitated from the hot reaction mixture and was recrystallized from the corresponding solvent and used as such. UV-Vis analysis (Figure A.1) of the dye showed a high extinction coefficient (ε = 73100 L mol^{-1} cm^{-1} at λ = 582 nm), thus proving suitability of the molecule for the envisaged application. The frontier orbital energy levels, as determined from the oxidation and reduction onsets derived from cyclic voltammetry (CV), are E_{HOMO} = -5.70 eV and E_{LUMO} = -4.03 eV. Figure A.2a and A.2b show the ^{1}H and ^{13}C NMR spectrum of **Br-CPDT-Fur**, respectively.

4.4.2 Diazonium Electrografting

Successful electrografting of the arylboronic ester groups on the B:NCD surface by the diazonium approach was confirmed by CV (Figure 4.5). The first CV cycle shows two reduction peaks. The broader peak at -0.6 V (vs Ag/AgCl) can be assigned to the formation of arylboronic ester radicals. During the second cycle, this reduction wave disappears and the cyclic voltammogram only exhibits a very small reduction current, which suggests passivation of the diamond surface by the grafted layer, hence blocking the access of the diazonium cations to the surface. A smaller reduction peak appearing at -0.1 V (vs Ag/AgCl) was previously noticed as well for electrografting of 4-nitrophenyl- and 4-carboxyphenyl-diazonium cations, but its origin is not yet clearly understood [7].

XPS spectra of the hydrogenated and arylboronic ester functionalized B:NCD films are shown in Figure 4.6. As can be seen clearly from the high-resolution XPS spectra (Figure 4.6b), the B 1s peak of the dopant boron atoms in B:NCD is

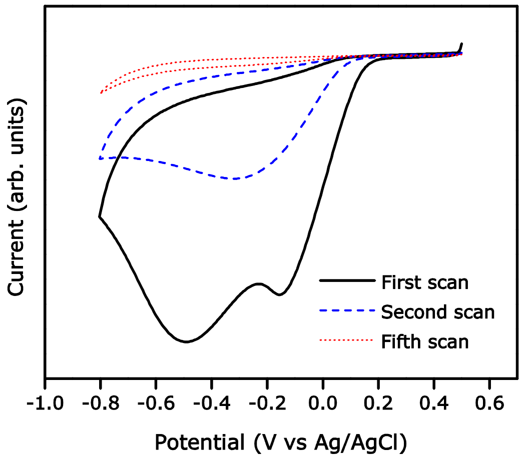

Figure 4.5 *In situ* electrochemical generation of boronic ester derivatized phenyldiazonium cations, showing five CV reduction cycles (first cycle, black solid line; second cycle, blue dashed line; fifth cycle, red dotted line) with applied voltage between +0.5 and -0.8 V (scan rate 100 mVs^{-1}).

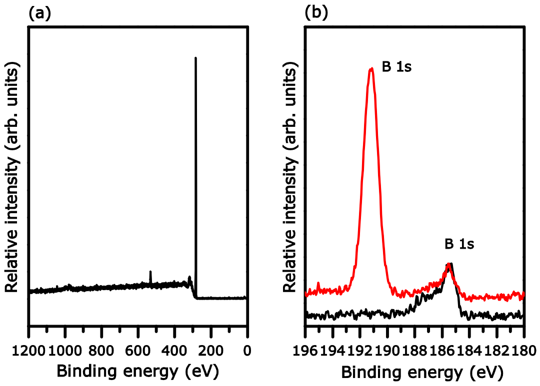

Figure 4.6 (a) XPS survey spectrum of hydrogenated B:NCD. (b) High-resolution XPS spectra showing the B 1s peaks for hydrogenated (black line) and arylboronic ester grafted B:NCD (red line), respectively.

found at ~186 eV (Figure 4.6b, black solid line). After electrografting of the arylboronic ester groups on the B:NCD surface, an additional intense signal appears at ~191 eV (Figure 4.6b, red solid line). This peak is assigned to the B 1s core level in boron atoms from the grafted arylboronic ester layer [16]. High-resolution XPS clearly shows the presence of two chemically distinct boron species.

4.4.3 Suzuki cross-coupling

The arylboronic ester surface provides an excellent solid phase platform for further C-C extension via Suzuki cross-coupling. As such, an ‘all-carbon’ molecular photovoltaic system could be realized. However, a diamond surface with high chromophore loading is required for this purpose and this high coverage is not trivially obtained. To tackle this, a careful search for the optimum Suzuki conditions on arylboronic ester functionalized B:NCD was conducted. Table 4.1 and 4.2 gather some of the different catalytic systems (changing the Pd catalyst, ligand, base and/or solvent) investigated for the two different chromophores (or their precursors). It should be mentioned at this point that the ‘opposite’ strategy, coupling 5-(5-formyl-2-thienyl)-2-thiopheneboronic acid ($(HO)_2B$-BT-CHO) to a bromophenyl decorated B:NCD surface (obtained via spontaneous grafting of 4-bromobenzenediazonium tetrafluoroborate), was employed as well, but the obtained results were inferior to the procedure outlined here.

Successful coupling was confirmed by monitoring the S and N markers present in the dye molecules by XPS (Figure 4.7). To determine the surface coverage, the S 2p peak intensities were calibrated against the XPS 2p intensity of a dodecanethiol self-assembled monolayer (SAM) on Au [17] where the coverage of the latter was assumed to be 1 ML (see Experimental). The coverages for both molecular dyes as determined by this method are listed in Table 4.1 and 4.2.

Table 4.1 Optimization of the Suzuki cross-coupling conditions for **Br-BT-CHO** and **Br-BT-Rho**.

Entry	Catalyst/Ligand[a]	Base	Solvent	Surface Coverage[b]	
				Br-BT-CHO[c]	**Br-BT-Rho**
1	$Pd(PPh_3)_4$ (10 mol%)	NaOAc (1 equiv)	THF	0.05	0.01
2	$Pd(PPh_3)_4$ (10 mol%)	Na_2CO_3 (4 equiv)	$THF:H_2O$ (5:1)	0.02	0.005
3	$Pd(OAc)_2$ (5 mol%) - $P(o\text{-tol})_3$ (10 mol%)	K_3PO_4 (5 equiv)	THF	0.03	/
4	$Pd(OAc)_2$ (5 mol%) - $P(o\text{-tol})_3$ (10 mol%)	CsOAc (1 equiv)	THF	0.05	/
5	$Pd(OAc)_2$ (5 mol%) - $P(o\text{-tol})_3$ (10 mol%)	CsF (1 equiv)	THF	Not successful	/
6	$Pd(OAc)_2$ (5 mol%) - $P(o\text{-tol})_3$ (10 mol%)	NaOAc (1 equiv)	THF	0.24	0.08
7	$Pd(OAc)_2$ (3 mol%) - SPhos (3 mol%)	K_3PO_4 (5 equiv)	dioxane:H_2O (5:1)	0.43	/
8	$Pd(OAc)_2$ (3 mol%) - SPhos (3 mol%)	CsOAc (2 equiv)	THF:MeOH (5:1)	0.36	0.58

[a] General conditions: 80 °C, 18 h, 6 mL solvent, 100 μmol Ar-Br. [b] The XPS S 2p intensity was used to estimate the surface coverage. [c] Precursor used as a model compound.

Table 4.2 Optimization of the Suzuki cross-coupling conditions for **Br-CPDT-CHO** and **Br-CPDT-Fur**.

Entry	Catalyst/Ligand[a]	Base	Solvent	Surface Coverage[b]	
				Br-CPDT-CHO[c]	**Br-CPDT-Fur**
1	$Pd(PPh_3)_4$ (10 mol%)	NaOAc (1 equiv)	THF	0.04	0.02
2	$Pd(OAc)_2$ (5 mol%) - P(*o*-tol)$_3$ (10 mol%)	NaOAc (1 equiv)	THF	/	0.06
3	$Pd(OAc)_2$ (5 mol%) - P(*o*-tol)$_3$ (10 mol%)	CsF (2 equiv)	THF:MeOH (5:1)	0.10	/
4	$Pd(OAc)_2$ (3 mol%) - SPhos (3 mol%)	K_3PO_4 (5 equiv)	dioxane:H_2O (5:1)	0.55	/
5	$Pd(OAc)_2$ (3 mol%) - SPhos (3 mol%)	CsF (2 equiv)	THF:MeOH (5:1)	0.06	/
6	$Pd(OAc)_2$ (3 mol%) - SPhos (3 mol%)	CsOAc (2 equiv)	THF:MeOH (5:1)	0.60	0.56

[a] General conditions: 80 °C, 18 h, 6 mL solvent, 100 µmol Ar-Br. [b] The XPS S 2p intensity was used to estimate the surface coverage. [c] Precursor used as a model compound.

When the standard catalytic system outlined in Entry 1 ($Pd(PPh_3)_4$, NaOAc, THF) was used, the obtained surface loadings (0.01 and 0.02 ML, respectively) were relatively low as compared to the results obtained by Zhong *et al.* [17] There are three possible reasons for the low surface coverage. First, the relative reactivity for the Suzuki cross-coupling is known to be R–I (Zhong and co-workers used an iodinated bithiophene) > R–Br >> R–Cl [25]. Secondly, $Pd(PPh_3)_4$ is known to be easily degrading, even in the presence of the smallest amount of oxygen, thus reducing the coupling efficiency [26]. Thirdly, for sterically demanding molecules as the two molecular dyes used here, catalytic systems with electron-rich ligands are often more appropriate [27].

A slightly better coverage was observed when an *in situ* generated Pd catalyst, via combination of tri(*o*-tolyl)phosphine (P(*o*-tol)$_3$) and palladium(II) acetate ($Pd(OAc)_2$), was used (Entry 6, Table 4.1; Entry 2, Table 4.2). The more electron-donating tri(*o*-tolyl)phosphine ligand enhances the oxidative insertion of Pd into the Ar-Br bond [27]. Moreover, the steric congestion of the ligand can also facilitate dissociation of the ligand from the Pd complex.

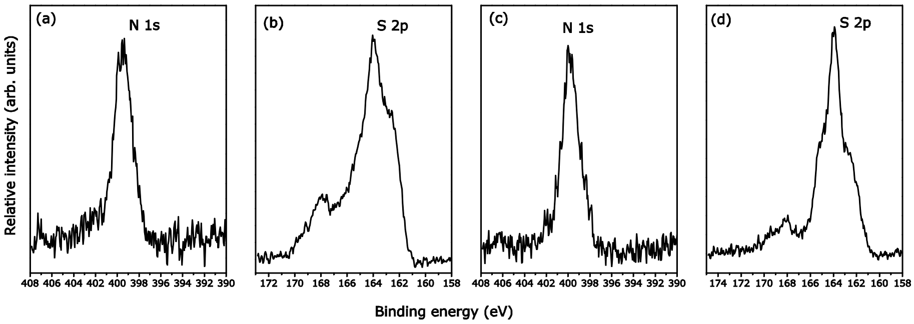

Figure 4.7 XPS spectra showing the N 1s and S 2p peaks for the **Br-CPDT-Fur** (a-b) (Table 4.2, Entry 6) and **Br-BT-Rho** (c-d) (Table 4.1, Entry 8) based molecular dyes (Pd(OAc)$_2$/SPhos catalytic system).

Over the past 20 years, the Buchwald group has made important contributions to the design of sterically hindered electron-rich biarylmonodentate phosphine ligands such as SPhos and XPhos (2-dicyclohexylphosphino-2’,4’,6’-triisopropylbiphenyl) which, when combined with catalytic amounts of Pd(0), enable to prepare extremely hindered biaryls via Suzuki-Miyaura cross-coupling reactions in an efficient manner [28]. Recently, Zhou *et al.* successfully applied these conditions towards extension of the CPDT chromophore [29]. Triggered by the effectiveness of the method and the similar CPDT building blocks used, we applied this catalytic system to the Suzuki cross-coupling on the B:NCD surface. Zhou and co-workers applied a dioxane:water mixture as the reaction solvent and K_3PO_4 as a base. This catalytic system might, however, cleave our acceptor groups from the molecular dyes due to hydrolysis. We thus first tested the catalytic system for two ‘precursor’ systems (**Br-BT-CHO** and **Br-CPDT-CHO**) devoid of the respective acceptor groups. As shown in Table 4.1 (Entry 7) and Table 4.2 (Entry 4), the surface coverages increased tremendously. When the

$Pd(OAc)_2$/SPhos catalyst was used in combination with CsOAc base in a water-free THF:MeOH (5:1) mixture (Entry 8, Table 4.1 and Entry 6, Table 4.2), a comparable surface coverage was achieved. Hence, these conditions were also applied for the full molecular wire systems. As illustrated in Table 4.1 (Entry 8) and 4.2 (Entry 6), the overall coupling efficiency was noticeably higher when SPhos was used as the supporting ligand. A surface coverage of 0.58 and 0.56 ML was achieved for the **Br-2T-Rho** and **Br-CPDT-Fur** chromophores, respectively, the highest reported surface coverages so far for Suzuki cross-coupling on B:NCD films (Figure 4.7). An increase in coverage of 17% is achieved despite the use of a less reactive Br-Ar function and a more complex molecular structure (0.56 ML for **Br-CPDT-Fur**) as compared to the results of Zhong and co-workers (0.41 ML for 2-(dicyanovinyl)-5-iodobithiophene) [17]. Moreover, the Pd catalyst usage is also quite low (3 mol%) as compared to standard $Pd(PPh_3)_4$, which requires a loading of 10 mol% [17].

4.4.4 Ultraviolet Photoelectron Spectroscopy (UPS)

UPS was applied to probe the electronic properties of the valence band of the functionalized B:NCD samples. Figures 4.8 (a) and (c) show the UPS spectra of the **Br-BT-Rho** and **Br-CPDT-Fur** functionalized B:NCDs, respectively, compared to the respective pure molecular wire systems (drop-casted on an Au substrate). When the UPS intensity is plotted on a logarithmic scale, the weak valence band feature can be distinguished. The first valence band peak for both Br-BT-Rho and Br-BT-Rho functionalized B:NCD appears around 0.9 eV. On the other hand, for Br-CPDT-Fur and Br-CPDT-Fur functionalized B:NCD, the first valence band peak appears around 1.1 eV.

To determine the HOMO energy levels of both molecular wire systems, the UPS spectra of the functionalized diamond films were compared to bare hydrogen-terminated B:NCD thin films (Figures 4.8 b, d). By linear extrapolation of the hydrogen-terminated B:NCD thin film UPS data, the position of the valence band

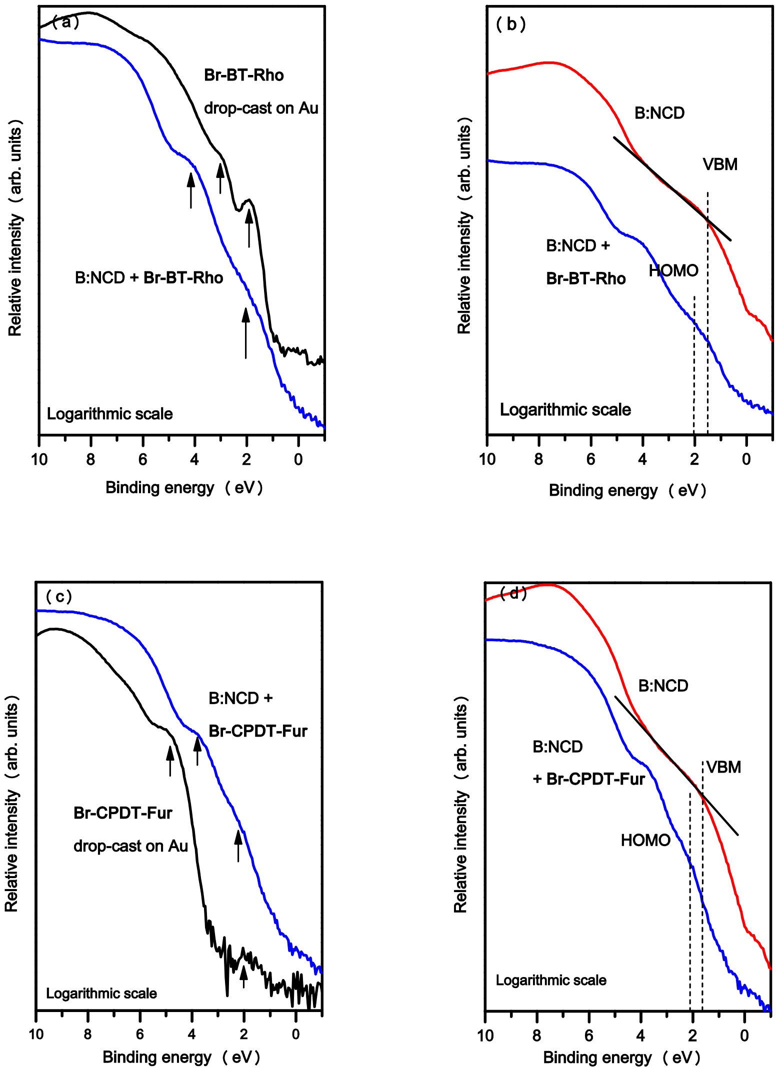

Figure 4.8 (a,c) Comparison of the UPS spectra of the molecular dye-functionalized B:NCDs (blue line) and the pure molecular dyes (drop-casted on an Au substrate) (black line) for (a) **Br-BT-Rho** and (c) **Br-CPDT-Fur** on an logarithmic scale. (b,d) Comparison of the UPS spectra of the molecular dye-functionalized B:NCDs (blue line) and a bare hydrogen-terminated B:NCD film (red line) for (b) **Br-BT-Rho** and (d) **Br-CPDT-Fur**. Linear extrapolation of the valence band edge yields an estimate of the VBM the of B:NCD thin film.

maximum (VBM) of diamond with respect to its Fermi level can be determined. It is approximately 0.6 eV below the (surface) Fermi level.

Previous studies have shown that E_F-VBM is 0.25 eV in bulk B-doped diamond. However, it can increase up to 0.7 eV at the surface of a clean H-terminated diamond [30 – 33]. Accordingly, the HOMO levels of the **Br-BT-Rho** and **Br-CPDT-Fur** functionalized diamond samples lie 0.3 and 0.5 eV below the VBM of B:NCD, respectively. These energy differences have implications on the possibility for hole transport between the B:NCD thin film and the functionalized molecular dyes. Based on the principle of charge transfer in dye-sensitized solar cells with p-semiconducting photocathode (p-DSSCs), upon photogeneration of an exciton, the electron is transferred to an acceptor site and subsequently to the oxidized form of the electrolyte redox mediator. In turn, the hole is transferred from the donor site to the semiconductor electrode. Hence, a good match between the HOMO of the donor molecule and the valence band of the electrode is important for efficient hole injection. For B:NCD, the VBM is situated rather close to the HOMO of both molecular dyes, which should favor hole injection from the light-harvesting chromophores to the B:NCD thin film [17, 33]

4.4.5 Photoelectrochemical Measurements

As a proof of concept, photoelectrochemical measurements were performed using either a hydrogen-terminated, **Br-CPDT-Fur** or **Br-BT-Rho** functionalized B:NCD film as the working electrode in a standard three-electrode electrochemical system (Figure 4.9). After equilibration in darkness, the light source was switched on and off approximately every 10 s for several cycles. At Time = 0, the electrode was in dark, and each light-on triggered the cathodic photocurrent. The process was fully reversible, and was stopped at Time ≈ 300 s, when the electrode was relaxed again in dark. We observed an increased photocurrent intensity for both molecular wire functionalized B:NCD electrodes as compared to the control system. In accord with previous work [17], negative bias enhances the photocurrent considerably. This agrees well with the mechanism that, upon light generation of electron-hole pairs in the molecular dyes, the separated electrons flow toward the MV^{2+} (dimethyl viologen) electron carrier and the holes toward the B:NCD electrode (at negative bias) [16,17]

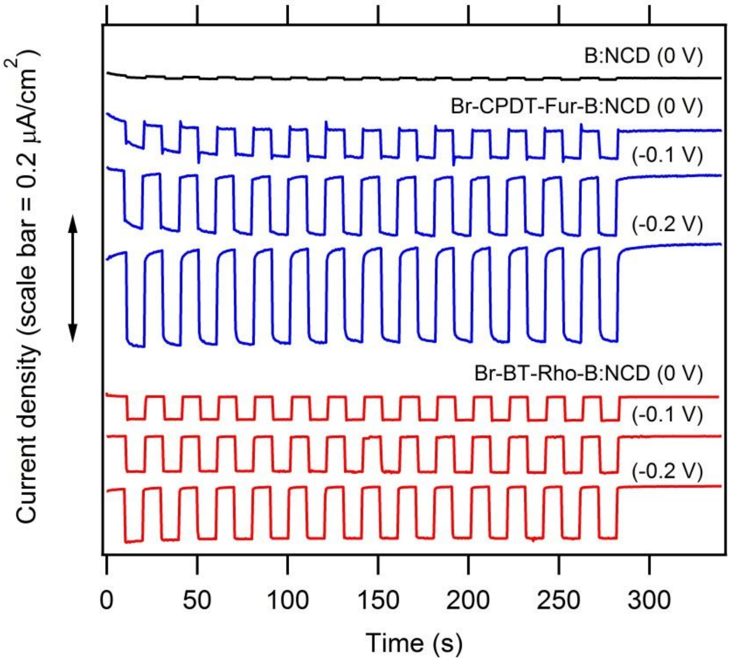

Figure 4.9 Photocurrent response of B:NCD (black line), **Br-CPDT-Fur**-B:NCD (blue lines), and **Br-BT-Rho**-B:NCD (red lines) electrodes in a 5 mM methyl viologen solution (in 0.1 M Na_2SO_4) at varying bias (vs Ag/AgCl). White light illumination by a Xe-lamp (15 mW/cm^2). Curves are offset for clarity, but the intensity scale is identical in all cases.

Our photocurrents are comparable to those reported earlier for similar systems: Zhong et al [16] observed a photocurrent of ca. 150 nA/cm^2 under white light (150 W halogen lamp) illumination of B:NCD sensitized by dicyanovinyl-bithiophene and C_{60}-bithophene. Later on, the same group reported ca. 4-6 µA/cm^2 under 1 sun illumination (AM1.5G; 100 mW/cm^2) [17]. In general, photocurrents on sensitized diamond electrodes are very small compared to those observed for the state-of-art n-DSSCs with titania photoanode (≈ 20 mA/cm^2 at 1 sun). Among other reasons, the difference can be rationalized in terms of surface morphology of the aforementioned semiconductor photoelectrodes. Early works on flat titania surface, sensitized with Ru-bipyridine complexes, reported photocurrents of several nA under white light ($450<\lambda/\mathrm{nm}<650$) illumination from a 150 W Xe-lamp [30]. In principle, the flat electrode cannot deliver external quantum efficiencies larger than ≈ 0.3%, whereas mesoporous electrodes can give values exceeding 90% for the same dye/electrolyte systems [31]. The B:NCD films made by CVD are usually quite compact, with double-layer capacitances approaching those of flat surfaces (ca. 3 $\mu F/cm^2$) [32]. Also our SEM image shown below (Figure 4.2) confirms quite dense packing of the diamond crystals without any noticeable mesoporosity. Hence, surface engineering of the B:NCD photocathode is a straightforward task in the future development of diamond-based p-DSSCs.

4.5 Conclusions

In summary, we have demonstrated that a proper choice of the catalytic system used for Suzuki cross-coupling can effectively increase the coupling efficiency, also on a diamond surface. Best results, leading to unprecedented surface loadings, were obtained for the $Pd(OAc)_2$/SPhos combination. The resulting B:NCD films decorated with light-harvesting molecular dyes can potentially be applied for ‘all-carbon’ photovoltaic applications. Preliminary photoelectrochemical measurements using the novel molecular wire systems show photocurrent generation. More detailed studies concerning full devices and quantum efficiencies will be carried out and reported in near future.

4.6 Acknowledgements

This work was financially supported by the Special Research Fund of Hasselt University, the Research Foundation Flanders (FWO) (G.0555.10N), and the EU FP7 Collaborative Project “MOLESOL” (No. 256617). X.L. acknowledges support from The Swedish Research Council Linnaeus grant LiLi-NFM. L.K. acknowledges support from the Grant Agency of the Czech Republic (contract No. 13-31383S). We thank Huguette Penxten for the cyclic voltammetry measurements.

4.7 References

1. (a) Williams, O.; Nesladek, M.; Mares, J. J.; Hubik, P., Growth and Properties of Nanocrystalline Diamond Films. In: *Physics and Applications of CVD Diamond*; Koizumi, S.; Nebel, C.; Nesladek, M., Eds.; Wiley-VCH: Weinheim, Germany, **2008**; pp 13-27.; (b) Janssens, S. D.; Pobedinskas, P.; Vacik, J.; Petrakova, V.; Ruttens, B.; D'Haen, J.; Nesladek, M.; Haenen, K.; Wagner, P., Separation of Intra- and Intergranular Magnetotransport Properties in Nanocrystalline Diamond Films on The Metallic Side of The Metal-Insulator Transition. *New J. Phys.* **2011**, *13*, 083008.

2. Williams, O. A.; Nesladek, M.; Daenen, M.; Michaelson, S.; Hoffman, A.; Osawa, E.; Haenen, K.; Jackman, R. B., Growth, Electronic Properties and Applications of Nanodiamond. *Diam. Relat. Mater.* **2008**, *17*, 1080.

3. Lim, C. H. Y. X.; Zhong, Y. L.; Janssens, S.; Nesladek, M.; Loh, K. P., Oxygen-Terminated Nanocrystalline Diamond Film as an Efficient Anode in Photovoltaics. *Adv. Funct. Mater.* **2010**, *20*, 1313.

4. (a) Balmer, R. S.; Brandon, J. R.; Clewes, S. L.; Dhillon, H. K.; Dodson, J. M.; Friel, I., Inglis, P. N.; Madgwick, T. D.; Markham, M. L.; Mollart, T. P.; Perkins, N.; Scarsbrook, G. A.; Twitchen, D. J.; Whitehead, A. J.; Wilman, J. J.; Woollard, S. M., Could One Make A Diamond-Based Quantum Computer? *J. Phys. Condens. Mat.* **2009**, 21, 36422; (b) Kirste, A.; Schnakenburg, G.; Stecker, F.; Fischer, A.; Waldvogel, S. R. Anodic Phenol-Arene Cross-Coupling Reaction on Boron-Doped Diamond Electrodes. *Angew. Chem. Int. Ed.* **2010**, *49*, 971; (c) Wang, Q.; Subramanian, P.; Li, M. S.; Yeap, W. S.; Haenen, K.; Coffinier, Y.; Boukherroub, R.; Szunerits, S., Non-Enzymatic Glucose Sensing On Long and Short Diamond Nanowire Electrodes. *Electrochem. Commun.* **2013**, *34*, 286; (d) Inagi, S.; Nagai, H.; Tomita, I.; Fuchigami, T. Parallel Polymer Reactions of a Polyfluorene Derivative by Electrochemical Oxidation and Reduction. *Angew. Chem. Int. Ed.* **2013**, *52*, 6616; (e) Read, T. L.; Bitziou, E.; Joseph, M. B.; Macpherson, J. V., In Situ Control of Local pH Using a Boron Doped Diamond Ring Disk Electrode: Optimizing Heavy Metal (Mercury) Detection. *Anal. Chem.* **2014**, *86*, 367; (f) Nakata, K.; Ozaki, T.; Terashima, C.;

Fujishima, A.; Einaga, Y., High-Yield Electrochemical Production of Formaldehyde from CO2 and Seawater. *Angew. Chem. Int. Ed.* **2014**, *53*, 871.

5. Wang, X. Y.; Landis, E. C.; Franking, R.; Hamers, R. J., Surface Chemistry for Stable and Smart Molecular and Biomolecular Interfaces via Photochemical Grafting of Alkenes. *Acc. Chem. Res.* **2010**, *43*, 1205.

6. Wang, X.; Kurihara, S.; Hasegawa, M.; Ruslinda, A. R.; Kawarada, H., High Priority of Nanocrystalline Diamond as a Biosensing Platform. *Jpn. J. Appl. Phys.* **2012**, *51*, 090125.

7. Belanger, D.; Pinson, J., Electrografting: A Powerful Method for Surface Modification. *Chem. Soc. Rev.* **2011**, *40*, 3995.

8. Lahann. J., Click Chemistry: A Universal Ligation Strategy for Biotechnology and Materials Science. In *Click Chemistry for Biotechnology and Materials Science;* Lahann, J., Eds.; John Wiley & Sons Ltd: West Sussex, **2009**; pp 1-8.

9. Miyaura, N.; Suzuki, A., Palladium-Catalyzed Cross-Coupling Reactions of Organoboron Compounds. *Chem. Rev.* **1995**, *95*, 2457.

10. Bujak, P.; Kulszewicz-Bajer, I.; Zagorska, M.; Maurel, V.; Wielgus, I.; Pron, A., Polymers for electronics and spintronics. *Chem. Soc. Rev.* **2013**, *42*, 8895.

11. Pron, A.; Gawrys, P.; Zagorska, M.; Djurado, D.; Demadrille, R., Electroactive Materials for Organic Electronics: Preparation, Strategies, Structural Aspects and Characterization Techniques. *Chem. Soc. Rev.* **2010**, *39*, 2577.

12. (a) Bijleveld, J. C.; Shahid, M.; Gilot, J.; Wienk, M. M.; Janssen, R. A. J., Copolymers of Cyclopentadithiophene and Electron-Deficient Aromatic Units Designed for Photovoltaic Applications. *Adv. Funct. Mater.* **2009**, 19, 3262; (b) Watters, D. C.; Yi, H.; Pearson, A. J.; Kingsley, J.; Iraqi, A.; Lidzey, D., Fluorene-Based Co-polymer with High Hole Mobility and Device Performance in Bulk Heterojunction Organic Solar Cells. *Macromol. Rapid Commun*. **2013**, 34, 1157.

13. Wu, W.; Huang, L.; Xiao, L.; Huang, Q.; Tang, R.; Ye, C.; Qin, J.; Li, Z., New Second-Order Nonlinear Optical (NLO) Hyperbranched Polymers Containing Isolation Chromophore Moieties Derived from One-Pot "A(2)+B-4" Approach via Suzuki Coupling Reaction. *RSC Adv.* **2012**, *2*, 6520.

14. (a) Cheng, F.; Adronov, A., Suzuki Coupling Reactions for the Surface Functionalization of Single-Walled Carbon Nanotubes. *Chem. Mater.* **2006**, *18*, 5389; (b) Gao, J.; Bao, F.; Zhu, Q.; Tan, Z.; Chen, T.; Cai, H.; Zhao, C.; Cheng, Q.; Yang, Y.; Ma, R., Attaching Hexylbenzene and Poly(9,9-dihexylfluorene) to Brominated Graphene via Suzuki Coupling Reaction. *Polym. Chem.* **2013**, *4*, 1672.

15. Hasobe, T.; Imahori, H.; Yamada, H.; Sato, T.; Ohkubo, K.; Fukuzumi, S., Enhancement of Light Harvesting and Photocurrent Generation by ITO Electrodes Modified with Meso,meso-linked Porphyrin Oligomers. *Nano Lett.* **2003**, *3*, 409.

16. Zhong, Y. L.; Loh, K. P.; Midya, A.; Chen, Z. K., Suzuki Coupling of Aryl Organics on Diamond. *Chem. Mater.* **2008**, *20*, 3137.

17. Zhong, Y. L.; Midya, A.; Ng, Z.; Chen, Z. K.; Daenen, M.; Nesladek, M.; Loh, K. P., Diamond-Based Molecular Platform for Photoelectrochemistry. *J. Am. Chem. Soc.* **2008**, *130*, 17218.

18. Yeap, W. S.; Chen, S.; Loh, K. P., Detonation Nanodiamond: An Organic Platform for the Suzuki Coupling of Organic Molecules. *Langmuir* **2009**, 25, 185.

19. (a) Peet, J.; Kim, J. Y.; Coates, N. E.; Ma, W. L.; Moses, D.; Heeger, A. J.; Bazan, G. C., Efficiency Enhancement in Low-Bandgap Polymer Solar Cells by Processing with Alkane Dithiols. *Nat. Mater.* **2007**, 6, 497; (b) Li, R.; Liu, J.; Cai, N.; Zhang, M.; Wang, P., Synchronously Reduced Surface States, Charge Recombination, and Light Absorption Length for High-Performance Organic Dye-Sensitized Solar Cells. *J. Phys. Chem. B* **2010**, 114, 4461; (c) Tsao, H. N.; Cho, D. M.; Park, I.; Hansen, M. R.; Mavrinskiy, A.; Yoon, D. Y.; Graf, R.; Pisalu, W.; Spiess, H. W.; Müllen, K., Ultrahigh Mobility in Polymer Field-Effect Transistors by Design. *J. Am. Chem. Soc.* **2011**, 133, 2605; (d) Van Mierloo, S.; Hadipour, A.; Spijkman, M.; Van den Brande, N.; Ruttens, B.; Kesters, J.; D’Haen, J.; Van

Assche, G.; de Leeuw, D. M.; Aernouts, T.; Manca, J.; Lutsen, L.; Vanderzande, D.; Maes, W., Improved Photovoltaic Performance of a Semicrystalline Narrow Bandgap Copolymer Based on 4*H*-Cyclopenta[2,1-*b*:3,4-*b′*]dithiophene Donor and Thiazolo[5,4-*d*]thiazole Acceptor Units. *Chem. Mater.* **2012**, 24, 587; (e) Gao, P.; Tsao, H. N.; Grätzel, M.; Nazeeruddin, M. K., Fine-tuning the Electronic Structure of Organic Dyes for Dye-sensitized Solar Cells. *Org. Lett.* **2012**, 14, 4330; (f) Marszalek, M.; Nagane, S.; Ichake, A.; Humprey-Baker, R.; Paul, V.; Zakeeruddin, S. M.; Grätzel, M., Structural variations of D–π–A Dyes Influence on the Photovoltaic Performance of Dye-sensitized Solar Cells. *RSC Adv.* **2013**, 3, 7921; (g) Delcamp, H. J.; Shi, Y.; Yum, J.; Sajoto, T.; Dell'Orto, E.; Barlow, S.; Nazeeruddin, M. K.; Marder, S. R.; Grätzel, M., The Role of π Bridges in High-Efficiency DSCs Based on Unsymmetrical Squaraines. *Chem. Eur. J.* **2013**, 19, 1819.

20. (a) Bard, A. L.; Faulkner, L. R., *Electrochemical Methods: Fundamentals and Applications*, John Wiley & Sons Inc: New York, **2001**; (b) Trasatti, S., The Absolute Electrode Potential: An Explanatory Note. *Pure Appl. Chem.* **1986**, 58, 955.

21. (a) Van Mierloo, S.; Adriaensens, P. J.; Maes, W.; Lutsen, L.; Cleij, T. J.; Botek, E.; Champagne, B.; Vanderzande, D. J., A three-step synthetic approach to asymmetrically functionalized 4H-cyclopenta[2,1-b:3,4-b']dithiophenes. *J. Org. Chem.* **2010**, 75, 7202; (b) Vanormelingen, W.; Verstappen, P.; Maes, V.; Bevk, D.; Lutsen, L.; Vanderzande, D.; Maes, W., Synthetic Routes toward Asymmetrically Substituted (Functionalized) 4H-Cyclopenta[2,1-b:3,4-b'] Dithiophenes. *Synlett.* **2013**, 24, 2389.

22. Ermer, S.; Lovejoy, S. M.; Bedworth, P. V.; Leung, D. S.; Warren, H. B.; Epstein, J. A.; Girton, D. G.; Dries, L. S.; Taylor, R. E.; Barto, R. R.; Eades, W.; Van Eck, T. E.; Moss, A. S; Anderson, W. W., Low-Voltage Electro-Optic Modulation Using Amorphous Polycarbonate Host Material. *Adv. Funct. Mater.* **2002**, 12, 605.

23. Gajewski, W.; Achatz, P.; Williams, O. A.; Haenen, K.; Bustarret, E.; Stutzmann, M.; Garrido, J. A., Electronic and Optical Properties of Boron-Doped Nanocrystalline Diamond Films. *Phys. Rev. B* **2009**, 79, 045206.

24. Laibinis, P. E.; Bain, C. D.; Whitesides, G. M., Attenuation of Photoelectrons in Monolayers of Normal-Alkanethiols Adsorbed on Copper, Silver, and Gold. *J. Phys. Chem.* **1991**, *95*, 7017.

25. Suzuki, A., Carbon-Carbon Bonding Made Easy. *Chem. Commun.* **2005**, 38, 4759.

26. (a) Billingsley, K. L.; Barder, T. E.; Buchwald, S. L., Palladium-Catalyzed Borylation of Aryl Chlorides: Scope, Applications, and Computational Studies. *Angew. Chem., Int. Ed.* **2007**, *46*, 5359; (b) Han, F., Transition-Metal-Catalyzed Suzuki-Miyaura Cross-Coupling Reactions: A Remarkable Advance from Palladium to Nickel Catalysts. *Chem. Soc. Rev.* **2013**, *42*, 5270.

27. Barder, T. E.; Walker, S. D.; Martinelli, J. R.; Buchwald, S. L., Catalysts for Suzuki-Miyaura Coupling Processes: Scope and Studies of The Effect of Ligand Structure. *J. Am. Chem. Soc.* **2005**, *127*, 4685.

28. Hartwig, J. F., Evolution of a Fourth Generation Catalyst for The Amination and Thioetherification of Aryl Halides. *Acc. Chem. Res.* **2008**, *41*, 1534.

29. Zhou, D. F.; Cai, N.; Long, H. J.; Zhang, M.; Wang, Y. H.; Wang, P., An Energetic and Kinetic View on Cyclopentadithiophene Dye-Sensitized Solar Cells: The Influence of Fluorine vs Ethyl Substituent. *J. Phys. Chem. C* **2011**, *115*, 3163.

30. Bandis, C.; Pate, B. B., Photoelectric Emission from Negative-Electron-Affinity Diamond (111) Surfaces: Exciton Breakup versus Conduction-Band Emission. *Phys. Rev. B* **1995**, 52, 12056.

31. Diederich, L.; Küttel, O. M.; Aebi, P.; Schlapbach, L., Electron Affinity and Work Function of Differently Oriented and Doped Diamond Surfaces Determined by Photoelectron Spectroscopy. *Surf. Sci.* **1998**, 418, 219.

32. Himpsel, F. J.; van der Veen, J. F.; Eastman, D. E., Experimental Bulk Energy Bands for Diamond Using *hv*-Dependent Photoemission. *Phys. Rev. B* **1980**, 22, 1967.

33. Zegkinoglou, I.; Cook, P. L.; Johnson, P. S.; Yang, W. L.; Guo, J. H.; Pickup, D.; Gonzalez-Moreno, R.; Rogero, C.; Ruther, R. E.; Rigsby, M. L.; Ortega, J. E.; Hamers, R. J.; Himpsel, F. J., Electronic Structure of Diamond Surfaces Functionalized by Ru(tpy)$_2$. *J. Phys. Chem. C* **2012**, *116*, 13877.

34. Dare-Edwards, M. P.; Goodenough, J. B.; Hamnett, A.; Seddon, K. R.; Wright, R. D., Sensitisation of Semiconducting Electrodes with Ruthenium-Based Dyes. *Discuss. Farad. Soc*. **1980**, 70, 285.

35. Kavan, L., Electrochemistry of Titanium Dioxide: Some Aspects and Highlights. *Chem. Record* **2012**, 12, 131.

36. Fujishima, A.; Einaga, Y.; Rao, T. N.; Tryk, D. A., Fundamental and Applied Aspects of Diamond Electrodes. In *Diamond Electrochemistry*; Fujishima, A.; Einaga, Y.; Rao, T. N.; Tryk, D. A., Eds.; Elsevier: Amsterdam, **2005**; pp 556-574.

Chapter 5

Boron-Doped Diamond Functionalization by an Electrografting - Alkyne-Azide Click Chemistry Sequence

Published in *CHEMELECTROCHEM, **1**, 1145–1154.* (2014)

W.S. Yeap[1], M.S. Murib[1], W. Cuypers[1], X. Liu[2], B. van Grinsven[1], M. Ameloot[3], M. Fahlman[2], P. Wagner[1,4], W. Maes[1,4], and K. Haenen[1,4]

[1] Hasselt University, Institute for Materials Research (IMO), B-3590 Diepenbeek, Belgium

[2] Linköping University, Department of Physics, Chemistry and Biology, S-58183 Linköping, Sweden

[3] Hasselt University, BIOMED, Agoralaan, B-3590 Diepenbeek, Belgium

[4] IMEC vzw, IMOMEC, B-3590 Diepenbeek, Belgium

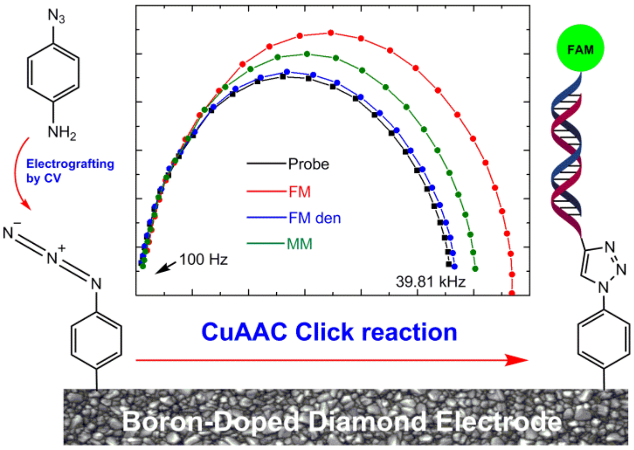

5.1 Abstract

A straightforward protocol for the covalent functionalization of boron-doped diamond electrodes with either ferrocene or single-stranded deoxyribonucleic acid (ss-DNA) is reported. The functionalization method is based on a combination of diazonium salt electrografting and click chemistry. An azide-terminated organic layer is first electrografted on the diamond surface by electrochemical reduction of 4-azidophenyldiazonium chloride. The azidophenyl-modified surface then reacts rapidly and efficiently with molecules bearing a terminal alkyne moiety by means of a Cu(I)-catalyzed alkyne-azide cycloaddition. Covalent attachment of ferrocene moieties was analyzed by means of X-ray photoelectron spectroscopy (XPS) and cyclic voltammetry (CV), whereas impedance spectroscopy was applied for the characterization of the immobilized DNA.

Keywords: azide, boron-doped diamond, click chemistry, diazonium electrografting, DNA

5.2 Introduction

Chemical Vapor Deposition (CVD) diamond recently receives great interest, both in science and technology [1]. The large attention for this material can be attributed to its outstanding properties such as biocompatibility [2], chemical inertness, hardness and excellent thermal conductivity [3]. Synthetic CVD diamond can be boron-doped during its growth and shows p-type conductivity. In case of heavy B-doping, for concentrations above ~3 x 10^{20} cm^{-3}, metal-like conductivity is observed [4]. Boron-doped diamond shows a negligible rate of water electrolysis over a wide potential range. Due to this wide potential window, CVD diamond surfaces are regarded as appealing electrodes [5].

Another particular advantage of CVD diamond surfaces is the fact that surface functionalization can be readily achieved. Various strategies have been successfully applied to derivatize diamond surfaces [6]. The well-known photochemical surface modification using vinyl derivatives is a promising method for stable immobilization of molecular monolayers linked to the diamond substrate by C-C bonds [7]. The mechanism proposed for such photochemical modification involves a photoemission-induced radical reaction, possibly enabled by the negative electron affinity of hydrogen-terminated diamond surfaces [8]. Even though this method is widely accepted, it requires long reaction times and an inert atmosphere. Surface functionalization through esterification on UV-ozone oxidized diamond, as demonstrated by the group of Boukherroub and Szunerits [9, 10], allows molecules bearing carboxylic acid end groups to attach on diamond surfaces. It is, however, quite hard to achieve a homogenous hydroxyl layer on the diamond surface, as UV-ozone oxidation usually creates other oxygen functionalities as well, such as carboxylic and carbonyl moieties [11]. One-step functionalization of amine derivatives on diamond surfaces was recently demonstrated by Agnes et al. [12] This rapid new grafting protocol is based on the high affinity of hydrogenated diamond towards primary amines. However, as stated, this procedure is limited to the coupling of (bio)molecules bearing a primary amine group. Several groups have also demonstrated the coupling of arenediazonium salts onto diamond surfaces [13], either by electrografting [14, 15] or spontaneous grafting [16]. Electrografting is more attractive since it requires a shorter reaction time [15]. In general, this potential assisted method offers several advantages: i) an instantaneous surface modification, generally requiring only a few seconds for the formation of a saturated monolayer; ii) it does not require an inert atmosphere for efficient reaction; and iii) an easy control over the functionalization degree (i.e. surface coverage) [15]. Electrografting on diamond surfaces has already been demonstrated for a variety of substituted aryl derivatives [13], but not for azidophenyldiazonium salts.

Recently, the search for more efficient and controlled strategies for the functionalization of conductive surfaces, at the molecular level, with biological [17], redox-active [18], or photo/chemical sensitive molecules has become a central interest in the development of molecular electronics [19], energy conversion systems [20], and chemical or biological sensors [21]. It has, however, been proven difficult to successfully realize the formation of these materials due to their inherent structural and functional properties [22]. Moreover, most coupling methods are hampered by the difficulty to introduce the required reactive groups, a lack of specificity, or a low yield [23]. Ligation strategies can offer a solution by interacting with specific kinds of functional groups. Click chemistry reactions can be seen as “the most advanced examples” providing a set of powerful, highly reliable and selective reactions [22]. The copper(I)-catalyzed alkyne-azide cycloaddition (CuAAC) reaction – 1,2,3-triazole formation through classical Huisgen 1,3-dipolar cycloaddition – is one of the most popular and renown click reactions [24]. This heterogenous coupling strategy was found to be fast, reproducible, with a minimum of side reactions, and highly tolerant to diverse reaction conditions. Click reactions have already been tested on various surfaces. For example, Arnold et al. recently demonstrated the clicking of 5-azidofluorescein to 4-(trimethylsilyl) ethynylstyrene polymer brushes that were grown on a silicon surface [25]. Grabosch *et al.* presented a 'dual click' strategy for the fabrication of bioselective glycosylated self-assembled monolayers as glycocalyx models [26]. They showed that their click reaction provides a rather mild surface immobilization with excellent coupling yields, versatility, regioselectivity, functional group tolerance, and stability of the catalytic process in different solvents and pHs.

In this work, we report on the modification of boron-doped CVD-grown diamond electrodes by electrografting an azidophenyl layer on the diamond surface through electrochemical reduction of the corresponding (*in situ* generated) 4-azidophenyldiazonium chloride salt, and subsequent chemoselective CuAAC coupling of terminal alkyne-bearing molecules. The surface coverage with reactive azide moieties was quantified electrochemically through complementary coupling of a simple redox-active probe, i.e. ethynylferrocene. Finally, the utility of the azide-functionalized diamond electrode for fast and efficient covalent attachment of a ss-DNA probe was demonstrated by reaction with an alkyne-functionalized DNA probe. The resulting device and its capability to work as a DNA-based sensor were evaluated by impedance spectroscopy. Due to the highly chemoselective nature of the alkyne-azide click reaction, azide-terminated boron-doped diamond electrodes can be regarded as a generic platform, providing a reliable coverage, for coupling with a wide range of ethynyl-terminated species of interest for various (sensing) applications.

5.3 Experimental

5.3.1 Chemicals and Reagents

Sodium nitrite, sodium acetate, 4-azidoaniline hydrochloride, 4-ethynylferrocene, tetrabutylammonium hexafluorophosphate ($TBAPF_6$), L-ascorbic acid (L-AA), and $CuSO_4.5H_2O$ were used as received from Sigma Aldrich. All these products were used at their highest purity and used without further purification. The DNA sample was customized, synthesized and purchased from Base Click (Purity 95-98%). The kit used for clicking DNA on diamond was also purchased from Base Click. The kit contains CuBr, tris(benzyltriazolylmethyl)amine (TBTA) ligand and a solvent mixture of *tert*-butanol (*t*-BuOH) and dimethylsulfoxide (DMSO) in 1:3 v/v%. The solvents used for rinsing were of technical grade. Acetonitrile (MeCN) used for the electrochemical work was of HPLC grade and was freshly distilled over CaH_2 prior to use. The water used for the electrochemical work was type 1 ultrapure water by Sartorius stedim biotech.

5.3.2 Preparation of the Substrates

Commercially available freestanding electrochemical grade boron-doped microcrystalline CVD diamond plates from Element Six (E6) with [B] ~10^{21} cm^{-3} [27] and home-grown boron-doped nanocrystalline diamond (NCD) thin films were used in this work. The latter were grown on fused silica substrates, which make them not suitable for our impedance measurements. As a result, the former is chosen for the impedance measurements and are referred to as B:MCD. The in-house deposited material is named as B:NCD in this article. Sheet resistances (R_s), as measured by four-point probe measurements for B:NCD and B:MCD, were 1.06 and 207 Ω sq^{-1}, respectively. B:NCD films were grown by microwave plasma-enhanced chemical vapor deposition from methane/hydrogen mixtures (1% CH_4) in an ASTeX 6500 reactor. The growth conditions used were as follows: substrate temperature 700-900 °C, total gas flow of 500 sccm, total pressure in the reactor 30 Torr, microwave power 3500 W. Trimethylborane gas was added during the growth with a ratio of 10000 ppm B/C to ensure good electrical conductivity [4].

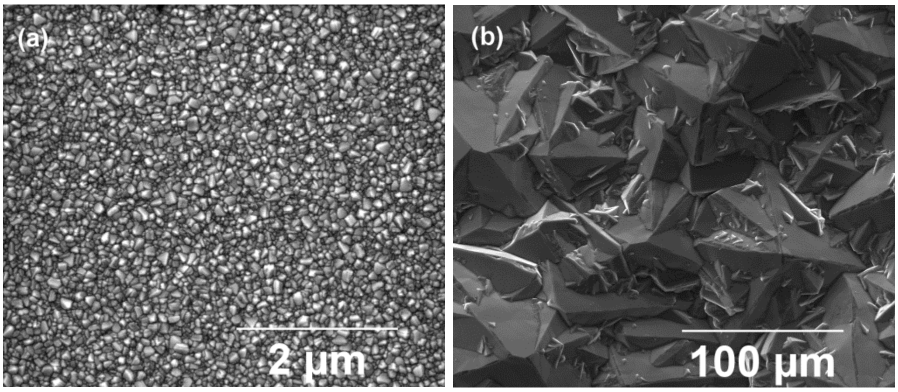

Figure 5.1 Typical SEM images of (a) B:NCD and (b) B:MCD films.

Based on previous experiments [28], this ratio corresponds to a boron film concentration 10^{21} cm^{-3}. Prior to the diamond growth, the fused silica substrates were cleaned for 15 min each in RCA 1 (30% NH_3 + 30% H_2O_2 + H_2O; 1:1:5) and RCA 2 (37% HCl + 30% H_2O_2 + H_2O; 1:1:5) solutions at 90 °C. Following this, the cleaned fused silica substrates were seeded with nanodiamond powder in water to improve the nucleation density [4]. After deposition, the diamond samples were allowed to cool down in the reactor for 30 min under a hydrogen flow. To remove any graphitic layers, the as-deposited diamond films were boiled in an acid mixture of 99% H_2SO_4 + 30% HNO_3 (3:1) at 90 °C for 30 min. After rinsing and sonicating thorougly with deionized water, the samples were subjected to hydrogenation. Figure 5.1 displays the scanning electron microscopy (SEM) images of (a) a typical as-grown 150 nm B:NCD thin film and (b) microcrystalline CVD diamond plates from Element Six (E6).

Hydrogenation on all diamond samples was performed using the same plasma-enhanced microwave CVD reactor that was used to grow the B:NCD. To create a hydrogen-terminated surface, all diamond samples were treated with hydrogen plasma under the following conditions: i) 500 sccm of hydrogen flux, 30 Torr reactor pressure with a 3500 W microwave power for 2 min; ii) 500 sccm of hydrogen flux, 15 Torr reactor pressure with a 2500 W microwave power for 5 min. At the end of the plasma treatment, the microwave power was switched off and the samples were allowed to cool down under hydrogen flux for 40 min. This hydrogenation step ensures full hydrogen termination and also serves to minimize dandling bonds [29].

5.3.3 In situ Generation of The Diazonium Salt

4-Azidoaniline (10 mg, 58.6 µmol) was used for the derivatization of the hydrogen-terminated diamond samples. It was diazotized with an equimolar amount of $NaNO_2$ (4 mg, 58.6 µmol) [13]. It was first dissolved in a N_2-purged 0.5 M HCl solution (9.5 mL). Thereafter, 0.1 M $NaNO_2$ solution (0.5 mL) was added, bringing the final concentration to 5 mM. This electrolytic solution was then used for the electrografting procedure by means of cyclic voltammetry (CV).

5.3.4 Electrografting of the Phenylazide Groups

Functionalization of the diamond surface with 4-azidophenyl groups via electrochemical reduction of the *in situ* generated diazonium salt was carried out by CV [14]. The electrografting reactions were performed with an Autolab PGSTAT30 potentiostat (Eco Chemie B.V.) and controlled by the GPES Manager program. A one-compartment electrochemical cell was used with three-electrode configuration. The working electrode was a hydrogen-terminated diamond electrode. A platinum wire and Ag/AgCl/KCl$_{(sat)}$ electrodes were used as the counter and reference electrodes, respectively. All potentials are reported versus this reference electrode at room temperature. Half of the diamond sample was immersed in the reaction solution for larger area functionalization. Optimization of the electrografting process was carried out with B:NCD. As outlined above, 5 mM of 4-azidoaniline was diazotized with an equimolar amount of $NaNO_2$ in a N_2-purged HCl solution which was directly used for cyclic voltammetric scanning with 3 different potentials [+0.5 to -0.1 V (vs Ag/AgCl); +0.5 to -0.8 V (vs Ag/AgCl) and +0.5 to -1.2 V (vs Ag/AgCl)] at a scan rate of 100 mV/s for 10 scans. After the modifications, the B:NCD samples were rinsed with and sonicated in ultrapure water. Finally, these samples were dried by means of a nitrogen flow. The samples are referred to as listed in Table 5.1. B:MCD was derivatized with phenylazide groups with a single fixed potential (+0.5 to -0.8 V vs Ag/AgCl).

Table 5.1 B:NCD samples and their sample codes.

Applied potential	**Sample code**
+0.5 to -0.1 V (vs Ag/AgCl)	EG 1
+0.5 to -0.8 V (vs Ag/AgCl)	EG 2
+0.5 to -1.2 V (vs Ag/AgCl)	EG 3

5.3.5 Clicking Ferrocene Groups to Phenylazide-Functionalized B:NCD

The 4-azidophenyl-functionalized B:NCD surface was reacted with ethynylferrocene through CuAAC click chemistry. $CuSO_4.5H_2O$ (1 mg, 4 μmol) and L-AA (1.5 mg, 8.5 μmol) were dissolved in ultrapure water (7.5 mL), while ethynylferrocene (6 mg, 28.6 μmol) was dissolved in isopropanol (7.5 mL). Next, these two solutions were mixed and the azide-terminated diamond sample was immersed in the solution mixture. The reaction vessel containing the diamond sample and the solution mixture was covered with aluminium foil to protect L-AA from light [9]. After the reaction, the diamond sample was washed and sonicated with ultrapure water to remove any unbound molecules and kept in a desiccator under vacuum.

5.3.6 Clicking the Alkyne-terminated ss-DNA Probe onto Phenylazide-functionalized B:MCD

B:MCD was first modified with phenylazide groups and then the custom-synthesized alkyne-modified ss-DNA probe (Base Click) was covalently attached to it through a CuAAC click reaction [30]. For this coupling reaction, a special reaction kit for click reactions from Baseclick was used [30]. The click reaction was performed according to the protocol provided with slight modifications. The ss-DNA probe was first diluted with ultrapure water to make a 1 mM stock solution. The TBTA ligand (1 mg, 2 μmol) and CuBr (5 mg, 35 μmol) were dissolved in the reaction solvent. The diluted ss-DNA probe, the TBTA ligand and CuBr were then mixed in a reaction vessel and more reaction solvent was added until the final concentration of ss-DNA, TBTA ligand and CuBr reached 10, 30, and 15 μM respectively. A 20 μL volume of this solution mixture was then pipetted onto the 4-azidophenyl-functionalized B:MCD surface and the reaction was continued for 12 h in the dark at room temperature. After the reaction, the diamond samples were rinsed and washed thoroughly with the reaction solvent and ethanol. The ss-DNA probe-functionalized diamond samples were kept at 4 °C in PBS (phosphate buffered saline) buffer (pH 7) when they were not in use.

5.3.7 Hybridization

Two different types of target DNA labeled with 6-carboxyfluorescein (FAM) (Eurogentec) were used, a sequence complementary to the probe ss-DNA and a sequence with a 1-base mismatch at base pair 20 (Table 5.2). A 6 µL solution of DNA (100 pmol/µL) was added to 14 µL of 1 × Polymerase Chain Reaction buffer (PCR-buffer, diluted from 10 × PCR-buffer, Roche Diagnostics). This 20 µL of DNA/PCR solution was then added to the probe DNA-functionalized diamond samples and incubated at 35 °C for 2 hours. After the hybridization, the samples were first washed with 2 x SSC/0.5 % SDS, then with 0.2 × SSC at 30 °C, thereafter with 0.2 × SSC at room temperature, and finally with 1 × PBS at room temperature [31].

Table 5.2 Base sequences of the probe and the corresponding full match and mismatch target DNA.

Name	Sequence
Probe DNA	5´-Alkyne-AAAAAAACCCCTGCAGCCCATGTATACCCCCGAACC-3’
Full Match (FM)	5'-FAM-GGT TCG GGG GTA TAC ATG GGC TGC AGG GG-3'
Mismatch BP 20 (MM)	5'-FAM- GGT TCG GGG **C**TA TAC ATG GGC TGC AGG GG-3'

5.3.8 X-ray Photoelectronspectroscopy (XPS)

Photoemission experiments were carried out using a Scienta ESCA 200 spectrometer in ultrahigh vacuum with a base pressure of $1x10^{-10}$ mbar. The measurement chamber is equipped with a monochromatic Al Kα X-ray source (1486.6 eV). The XPS experimental conditions were set so that the full width at half maximum of the clean Au $4f_{7/2}$ line was 0.65 eV. All spectra were measured at a photoelectron take-off angle of 0°, i.e. normal emission, and at room temperature.

5.3.9 Water Contact Angle Measurements

A droplet of water (0.5 µL) was deposited onto the surface to be studied. Contact angle measurements were performed with an OCA 15 EC contact angle measuring instrument by Data Physics.

5.3.10 Electrochemical Measurements

CV was used for the analysis of the ferrocene moieties after the click reaction. CV was carried out with an Autolab PGSTAT30 potentiostat (Eco Chemie B.V.) and controlled by the GPES Manager program. All measurements were performed in a one-compartment cell with three-electrode configuration. A sample with an area of 0.5 cm^2 was immersed into the electrolyte solution or measurement solution. The electrochemical measurements were performed in freshly distilled acetonitrile (over CaH_2). $TBAPF_6$ was added as a supporting electrolyte. The electrolytic solution was purged with N_2-gas for 5 min prior to the electrochemical measurements, eliminating traces of oxygen in the CV experiments.

5.3.11 Impedance Spectroscopy

Impedance measurements were carried out with a home-built two electrode miniaturized impedance spectroscopy unit [32]. A transparent Perspex flow cell with an inner volume of 110 µL was used to exchange media. In this cell, the diamond sample acts as a working electrode and a gold wire (diameter 500 mm) acts as a counter electrode. The working electrode was pressed onto a copper lid using silver paste. The copper lid serves as a back electrode as well as heat sink. All impedance spectroscopy experiments were performed at the open-circuit potential with a 10 mV modulation, in PBS solution (pH 7) without any added redox agents. Under these conditions, there is no oxidation-reduction chemistry taking place, and the measurements are only measuring the intrinsic electrical properties of the interface. The full frequency spectrum of the impedimetrical data (100 Hz to 100 kHz) for DNA-modified diamond surfaces can be simulated with a 5-element circuit consisting of a resistor, representing the bulk solution inside the flow cell, in series with two complex resistors, representing the molecular layer and space-charge region, respectively [33]. This circuit is shown in Figure 5.2.

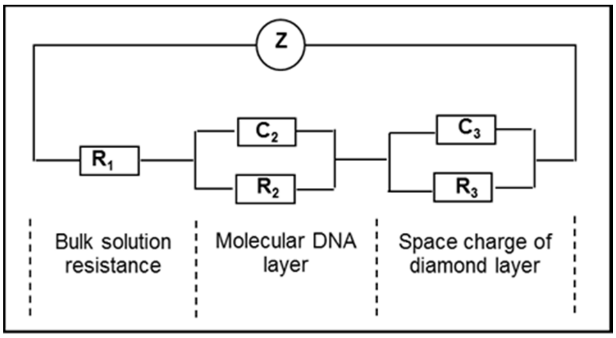

Figure 5.2 Circuit model used to analyze Cole-Cole plots.

5.3.12 Confocal Microscopy

Fluorescence images were taken on a Zeiss LSM 510 META Axiovert 200 M laser scanning confocal fluorescence microscope. To excite the FAM fluorescence dye, a 488 nm argon-ion laser was used with a maximum intensity at the sample surface of 30 µW, to avoid bleaching during the image acquisition. The fluorescent intensity was collected using a long pass filter 505 nm. The following filter sets were used: MBS HFT 488, DBS NFT 490, or mirror. All images were collected with a 10×/0.3 Plan Neofluar air objective with a working distance of 5.6 mm. The image size was 225 by 225 μm^2. The pinhole size was 150 µm. The detector gain, being a measure for the photomultiplier voltage in arbitrary units, was set to 950. The fluorescent intensity was analyzed using ImageJ software [31].

5.4 Results and Discussion

5.4.1 Electrografting of Phenylazide Groups

As shown in Figure 5.3, 4-azidophenyldiazonium chloride is formed *in situ* by diazotization when hydrochloric acid and sodium nitrite solutions are added to 4-azidoaniline [14]. Application of a potential reduces the diazonium salt to a radical species [15]. As the density and thickness of the functionalized layer depend on the potential applied [15, 34], we analyzed the effect of the potential on the formation of the 4-azidophenyl layer.

Commercially available freestanding electrochemical grade boron-doped microcrystalline CVD diamond plates from Element Six (E6) and home-grown boron-doped nanocrystalline diamond (NCD) thin films were used in this work. The latter were grown on fused silica substrates, which make them not suitable for our impedance measurements later. As a result, the former is chosen for the impedance measurements and are referred to as B:MCD. The in-house deposited material is named as B:NCD in this article. Figure 5.4 shows the cyclic voltammograms of three boron-doped nanocrystalline diamond (B:NCD) samples that underwent electrografting. Each sample was subjected to a different potential scan (cfr. Table 5.1, exp. section). The cyclic voltammogram of diamond sample EG 1 (Figure 5.4a) did not show any peak that can be related to the electroreduction of the diazonium salt, indicating that the diamond sample was not functionalized. When we applied a more negative potential (up to -0.8 V, sample EG 2), a broad irreversible reduction peak appeared during the first scan, which disappeared on the second scan (as indicated by the arrow in Figure 5.4b). This reduction peak can be related to the formation of radicals upon electroreduction of the diazonium salt [14, 15]. The disappearance of the reduction peak during the second scan (Figure 5.4b, blue line) is due to the passivation of the diamond surface by the electrochemically grafted organic layer, blocking the access of the diazonium cations to the electrode surface [15].

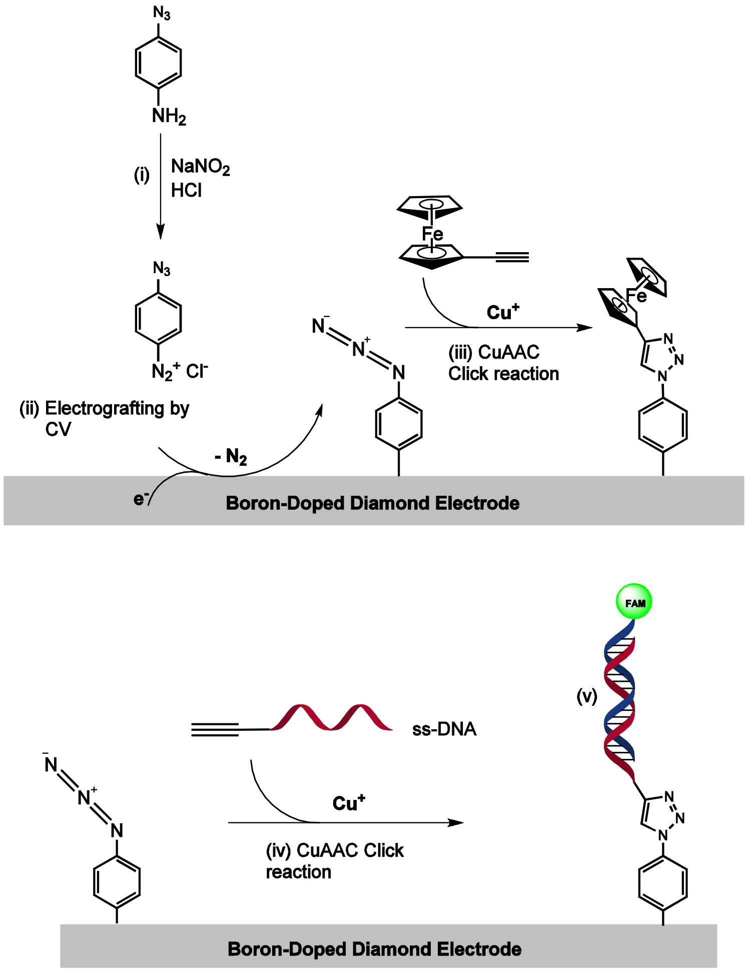

Figure 5.3 Illustration of the multistep functionalization of boron-doped diamond electrodes: i) Diazotization; ii) Electroreduction of the diazonium salt for electrografting of phenylazide molecules; iii) Cu(I)-catalyzed Huisgen 1,3-dipolar cycloaddition between the immobilized phenylazide molecules and ethynylferrocene; iv) Cu(I)-catalyzed Huisgen 1,3-dipolar cycloaddition between the immobilized phenylazide molecules and ss-DNA; v) Hybridization with fluorescein-labeled (FAM) target DNA molecules.

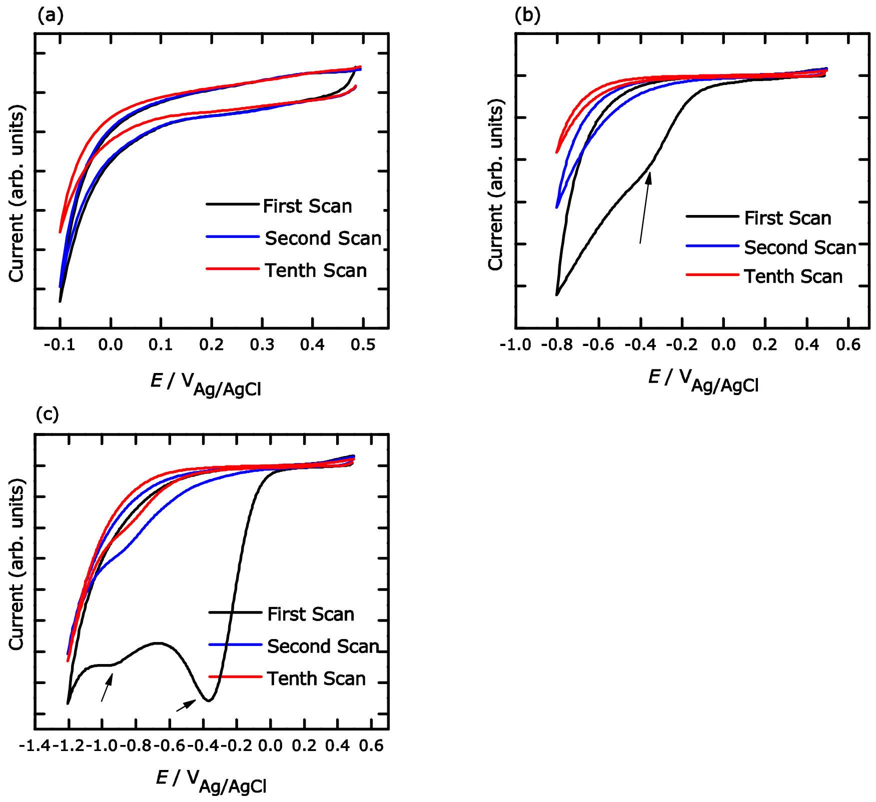

Figure 5.4 *In situ* electrochemical generation of 4-azidoaniline-derivatized aryl diazonium salts onto hydrogenated B:NCD samples, showing first, second and tenth CV reduction cycles with applied potential between a) +0.5 and -0.1 V; b) +0.5 and -0.8 V; c) +0.5 and -1.2 V at a scan rate of 100 mVs^{-1}.

When an even more negative potential (up to -1.2 V, sample EG 3) was applied, two reduction peaks clearly appeared (Figure 5.4c). Besides the broad irreversible reduction peak at -0.4 V, which indicates the presence of radicals, a smaller reduction peak appeared at around -0.9 V. Cycling to a more negative potential leads to the formation of anions by further reduction of the formed radicals [15].

5.4.2 Clicking Ferrocene Groups to Phenylazide-functionalized B:NCD

4-Ethynylferrocene was chosen as a model molecule to couple to the 4-azidophenyl-functionalized B:NCD with the intention to confirm the presence of the phenylazide groups and to demonstrate that the click reaction can effectively be carried out on this functionalized surface. The three different diamond samples EG 1–3 were all subjected to a CuAAC click reaction with ethynylferrocene in the presence of $CuSO_4.5H_2O$ and L-ascorbic acid (L-AA). The presence of the ferrocene groups after the click reaction was probed by CV in a solution of 0.1 M tetrabutylammonium hexafluorophosphate ($TBAPF_6$) in acetonitrile (MeCN). As shown in Figure 5.5, ferrocene groups could be observed for the EG 2 (red line) and EG 3 (blue line) diamond samples, with a redox peak $E°$ = ~ 0.19 V *vs.* $Ag/AgNO_3$ and a peak separation of ΔE = 37 mV (for both samples). The bound ferrocene moieties show a similar redox potential as compared to a ferrocene-modified crystalline silicon ($E°$ = ~ 0.15 V *vs.* Ag/AgCl) electrode [35]. It is known that the width of the current peaks depends strongly on the distribution of the individual ferrocenes.

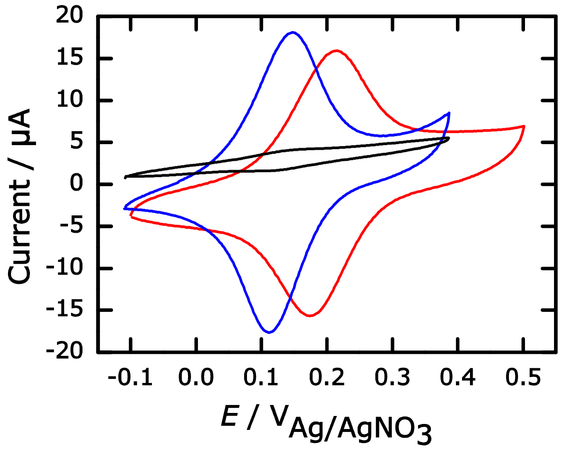

Figure 5.5 Cyclic voltammograms of diamond samples EG 1 (black line), EG 2 (red line), and EG 3 (blue line) after click reaction with ethynylferrocene in $TBAPF_6$ (0.1 M in MeCN), scan rate 100 mVs^{-1}.

For identical and non-interacting ferrocenes, the ideal full width at half-maximum (FWHM) is 90 mV [36]. The EG 2 and EG 3 samples show an FWHM of 125 and 127 mV, respectively.From these values, we conclude that the ferrocene entities formed are not significantly aggregated and are subject to almost identical redox conditions [36].

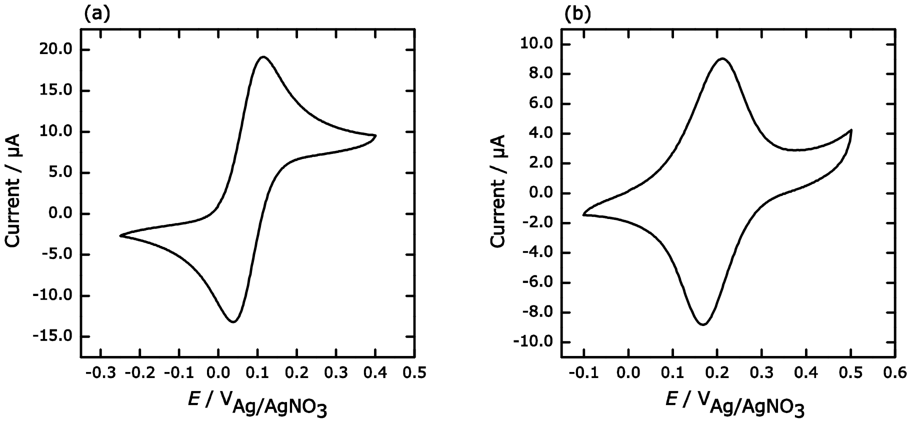

Figure 5.6 Cyclic voltammograms of (a) ferrocene in $TBAPF_6$ (0.1 M in MeCN) at a Pt-disc electrode, and (b) a ferrocene-terminated -B:NCD surface (EG 2) in $TBAPF_6$ (0.1 M in MeCN) (scan rate 100 mVs^{-1}).

The anodic-cathodic peak separation gives the first evidence that the ferrocene groups are covalently bound onto the diamond surface after the click reaction. As shown in Figure 5.6b, the peak separation (ΔE_p) for the EG 2 sample was 37 mV at a potential sweep rate of 100 mVs^{-1}, much smaller than the peak separation for a diffusion-controlled one-electron reversible redox system (Figure 5.6a, 59 mV) [37]. Results similar to those obtained with a ferrocene-modified diamond electrode prepared by a photochemical method were obtained [38]. The electron transfer mechanism for surface-bound redox active species depends on charge-transfer rather than diffusion-controlled kinetics [37].

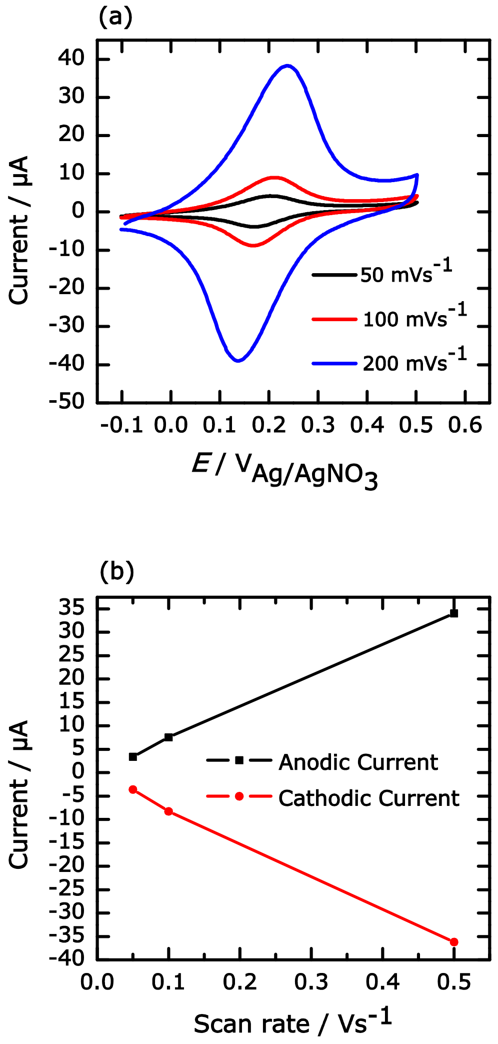

Figure 5.7 (a) Cyclic voltammograms of a ferrocene-functionalized HG-BDD surface in $TBAPF_6$ (0.1 M in MeCN), scan rate 50 mVs^{-1} (black), 100 mVs^{-1} (red), and 200 mVs^{-1} (blue). (b) Peak current as a function of scan rate for anodic (■) and cathodic (●) peak currents.

An analysis of the change in peak currents as a function of scan rate allows additional assessment of the fact that the ferrocene groups are surface-bound rather than physically adsorbed. Figure 5.7b shows that there is a linear relationship between either the anodic or cathodic peak current and the scan rate (*v*), suggesting a fast charge transfer process of the bonded ferrocene molecules with the electrode surface [10, 37, 38]. This characteristic points to a surface redox process controlled by charge transfer kinetics. A similar behavior has also been observed for ferrocenecarboxylic acid-modified single-crystal Si(111) surfaces [35] and ferrocene-based alkanethiol layers on gold [39]. The electrochemical stability of the ferrocene-functionalized B:NCD sample (EG 2) was examined by successive potential cycling in $TBAPF_6$ (0.1 M in MeCN) from -0.1 to +0.5 V *vs* $Ag/AgNO_3$ with a potential sweep rate of 100 mVs^{-1}. Figure 5.8 shows that the oxidation and reduction peaks are still clearly visible after 200 scans. Only a small decrease of the anodic peak height (~26%) is observed. This indicates that a strong covalent bond is formed between the ferrocene molecules and the 4-azidophenyl-functionalized diamond surface.

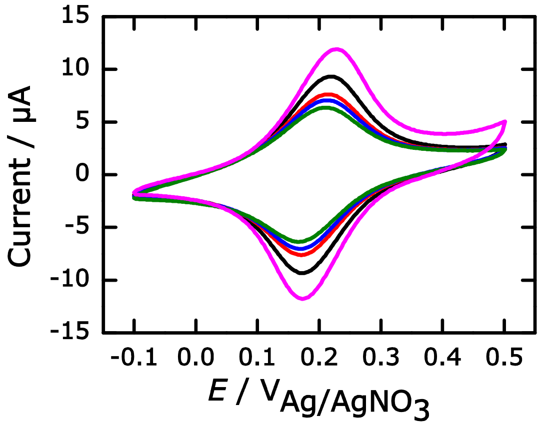

Figure 5.8 Cyclic voltammograms of ferrocene-functionalized B:NCD (EG 2) showing the 1st scan (pink line), 50th scan (black line), 100th scan (red line), 150th scan (blue line), and 200th scan (green line) in $TBAPF_6$ (0.1 M in MeCN), scan rate 100 mVs^{-1}. The anodic peak height shows a decrease of 26% after 200 scans.

The ferrocene coverage (Γ, molecules cm^{-2}) of the diamond electrode was estimated from the charge of the CV anodic peak, Q, assuming a one-electron reaction, using the following relationship;

$$\Gamma = QA / nFA \qquad \text{(Equation 5.1)}$$

where $n = 1$ is the number of electrons transferred during the redox reaction, F is Faraday's constant, and A is the area of exposed diamond electrode (= 0.5 cm^2). The ferrocene coverage was determined to be $1.48 \pm 0.5 \times 10^{14}$ molecules per cm^2 for the EG 2 sample, comparable to the values reported previously [10, 38]. From this value and comparison to the value reported before [37], we can conclude that a near to single monolayer of ferrocene entities is formed.

5.4.3 Water Contact Angle Measurements

Water contact angle measurements were conducted to identify the macroscopic changes in the wetting properties of the diamond surface after each functionalization step. A hydrogen terminated diamond surface is hydrophobic with a water contact angle of $\theta = 110.6°$. The water contact angle value decreased slightly to $\theta = 83.7°$ upon functionalization with the 4-azidophenyl layer. After clicking ferrocene groups to the phenylazide groups, the contact angle dropped further to $\theta = 73.9°$.

5.4.4 X-ray Photoelectron Spectroscopy (XPS)

X-ray photoelectron spectroscopy is a valuable tool to evaluate the changes in the surface chemical composition and binding that have occurred during surface derivatization. Figure 5.9(i) displays the XPS survey spectrum of a hydrogenated B:NCD surface. It shows a main peak at 285 eV (C 1s) from the bulk diamond and a small peak at 532 eV (O 1s) due to the adsorption of oxygen on the surface. After electrografting of the 4-azidophenyl groups, an additional small peak at ~ 400 eV was observed, in agreement with the chemical composition of the attached molecule (Figure 5.9(ii)). High-resolution XPS of the N 1s region of the 4-azidophenyl-functionalized B:NCD surface (Figure 5.10) showed a broad peak centered at ~ 400 eV and a second small peak centered at ~ 404 eV, suggesting the presence of chemically different nitrogen atoms. The central nitrogen atom of the azide group, with a characteristic peak at ~ 404 eV for the grafted electrode, has a low electron density and thus a higher binding energy [30].

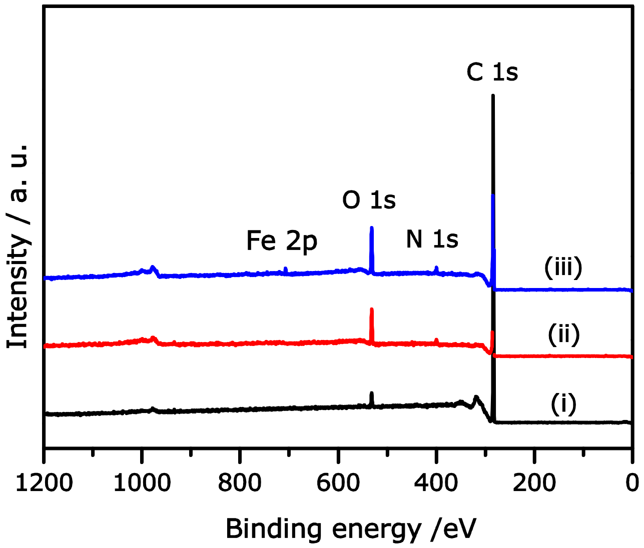

Figure 5.9 XPS spectra for (i) hydrogenated B:NCD, (ii) electrografted B:NCD, and (iii) electrografted B:NCD following click chemistry with ethynylferrocene.

XPS is particularly useful to monitor the click chemistry process as the intensity of this peak is greatly reduced after this reaction step. After clicking the ferrocene groups onto the 4-azidophenyl-functionalized B:NCD surface, the peak at ~ 404 eV disappeared almost completely and the peak at ~ 400 eV broadened (Figure 5.10, blue line). This can be seen as evidence for the transformation of the azide group into the 1,2,3-triazole unit attached to the terminal ferrocene. In addition, a high-resolution XPS scan of the Fe 2p region additionally demonstrated the presence of the ferrocene moieties on the B:NCD surface (Figure 5.11). The Fe $2p_{3/2}$ and $2p_{1/2}$ peaks are observed at 707.7 and

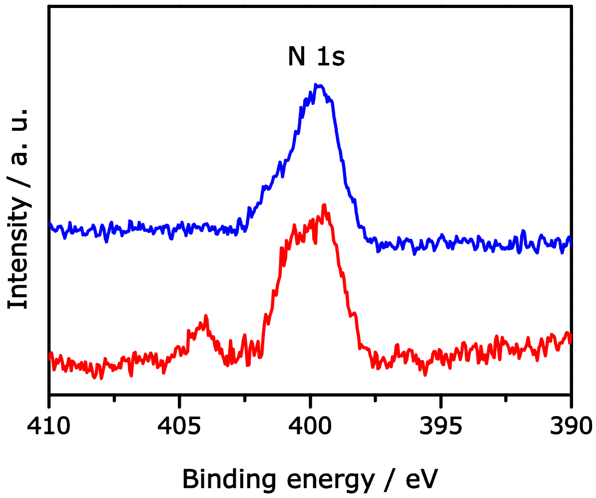

Figure 5.10 High-resolution XPS spectra of the N 1s region for electrografted B:NCD (red line), and electrografted B:NCD following click chemistry with ethynylferrocene (blue line).

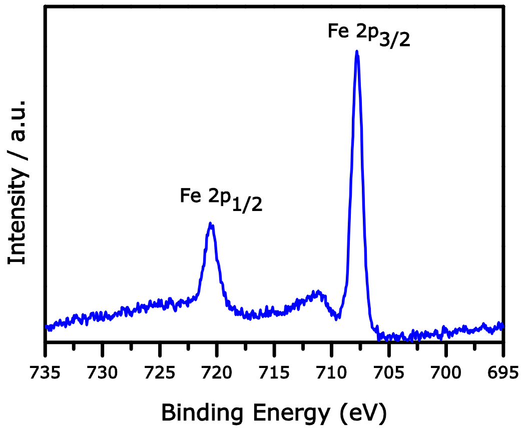

Figure 5.11 High-resolution XPS spectrum of the Fe 2p region for the electrografted B:NCD following click chemistry with ethynylferrocene.

720.6 eV, respectively. This indicates that the Fe moiety exists mainly in its +III oxidation state, in agreement with previously reported results on ferrocene groups anchored onto diamond [10] and silicon surfaces [35].

5.4.5 Clicking An Alkyne-terminated DNA Probe onto Phenylazide-functionalized B:MCD

The utility of the 4-azidophenyl-functionalized diamond electrode for fast and efficient attachment of a ss-DNA probe was demonstrated with the coupling of an alkynyl-derivatized ss-DNA probe followed by hybridization of the target DNA molecule (Figure 5.3).

To avoid oxidative cleavage of the ss-DNA molecules by L-ascorbic acid (L-AA), the DNA click reaction was carried out using CuBr and tris-(benzyltriazolylmethyl)amine (TBTA) instead of L-AA and $CuSO_4.5H_2O$ [33]. The ss-DNA probe was first immobilized onto a 4-azidophenyl-functionalized B:MCD sample, followed by hybridization with fully complementary DNA. This hybridization process could be verified with confocal microscopy since the target DNA was labelled with 6-carboxyfluorescein (FAM). The B:MCD sample on which the immobilization protocol was carried out (as described above) showed an intense fluorescence signal (Figure 5.12(a)). This confirms the hybridization of the target DNA to the probe DNA attached by the click reaction. The black bar in Figure 5.12(b) was induced by photobleaching of the FAM fluorophore. On the other hand, no hybridization was observed for the B:MCD sample without phenylazide layer (Figure 5.12(c)).

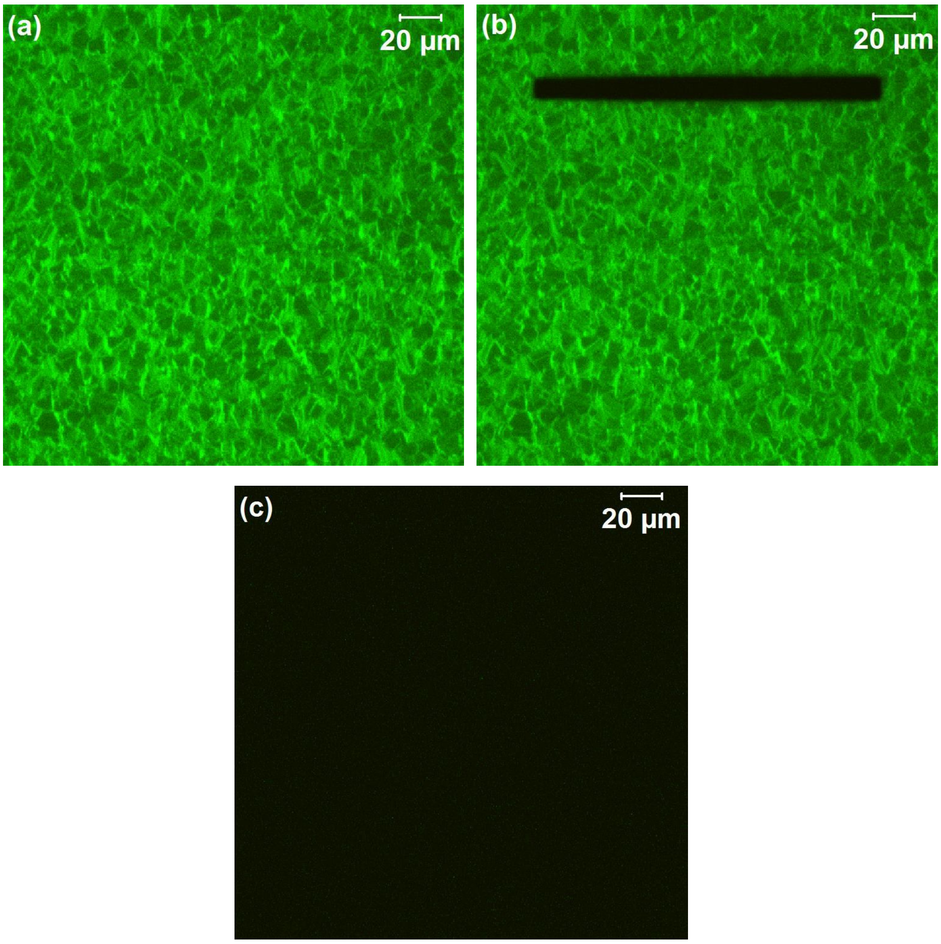

Figure 5.12 Confocal fluorescence images of B:MCD samples: (a) ss-DNA probe clicked to phenylazide-functionalized B:MCD and hybridized with FAM-tagged target DNA hybridized to the ss-DNA. (b) The black bar in the middle was induced by photobleaching of the FAM fluorophore. (c) ss-DNA probe and FAM-tagged target DNA exposed to bare hydrogenated B:MCD under the same condition as for (a).

5.4.6 Impedance spectroscopy of phenylazide- and DNA-modified diamond surfaces

As the dynamics of electron transfer at the electrode interfaces are strongly influenced by the nature of the electrode surface, surface immobilization with (bio)molecules can significantly alter the interfacial electron transfer properties. Hence, the 4-azidophenyl-functionalized and DNA-modified diamond surfaces were evaluated by impedance spectroscopy [32]. The measurements were performed with a miniaturized impedance spectroscopy unit, as described before [40]. Figure 5.13 shows the Cole-Cole plot for bare B:MCD (blue line) and phenylazide-grafted B:MCD (red line). A lower admittance is observed for the 4-azidophenyl-functionalized B:MCD as compared to the blank B:MCD. This is what is expected to be observed when an insulating organic molecular layer is chemically bonded onto an electrode [30].

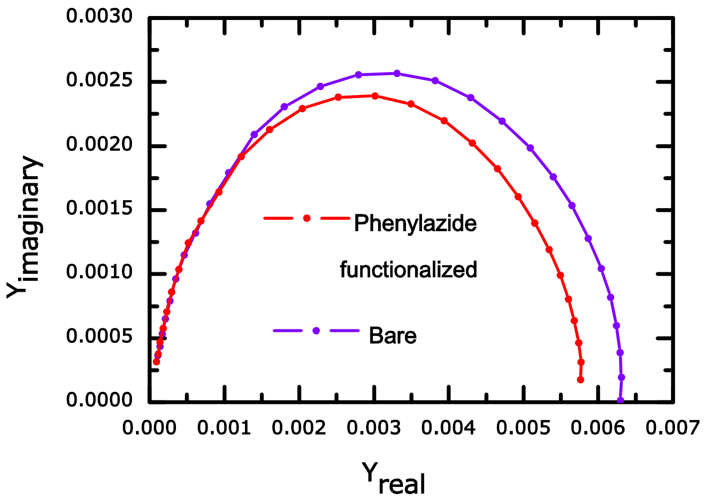

Figure 5.13 Cole-Cole plots showing the real and imaginary parts of the admittance for a blank B:MCD electrode (blue line) and a phenylazide-functionalized B:MCD electrode (red line).

Figure 5.14 shows the Cole-Cole plots for the DNA-modified B:MCD sample in its different states in PBS (phosphate buffered saline) buffer solution. The

4-azidophenyl-functionalized B:MCD was modified first with ss-DNA by click chemistry and then analyzed by impedance spectroscopy (black line). After hybridization with the target DNA, the impedance was measured again, resulting in an increase in Y_{real} and $Y_{imaginary}$ (red line). The hybridization-induced changes in Y_{real} and $Y_{imaginary}$ are quite apparent at frequencies above 1 kHz. These results agree well with previous findings showing that DNA molecules hybridizing at the interface induce a field effect in the diamond space-charge layer, and this lowers the impedance of the diamond [32]. Moreover, DNA is more conductive in its double-stranded form (i.e., after hybridization with a complementary sequence) compared to its single strand form [31].

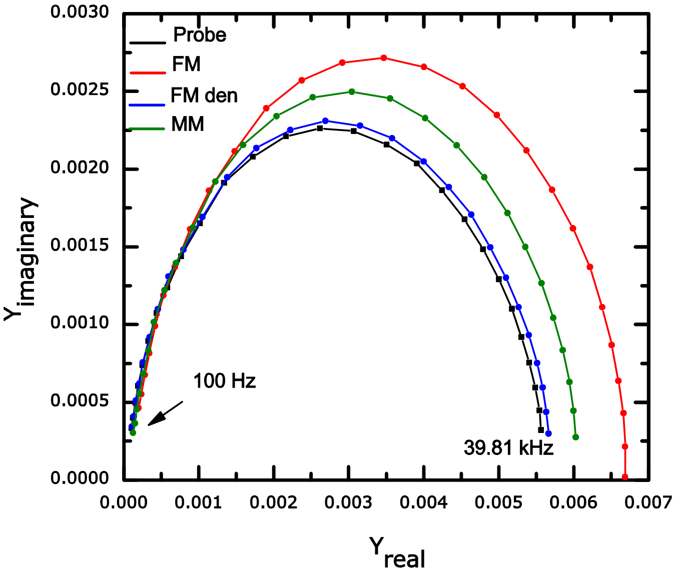

Figure 5.14 Cole-Cole plots showing the real and imaginary parts of the admittance for the B:MCD electrode, click immobilized with a ss-DNA molecule (black line), then hybridized with its fully complementary (FM, red line) and mismatch (MM, green line) DNA. After denaturation of the fully complementary DNA, the impedance signal falls back almost to its original position (FM den, blue line).

Then, when the DNA was denatured by introducing 0.1 M NaOH into the flow cell, a third Cole-Cole plot was determined (blue line). Y_{real} and $Y_{imaginary}$ moved back toward their original positions. After denaturation, the impedance did not completely reverse to its initial state. The lack of this complete reversibility is yet unclear but might be due to the induced changes in the molecular layer by NaOH [32, 41]. To determine the selectivity of DNA hybridization, the same ss-DNA modified B:MCD sample was hybridized with a non-complementary target DNA sequence (see Table 5.2, exp. section). Figure 5.14 (green line) clearly shows that the increase in the admittance due to hybridization with non-complementary DNA is smaller than observed upon hybridization with complementary DNA (red line) [32].

5.5 Conclusions

We have presented a simple yet efficient method to covalently attach functional organic molecules onto a boron-doped diamond electrode surface via a combination of diazonium electrografting and click chemistry. The functionalized diamond electrode was studied using cyclic voltammetry, impedance spectroscopy, and XPS to confirm the modification steps. This work also demonstrates, for the first time, the immobilization of DNA molecules on a diamond surface via CuAAC click chemistry. The DNA-click immobilized diamond electrode shows the possibility to be used as a DNA sensor. More in general, electrografted azidophenyl-functionalized diamond electrodes can be applied as a generic platform for coupling with a wide range of ethynyl-terminated species for various applications.

5.6 Acknowledgements

This work was financially supported by the Special Research Fund of Hasselt University, the Research Foundation Flanders (FWO) (G.0555.10N and G.0829.09N), and the EU FP7 Collaborative Project “MOLESOL” (No. 256617). We thank H. Penxten for the cyclic voltammetry measurements, B. Ruttens for the SEM images, and P. Robaeys for the four-point probe measurements.

5.7 References

1. (a) Balmer, R. S.; Brandon, J. R.; Clewes, S. L.; Dhillon, H. K.; Dodson, J. M.; Friel, I.; Inglis, P. N.; Madgwick, T. D.; Markham, M. L.; Mollart, T. P.; Perkins, N.; Scarsbrook, G. A.; Twitchen, D. J.; Whitehead, A. J.; Wilman, J. J.; Woollard, S. M., Chemical Vapour Deposition Synthetic Diamond: Materials, Technology and Applications. *J. Phys. Condens. Matter* **2009**, *21*, 364221; (b) Williams, O.; Nesladek, M.; Mareš, J. J.; Hubik, P. Growth and Properties of Nanocrystalline Diamond Films. In *Physics and Applications of CVD Diamond*; Koizumi, S.; Nebel, C.; Nesladek, M., Eds.; Wiley-VCH, Weinheim, Germany **2008**; pp 13-28.

2. Amaral, M.; Gomes, P. S.; Lopes, M. A.; Santos, J. D.; Silva, R. F.; Fernandes, M. H., Cytotoxicity Evaluation of Nanocrystalline Diamond Coatings by Fibroblast Cell Cultures. *Acta Biomater.* **2009**, *5*, 755.

3. Scajev, P.; Nargelas, S.; Jarasiunas, K.; Kisialiou, I.; Ivakin, E.; Deferme, W.; D'Haen, J.; Haenen, K., Crystallite Size Dependent Carrier Recombination Rate and Thermal Diffusivity in Undoped and Boron Doped CVD Diamond Layers. *Phys. Status Solidi A* **2013**, *210*, 2022.

4. Janssens, S. D.; Pobedinskas, P.; Vacik, J.; Petrakova, V.; Ruttens, B.; D'Haen, J.; Nesladek, M.; Haenen, K.; Wagner, P., Separation of Intra- and Intergranular Magnetotransport Properties in Nanocrystalline Diamond Films on The Metallic Side of The Metal-Insulator Transition. *New J. Phys.* **2011**, *13*, 083008.

5. (a) Wang, Q.; Subramanian, P.; Li, M. S.; Yeap, W. S.; Haenen, K.; Coffinier, Y.; Boukherroub, R.; Szunerits, S., Non-Enzymatic Glucose Sensing on Long and Short Diamond Nanowire Electrodes. *Electrochem. Commun.* **2013**, *34*, 286; (b) Shalini, J.; Lin, Y. C.; Chang, T. H.; Sankaran, K. J.; Chen, H. C.; Lin, I. N.; Lee, C. Y.; Tai, N. H., Ultra-Nanocrystalline Diamond Nanowires with Enhanced Electrochemical Properties. *Electrochim. Acta* **2013**, *92*, 9.

6. (a) Sotowa, K. I.; Amamoto, T.; Sobana, A.; Kusakabe, K.; Imato, T., Effect of Treatment Temperature on The Amination of Chlorinated Diamond. *Diamond Relat. Mater.* **2004**, *13*, 145; (b) Yang, N. J.; Uetsuka, H.; Watanabe, H.;

Nakamura, T.; Nebel, C. E., Photochemical Amine Layer Formation on H-terminated Single-crystalline CVD Diamond. *Chem. Mater.* **2007**, *19*, 2852; (c) Boukherroub, R.; Wallart, X.; Szunerits, S.; Marcus, B.; Bouvier, P.; Mermoux, M., Photochemical Oxidation of Hydrogenated Boron-doped Diamond Surfaces. *Electrochem. Commun.* **2005**, *7*, 937; (d) Ruther, R. E.; Rigsby, M. L.; Gerken, J. B.; Hogendoorn, S. R.; Landis, E. C.; Stahl, S. S.; Hamers, R. J., Highly Stable Redox-Active Molecular Layers by Covalent Grafting to Conductive Diamond. *J. Am. Chem. Soc.* **2011**, *133*, 5692; (e) Yao, S. A.; Ruther, R. E.; Zhang, L. H.; Franking, R. A.; Hamers, R. J.; Berry, J. F., Covalent Attachment of Catalyst Molecules to Conductive Diamond: CO_2 Reduction Using "Smart" Electrodes. *J. Am. Chem. Soc.* **2012**, *134*, 15632; (f) Nakamura, T.; Ohana, T., Surface Functionalization of Diamond Films by Photoreaction of Elemental Sulfur and Their Surface Properties. *Jpn. Appl. Phys.* **2012**, *51*, 085201.

7. (a) Härtl, A.; Schmich, E.; Garrido, J. A.; Hernando, J.; Catharino, S. C. R.; Walter, S.; Feulner, P.; Kromka, A.; Steinmüller, D.; Stutzmann, M., Protein-modified Nanocrystalline Diamond Thin Films for Biosensor Applications. *Nat. Mater.* **2004**, *3*, 736; (b) Yang, W. S.; Auciello, O.; Butler, J. E.; Cai, W.; Carlisle, J. A.; Gerbi, J.; Gruen, D. M.; Knickerbocker, T.; Lasseter, T. L.; Russell, J. N.; Smith, L. M.; Hamers, R. J., DNA-modified Nanocrystalline Diamond Thin-films as Stable, Biologically Active Substrates. *Nat. Mater.* **2002**, *1*, 253; (c) Tse, K. Y.; Nichols, B. M.; Yang, W. S.; Butler, J. E.; Russell, J. N.; Hamers, R. J., Electrical Properties of Diamond Surfaces Functionalized with Molecular Monolayers. *J. Phys. Chem. B* **2005**, *109*, 8523; (d) Wang, X.; Colavita, P. E.; Metz, K. M.; Butler, J. E.; Hamers, R. J., Direct Photopatterning and SEM Imaging of Molecular Monolayers on Diamond Surfaces: Mechanistic Insights Into UV-Initiated Molecular Grafting. *Langmuir* **2007**, *23*, 11623.

8. Wang, X. Y.; Landis, E. C.; Franking, R.; Hamers, R. J., Surface Chemistry for Stable and Smart Molecular and Biomolecular Interfaces via Photochemical Grafting of Alkenes. *Acc. Chem. Res.* **2010**, *43*, 1205.

9. Das, M. R.; Wang, M.; Szunerits, S.; Gengembre, L.; Boukherroub, R., Clicking Ferrocene Groups to Boron-doped Diamond Electrodes. *Chem. Commun.* **2009**, *19*, 2753.

10. Wang, M.; Das, M. R.; Li, M. S.; Boukherroub, R.; Szunerits, S., "Clicking" Thiophene on Diamond Interfaces. Preparation of a Conducting Polythiophene/ Diamond Hybrid Material. *J. Phys. Chem. C* **2009**, *113*, 17082.

11. Notsu, H.; Tatsuma, T.; Fujishima, A. Characterization of Oxygenated Diamond Electrodes. In *Diamond Electrochemistry;* Fujishima, A.; Einaga, Y.; Rao, T. N.; Tryk, D. A., Eds.; Elseveir: Amsterdam **2005**; pp 218-237.

12. Agnès, C.; Ruffinatto, S.; Delbarre, E.; Roget, A.; Arnault, J. C.; Omnès, F.; Mailey, P., New One Step Functionalization of Polycrystalline Diamond Films Using Amine Derivatives. *IOP Conf. Ser. Mater. Sci. Eng.* **2010**, *16*, 012001.

13. (a) Jian, W.; Firestone, M. A.; Auciello, O.; Carlisle, J. A., Surface Functionalization of Ultrananocrystalline Diamond Films by Electrochemical Rduction of Aryldiazonium Salts. *Langmuir* **2004**, *20*, 11450; (b) Lud, S. Q.; Steenackers, M.; Jordan, R.; Bruno, P.; Gruen, D. M.; Feulner, P.; Garrido, J. A.; Stutzmann, M., Chemical Grafting of Biphenyl Self-Assembled Monolayers on Ultrananocrystalline Diamond. *J. Am. Chem. Soc.* **2006**, *128*, 16884; (c) Zhong, Y. L.; Ng, W.; Yang, J. X.; Loh, K. P., Electrostatically Self-Assembled Polyoxometalates on Molecular-Dye-Functionalized Diamond. *J. Am. Chem. Soc.* **2009**, *131*, 18293; (d) Agnès, C.; Arnault, J. C.; Omnès, F.; Jousselme, B.; Billon, M.; Bidan, G.; Mailley, P., XPS Study of Ruthenium *tris*-Bipyridine Electrografted from Diazonium Salt Derivative on Microcrystalline Boron Doped Diamond. *Phys. Chem. Chem. Phys.* **2009**, *11*, 11647.

14. Zhong, Y. L.; Loh, K. P.; Midya, A.; Chen, Z. K., Suzuki Coupling of Aryl Organics on Diamond. *Chem. Mater.* **2008**, *20*, 3137.

15. Belanger, D.; Pinson, J., Electrografting: A Powerful Method for Surface Modification. *Chem. Soc. Rev.* **2011**, *40*, 3995.

16. Mesnage, A.; Lefevre, X.; Jegou, P.; Deniau, G.; Palacin, S., Spontaneous Grafting of Diazonium Salts: Chemical Mechanism on Metallic Surfaces. *Langmuir* **2012**, *28*, 11776.

17. Zhu, Z. W.; Wang, Y.; Zhang, X.; Sun, C. F.; Li, M. G.; Yan, J. W.; Mao, B. W., Electrochemical Impedance Spectroscopy and Atomic Force Microscopic

Studies of Electrical and Mechanical Properties of Nano-Black Lipid Membranes and Size Dependence. *Langmuir* **2012**, *28*, 14739.

18. Zhou, X. S.; Dong, Z. R.; Zhang, H. M.; Yan, J. W.; Gao, J. X.; Mao, B. W., Self-Assembly of A Rh(I) Complex on Au(111) Surfaces and Its Electrocatalytic Activity Toward The Hydrogen Evolution Reaction. *Langmuir* **2007**, *23*, 6819.

19. Aswal, D. K.; Lenfant, S.; Guerin, D.; Yakhmi, J. V.; Vuillaume, D., Self-Assembled Monolayers on Silicon for Molecular Electronics. *Anal. Chim. Acta* **2006**, *568*, 84.

20. (a) Grätzel, M., Photoelectrochemical Cells. *Nature* **2001**, *414*, 338; (b) Subban, C. V.; Ati, M.; Rousse, G.; Abakumov, A. M.; Van Tendeloo, G.; Janot, R.; Tarascon, J. M., Preparation, Structure, and Electrochemistry of Layered Polyanionic Hydroxysulfates: $LiMSO_4OH$ (M = Fe, Co, Mn) Electrodes for Li-Ion Batteries. *J. Am. Chem. Soc.* **2013**, *135*, 3653; (c) Dunn, B.; Kamath, H.; Tarascon, J. M., Electrical Energy Storage for the Grid: A Battery of Choices. *Science* **2011**, *334*, 928.

21. Willner, I.; Katz, E., Integration of Layered Redox Proteins and Conductive Supports for Bioelectronic Applications. *Angew. Chem. Int. Ed.* **2000**, *39*, 1180.

22. Lahann. J. Click Chemistry: A Universal Ligation Strategy for Biotechnology and Materials Science. In *Click Chemistry for Biotechnology and Materials Science;* Lahann, J., Eds.; John Wiley & Sons Ltd: West Sussex, **2009**; pp 1-8.

23. Frey, B. L.; Corn, R. M., Covalent Attachment and Derivatization of Poly(L-lysine) Monolayers on Gold Surfaces as Characterized by Polarization-Modulation FT-IR Spectroscopy. *Anal. Chem.* **1996**, *68*, 3187.

24. Kolb, H. C.; Finn, M. G.; Sharpless, K. B., Click chemistry: Diverse Chemical Function from A Few Good Reactions. *Angew. Chem. Int. Ed.* **2001**, *40*, 2004.

25. Arnold, R. M.; Locklin, J., Self-Sorting Click Reactions That Generate Spatially Controlled Chemical Functionality on Surfaces. *Langmuir* **2013**, *29*, 5920.

26. Grabosch, C.; Kind, M.; Gies, Y.; Schweighöfer, F.; Terfort, A.; Lindhorst, T. K., A 'Dual Click' Strategy for the Fabrication of Bioselective, Glycosylated Self-Assembled Monolayers as Glycocalyx Models. *Org. Biomol. Chem.* **2013**, 28, 4006.

27. Arihara, K.; Fujishima, A., Electrode, Ozone Generator and Ozone Generating Method. Central Japan Railway Company **2005**, EP1754804 A1.

28. Gajewski, W.; Achatz, P.; Williams, O. A.; Haenen, K.; Bustarret, E.; Stutzmann, M.; Garrido, J. A., Electronic and Optical Properties of Boron-Doped Nanocrystalline Diamond Films. *Phys. Rev. B* **2009**, 79, 045206.

29. (a) Fischer, A. E.; Show, Y.; Swain, G. M.; Electrochemical Performance of Diamond Thin-Film Electrodes from Different Commercial Sources. *Anal. Chem.* **2004**, *76*, 2553; (b) Vanhove, E.; de Sanoit, J.; Arnault, J. C.; Saada, S.; Mer, C.; Mailley, P.; Bergonzo, P.; Nesladek, M., Stability of H-terminated BDD Electrodes: An Insight into the Influence of the Surface Preparation. *Phys. Status. Solidi. A* **2007**, *204*, 2931.

30. Coates, M.; Nyokong, T., Electrode Modification Using Iron Metallophthalocyanine through Click Chemistry and Axial Ligation with Pyridine. *J. Electro. Chem.* **2012**, *687*, 111.

31. Lee, T. Y.; Shim, Y. B., Direct DNA Hybridization Detection Based on the Oligonucleotide-Functionalized Conductive Polymer. *Anal. Chem.* **2001**, *73*, 5629.

32. Yang, W. S.; Butler, J. E.; Russell, J. N.; Hamers, R. J., Interfacial Electrical Properties of DNA-Modified Diamond Thin Films: Intrinsic Response and Hybridization-Induced Field Effects. *Langmuir* **2004**, *20*, 6778.

33. Gramlich, P. M. E.; Wirges, C. T.; Manetto, A.; Carell, T., Postsynthetic DNA Modification through The Copper-Catalyzed Azide-Alkyne Cycloaddition Reaction. *Angew. Chem. Int. Ed.* **2008**, *47*, 8350.

34. Andrieux, C. P.; Pinson, J., The Standard Redox Potential of the Phenyl Radical/Anion Couple. *J. Am. Chem. Soc.* **2003**, *125*, 14801.

35. Rohde, R. D.; Agnew, H. D.; Yeo, W. S.; Bailey, R. C.; Heath, J. R., A Non-Oxidative Approach Toward Chemically and Electrochemically Functionalizing Si(111). *J. Am. Chem. Soc.* **2006**, *128*, 9518.

36. Collman, J. P.; Devaraj, N. K.; Chidsey, C. E. D., "Clicking" Functionality onto Electrode Surfaces. *Langmuir* **2004**, *20*, 1051.

37. Bard, A. L.; Faulkner, L. R. *Electrochemical Methods: Fundamentals and Applications*, John Wiley & Sons Inc: New York, **2001**.

38. Kondo, T.; Hoshi, H.; Honda, K.; Einaga, Y.; Fujishima, A.; Kawai, T., Photochemical Modification of A Boron-Doped Diamond Electrode Surface with Vinylferrocene. *J. Phys. Chem. C* **2008**, *112*, 11887.

39. Napper, A. M.; Liu, H. Y.; Waldeck, D. H., The Nature of Electronic Coupling Between Ferrocene and Gold through Alkanethiolate Monolayers on Electrodes: The importance of Chain Composition, Interchain Coupling, and Quantum Interference. *J. Phys. Chem. B* **2001**, *105*, 7699.

40. (a) van Grinsven, B.; Vandenryt, T.; Duchateau, S.; Gaulke, A.; Grieten, L.; Thoelen, R.; Ingebrandt, S.; De Ceuninck, W.; Wagner, P., Customized Impedance Spectroscopy Device As Possible Sensor Platform for Biosensor Applications. *Phys. Status Solidi A* **2010**, *207*, 919; (b) van Grinsven, B.; Bon, N. V.; Grieten, L.; Murib, M.; Janssens, S. D.; Haenen, K.; Schneider, E.; Ingebrandt, S.; Schoning, M. J.; Vermeeren, V.; Ameloot, M.; Michiels, L.; Thoelen, R.; De Ceuninck, W.; Wagner, P., Rapid Assessment of the Stability of DNA Duplexes by Impedimetric Real-Time Monitoring of Chemically Induced Denaturation. *Lab Chip* **2011**, *11*, 1656.

41. Murib, M. S.; van Grinsven, B.; Grieten, L.; Janssens, S. D.; Vermeeren, V.; Eersels, K.; Broeders, J.; Ameloot, M.; Michiels, L.; De Ceuninck, W.; Haenen, K.; Schoning, M. J.; Wagner, P., Electronic Monitoring of Chemical DNA Denaturation on Nanocrystalline Diamond Electrodes with Different Molarities and Flow Rates. *Phys. Status Solidi A* **2013**, *210*, 911.

Chapter 6

General Conclusions and Outlook

The importance of CVD diamond in biological and technological applications has recently been widely recognized. CVD diamond can find applications in biosensors, biochips, water treatment, radiation detection, high power electronics, magnetometry, novel lasers and other engineering applications. In this thesis, we have successfully demonstrated the application of diamond-based molecular platforms in the fields of photoelectrochemistry and biochemistry. A versatile chemistry to graft molecular linkers, molecular dyes and target sensing molecules onto otherwise inert diamond surfaces has been developed. Aryldiazonium grafting on H-terminated diamond was the major workhorse technique in this thesis. Spontaneous aryldiazonium grafting is found to be more attractive compared to diazonium electrografting as it does not require expensive electrochemical equipment or conductive materials. Moreover, it can be done on large area substrates which are an attractive point for industrial application.

Two surface post-modifications, i.e. Suzuki coupling and click chemistry, were carried out on this aryldiazonium pre-functionalized diamond. Surface Suzuki coupling was successfully demonstrated on 4-bromophenyl (Chapter 3) and arylboronic ester (Chapter 4) functionalized diamond, which later enable the direct coupling of molecular dyes on diamond. Surface click chemistry was successfully applied to couple molecules bearing a terminal alkyne moiety to azidophenyl-functionalized diamond. It should be noted that the Suzuki coupling and click reactions are just two of many possible coupling chemistries for a myriad of functional groups. The choice of which coupling chemistry to choose depends on the final targeted application. Suzuki coupling allows uninterrupted molecular conjugation of diamond surfaces to a large class of organic molecules which shows highly efficient charge transfer platform, but the reaction temperatures use in Suzuki coupling are usually high and it also requires long reaction time. On contrary, click reactions require mild reaction conditions and reaction usually complete within 2 hours which could preserve biomolecular activity after the reaction. This is especially an important key attribute for a successful bioconjugation reaction.

In Chapter 3 and 4, our work demonstrated the advantages of using B:NCD as a transparent electrode in photochemistry. The wide transparency and superb chemical stability are highly beneficial properties for p-type diamond as an electrode in dye-sensitized solar cells. We aim at developing B:NCD as essential component of novel generation of solar cells. This will allow an important breakthrough innovation and also at the same time the developed materials can mean a significant innovation and valorization for already developed photovoltaic technology platforms. In Chapter 3, we showed that commercially available N3 dye molecules can be covalently attached onto B:NCD surfaces through a diazonium, Suzuki and EDC-NHS reaction sequence. In Chapter 4, two novel donor-acceptor type light-harvesting molecular dyes, i.e. **Br-2T-Rho** and **Br-CPDT-Fur**, were synthesized and then covalently attached to a B:NCD surfaces via Suzuki cross-coupling on arylboronic ester pre-functionalized diamond. For all the Suzuki-coupling reactions, various catalytic systems were examined and compared to achieve high coupling yields. Calculations based upon the Ru presence as analyzed by XPS indicated that a dense layer of N3 molecules ($\sim 3\times10^{14}$ Ru/cm^2) was achieved. A surface coverage of 0.58 and 0.56 ML was achieved for the **Br-2T-Rho** and **Br-CPDT-Fur** molecular dyes, respectively.

Moreover, as evidenced by UPS measurements, the matching of the HOMO level of the molecular dyes with the VBM of the B:NCD thin film indicates that the holes generated during photoexcitation can possibly transfer from the dyes to the B:NCD thin film, which was further confirmed by proof of concept photocurrent measurements. This suggests the possibility of employing the p-type diamond electrode as photocathode to replace p-type NiO or as hole conductor to replace the highly corrosive triiodide electrolyte in dye-sensitized solar cells.

The ultimate goal of future research on diamond based solar cells is to fabricate a full device. We believe that systematic optimization of the solar cells with B:NCD films will bring improvement. Preparation of B:NCD films with low electrical resistivity can be used to replace the current platinum counter electrode use in DSSC technology. In general, photocurrents on sensitized diamond electrodes were very small compared to those observed for the state-of-art n-DSSCs with titania photoanodes. In principle, the flat electrode cannot deliver high external quantum efficiencies due to limited dye that could be attached onto the flat surface. Hence, surface engineering of the B:NCD photocathode should be the next direct task in the future development of diamond-based p-DSSCs. One possible way is the use of diamond foam developed lately by E. Nebel and co-workers at Fraunhofer IAF, Germany. This highly porous diamond foam has an increased surface area for the attachment of more molecular dyes. Hence, this may lead to higher photocurrent. Another possible way to improve the photocurrent on sensitized diamond electrodes would be a proper screening of other molecular dyes with a HOMO closer to the VBM of B:NCD by Density Functional Theory (DFT) calculations.

Our work also demonstrated the advantage of using BDD as an electrode in the field of biochemistry (Chapter 5). Successful surface functionalization of B:NCD via a combination of diazonium electrografting and click chemistry was achieved. An azide-terminated organic layer was first electrografted on the diamond surface by electrochemical reduction of 4-azidophenyldiazonium chloride. The azidophenyl-modified surface then reacted rapidly and efficiently with molecules bearing a terminal alkyne moiety by means of a Cu(I)-catalyzed alkyne-azide cycloaddition. The surface coverage with reactive azide moieties was first quantified electrochemically through complementary coupling of ethynylferrocene. The ferrocene coverage was determined to be 1.48 ± 0.5 x 10^{14} molecules per cm^2 and showed no significant aggregated. Later on, the utility of the azide-functionalized diamond electrode for fast and efficient covalent attachment of a ss-DNA probe was demonstrated by reaction with an alkyne-functionalized DNA probe. Finally, hybridization with labeled target DNA was carried out. The resulting device and its capability to work as a DNA-based sensor were evaluated by impedance spectroscopy. Due to the highly chemoselective and bioorthogonal nature of the alkyne-azide click reaction, azide-terminated boron-doped diamond electrodes can be regarded as a generic platform, providing a reliable coverage, for coupling with a wide range of ethynyl-terminated species of interest for various (sensing) applications. For instant, ethynyl-terminated antibody can be attached on diamond surface by using this method without affecting the antibody's bioactivity. The antibody-antigen binding activities then can be studied with electrochemical impedance spectroscopy.

The work in this thesis has certainly shown that diamond electrodes are very promising due to their unique properties. With advancing chemical vapour deposition growth technology, diamond can now be grown on a larger area, on different substrates and at lower cost. In addition, with further in-depth fundamental studies, diamond may reveal more of its hidden secrets. This should definitely have an attraction to get more scientists involved in diamond research in the near future.

Publications

1. Murib, M. S.; Yeap, W. S.; Martens, D.; Liu, X.; Bienstman, P.; Fahlman, M.; De Ceuninck, W.; Schöning, M. J.; Michiels, L.; Haenen, K.; Ameloot, M.; Serpengüzel, A.; Wagner, P., “Photonic Studies on Polymer-Coated Sapphire-Spheres: A Model System for Biological Ligands. *Sensor Actuat A-Phys,* **2015**, *222*, 212.

2. Murib, M. S.; Yeap, W. S.; Martens, D.; Bienstman, P.; De Ceuninck, W.; van Grinsven, B.; Schoning, M. J.; Michiels, L.; Haenen, K.; Ameloot, M.; Sperpenguzel, A.; Wagner, P., Photonic Detection and Characterization of DNA Using Sapphire Microspheres. *J. Biomed. Opt.* **2014**, *19*, 097006.

3. Yeap, W.S.; Bevk, D.; Liu, X.; Krysova, H.; Pasquarelli, A.; Vanderzande, D.; Lutsen, L.; Kavan, L.; Fahlman, M.; Maes, W.; Haenen, K., Diamond Functionalization with Light-Harvesting Molecular Wires: Improved Surface Coverage by Optimized Suzuki Cross-Coupling Conditions. *RSC Adv.*, **2014**, *4*, 42044.

4. Yeap, W. S.; Liu, X.; Bevk, D.; Pasquarelli, A.; Lutsen, L.; Fahlman, M.; Maes, W.; Haenen, K., Functionalization of Boron-Doped Nanocrystalline Diamond with N3 Dye Molecules. *ACS Appl. Mater. Interfaces*, **2014**, *6*, 10322.

5. Yeap, W. S.; Murib, M. S.; Cuypers, W.; Liu, X.; van Grinsven, B.; Ameloot, M.; Fahlman, M.; Wagner, P.; Maes, W.; Haenen, K., Boron-Doped Diamond Functionalization by an Electrografting - Alkyne-Azide Click Chemistry Sequence. *ChemElectroChem*, **2014**, *1*, 1145.

6. Heyer, S.; Jansses, W.; Turner, S.; Lu, Y.; Yeap, W. S.; Verbeeck, J.; Haenen, K.; Krueger, A., Toward Deep Blue Nano Hope Diamonds: Heavily Boron-Doped Diamond Nanoparticles. *ACS Nano*, **2014**, *8*, 5757.

7. Subramanian, P.; Motorina, A.; Yeap, W. S.; Haenen, K.; Coffinier, Y.; Zaitsev, V.; Niedziolka-Jonsson, J.; Boukherroub, R.; Szunerits, S., An Impedimetric Immunosensor Based on Diamond Nanowires Decorated with Nickel Nanoparticles. *Analyst*, **2014**, *139*, 1726.

8. Vanden Bon, N.; van Grinsven, B.; Murib, M. S.; Yeap, W. S.; Haenen, K.; De Ceuninick, W.; Wagner, P.; Ameloot, M.; Vermeeren, V.; Michiels, L., Heat-Transfer-Based Detection of SNPs in The PAH Gene of PKU Patients. *Int. J. Nanomedicine*, **2014**, *9*, 1629.

9. Wang, Q.; Subramanian, P.; Li, M. S.; Yeap, W. S.; Haenen, K.; Coffinier, Y.; Boukherroub, R.; Szunerits, S., Non-Enzymatic Glucose Sensing on Long and Short Diamond Nanowire Electrodes. *Electrochem. Commun.* **2013**, *34*, 286.

Appendix:

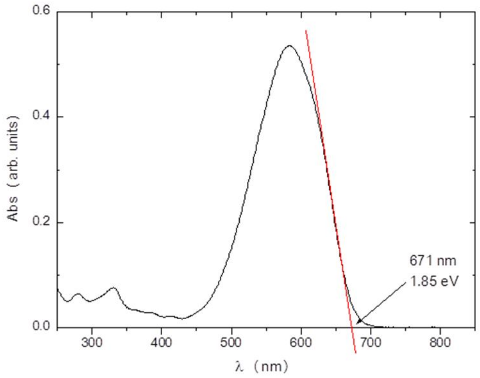

Figure A.1 UV-Vis absorption spectrum of Br-CPDT-Fur in CH_2Cl_2 solution.

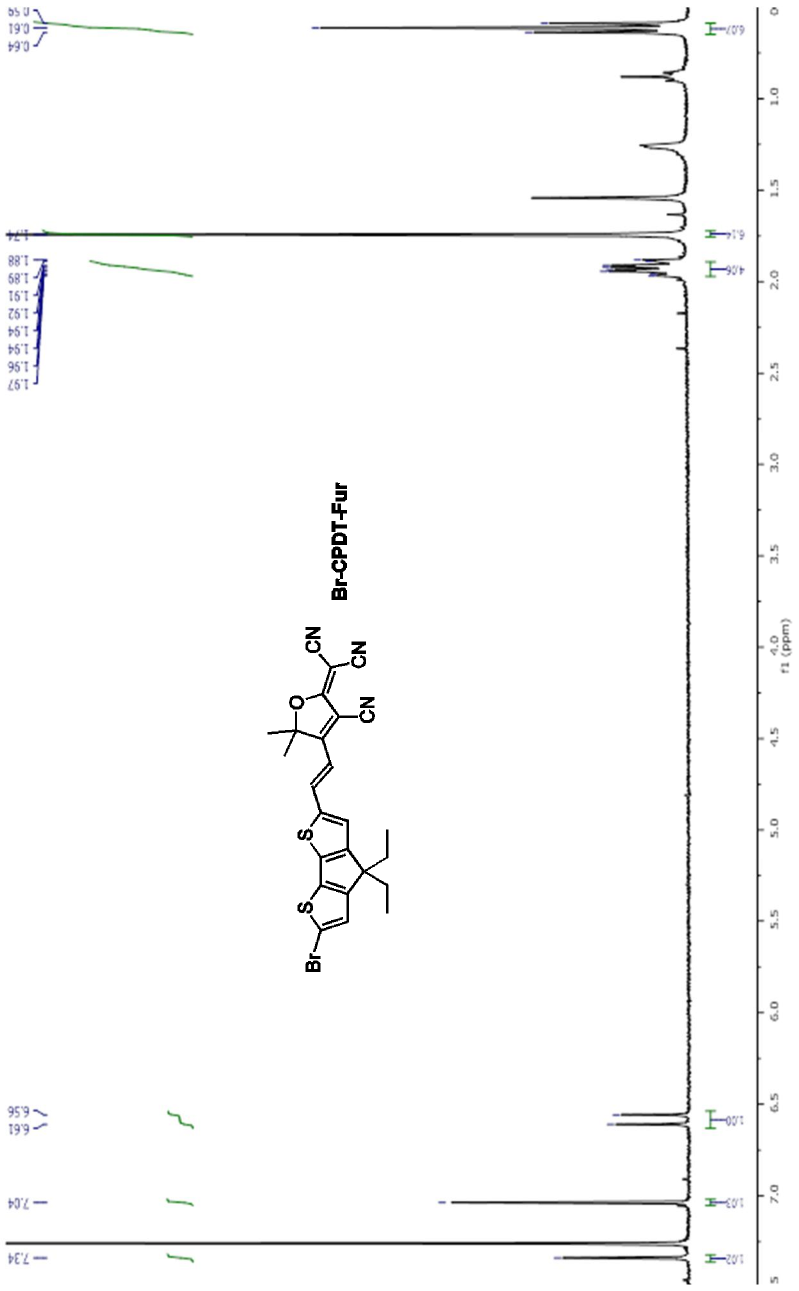

Figure A.2a ^{1}H NMR spectrum of **Br-CPDT-Fur**.

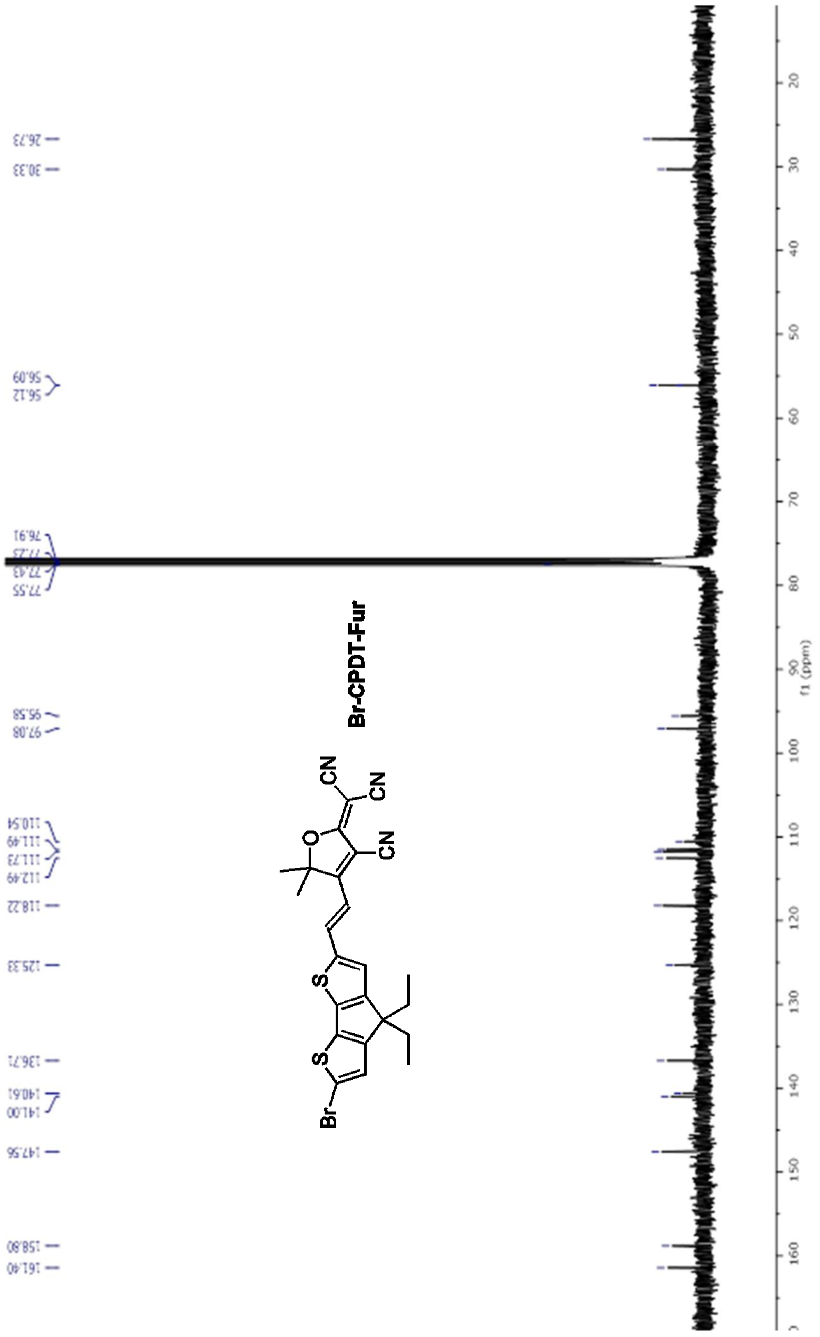

Figure A.2b ^{13}C NMR spectrum of **Br-CPDT-Fur**.